EVALUATION OF PREMALIGNANT LESIONS OF RAT COLON BY ^{1}H NUCLEAR MAGNETIC RESONANCE AND INFRARED SPECTROSCOPY

by

Eduardo Krupnik

A Thesis
Submitted to the Faculty of Graduate Studies
in Partial Fulfilment of the Requirements
for the Degree of

DOCTOR OF PHILOSOPHY

Department of Anatomy
University of Manitoba
Winnipeg, Manitoba

and

Biosystems Group, Institute for Biodiagnostics
National Research Council of Canada
Winnipeg, Manitoba

THE UNIVERSITY OF MANITOBA

FACULTY OF GRADUATE STUDIES

*****

COPYRIGHT PERMISSION PAGE

EVALUATION OF PREMALIGNANT LESIONS OF RAT COLON BY ^{1}H NUCLEAR MAGNETIC RESONANCE AND INFRARED SPECTROSCOPY

BY

EDUARDO KRUPNIK

A Thesis/Practicum submitted to the Faculty of Graduate Studies of The University of Manitoba in partial fulfillment of the requirements of the degree of

DOCTOR OF PHILOSOPHY

Abstract

^{1}H magnetic resonance spectroscopy (^{1}H MRS) and Fourier transform infrared (FTIR) spectroscopy are being widely used to study the biochemical changes associated with cancer. In particular, based upon the hypothesis that biochemical changes associated with cancer precede morphological manifestations of the disease, these spectroscopic techniques are being evaluated as potential diagnostic and prognostic tool.

In the current study, ^{1}H MRS and FTIR spectroscopy were applied to the study of colonic tissue from rats treated with the specific colon carcinogen azoxymethane (AOM) to determine whether tumor induction was associated with identifiable spectroscopic changes in the colon. In particular the attention was centered on aberrant crypt foci or ACF, small lesions of the colon, which are hypothesized to represent an early preneoplastic stage in the adenoma-carcinoma sequence.

The ^{1}H MRS analysis of control mucosa taken from healthy male Sprague Dawley rats, ACF, colonic mucosa and tumor samples taken from AOM treated rats revealed that the peak intensities and areas of ACF lie between those from normal and normal-appearing carcinogen-treated mucosa samples and tumors. Application of pattern recognition algorithms such as linear discriminant analysis (LDA) allowed non-subjective classification of the spectra into four groups with a high degree of accuracy (81.5%). The results place the ACF mainly as an

independent group, but with ^{1}H MRS features that put them between those of the normal mucosa samples and the tumors, supporting the hypothesis that ACF represent an intermediate step in colon carcinogenesis.

For the FTIR analysis, and due to the heterogeneity of the colon, we first studied the mid-infrared spectroscopic characteristics of cryostat sections of the different layers of the colon with the aid of an infrared microscope. The spectra of the muscularis, submucosa and mucosa were significantly different, allowing identification of mucosal tissue with relative ease. The spectroscopic characteristics of healthy mucosa, AOM-treated mucosa, and tumors were then studied. Spectra of the three tissues were similar. However, subtle differences in the absorbance bands assigned to nucleic acids were seen, indicative of alterations in the structure of the nucleic acids. Spectra indicate a progressive alteration in nucleic acid structure from normal mucosa through treated mucosa to tumors. LDA allowed non-subjective classification of spectra as arising from normal mucosa, treated mucosa and tumors with an accuracy of 85%. Similarly, LDA allowed classification of spectra of AOM-treated mucosa, ACF and tumor biopsies with an accuracy of 79.2%. Misclassification of spectra arising from ACF as arising from both tumor and mucosa suggests that the ACF exhibit biochemical characteristics intermediate between the control and AOM-mucosa samples and the tumor groups.

Several biochemical characteristics of the ACF, detected by ^{1}H MRS and FTIR, suggest that these lesions are an early event in the development of colon carcinogenesis. The application of pattern recognition algorithms to classify the different classes of colon tissues supports this conclusion, since ACF samples were grouped between the normal tissue samples and the tumors.

Given the importance of early diagnosis, the multidisciplinary approach presented in this thesis could serve as an important complement to the routine histopathological assessment for a better and more efficient diagnosis of colorectal cancer.

Esta tesis esta dedicada a vos Minnie

Acknowledgements

I would like to begin by acknowledging my supervisor, Dr. Ian C.P. Smith for his continuos support and encouragement throughout my thesis.

I also like to thank Dr. J. Paterson for her guidance and friendship, Dr. R.P.Bird for her continuous support, Dr. J. Anderson for her great teaching and Dr. M. Jackson for showing me the light (infrared) and for his friendship.

I would also like to thank all the people at the Institute for Biodiagnostics, National Research Council, especially the animal care personnel, commissioners, Anne Daley, Pauline Kulbaba and David Colborne.

This thesis would have not been possible without the support, friendship, and scientific discussions with my fellow students at the Institute for Biodiagnostics. The members of the Human Cancer group Lanette Friesen, Dr. Tedros Bezabeh, and Scott King, Dr. Lin-P'ing Choo-Smith, Edward Hoffenberg, Mauricio Ede and Hooman Gomeshi; and my good friend from anatomy Jon Meltzer.

Most of all I would like to acknowledge my office- coffee- hockey-pool-mate, classical NMR teacher, and best friend of all, Scott King, who I am going to miss dearly.

And my family: Marcelo, Valeria y Daniel, who were so supportive even though it meant having their son and brother so many miles away.

And Barbara, who always has found time to teach me English and friendship.

And my friends in Argentina, Canada, Mexico and Israel: Abbes, Andres, Claudio, Daniel, Gabriel, Gaston, Marcela, Marcelo, and Ricardo.

And Paola, my friend of life who with her love always heals my emotions.

And to you Minnie, my friend, my abu, to whom this thesis is dedicated with all my love.

Table of Contents

List of Figures

List of Tables

List of Abbreviations

ACF	*aberrant crypt foci*
AOM	*azoxymethane*
B_0	*external static magnetic field*
B_1	*radiofrequency magnetic field*
BUdR	*bromodeoxyuridine*
δ	*chemical shift*
DCC	*Deleted in Colon Carcinoma*
DMH	*dimethylhydrazine*
DNA	*deoxyribonucleic acid*
D_2O	*deuterium oxide*
GA	*genetic algorithm*
γ	*gyromagnetic ratio*
FID	*free induction decay*
FM	*fixed mirror*
FT-IR	*Fourier transform infrared*
λ	*wavelength of light*
h	*Planck's constant*
H&E	*hematoxilyn and eosin*
^1H	*proton*
^3HTdR	*tritiated-thymidine*
I	*spin quantum number*
k	*Boltzman's constant*
LDA	*linear discriminant analysis*
m	*magnetic nuantum number*
M	*magnetization vector*

M_0	*net magnetization vector*
MANOVA	*multivariate analysis of variance*
MM	*moving mirror*
MR	*magnetic resonance*
MRS	*magnetic resonance spectroscopy*
MRI	*magnetic resonance imaging*
N	*spin population*
NMR	*nuclear magnetic resonance*
OCT	*Optimal Cutting Temperature*
PABA	*para-aminobenzoic acid*
PBS	*phosphate buffered saline*
ppm	*parts per million*
P-Tyr	*phosphorylated cellular tyrosine*
rf	*radiofrequency*
RNA	*ribonucleic acid*
RSV	*Rous sarcoma virus*
S/N	*signal-to-noise ratio*
SD	*Sprague Dawley*
T	*Tesla*
T	*absolute temperature*
T_1	*spin-lattice (longitudinal) relaxation*
T_2	*spin=spin (transverse) relaxation*
TGF-α	*transforming growth factor α*
μ	*nuclear magnetic moment*
ν	*frequency*
$\bar{\upsilon}$	*wavenumber*
ω_0	*Larmor precession frequency*

Introduction

Cancer, a word that needs no translation. A word commonly associated with death. Cancer is the third leading cause of death in the general population after injuries and heart disease, and also one of the leading cause of emotional and physical suffering among families. Early diagnosis of this killer disease greatly improves the prognosis. Thus, the importance of the research to improve the methods of diagnosis is vital. Of great value would be to identify and study preneoplastic lesions to aid the development of methods for early detection of risk for developing cancer. Aberrant crypt foci (ACF) are the focus of this thesis. These tiny structures of the colon were proposed to represent preneoplastic lesions of colorectal cancer (Bird, 1987). Morphological, immunological, and genetic data support this hypothesis (Bird, 1995).

^{1}H magnetic resonance spectroscopy (MRS) and infrared (IR) spectroscopy are rapid, sensitive techniques, which can provide detailed information at the molecular level concerning the composition and architecture of biological materials. All diseases are associated with biochemical changes in the tissues and cells, which should be detectable spectroscopically. In addition, such changes associated with the disease process must precede clinical manifestation, allowing the potential for an early detection by MRS and IR spectroscopy.

^{1}H MRS and IR spectroscopy are two complementing techniques. While ^{1}H MRS allows the study of small molecular weight metabolites, FT-IR reveals

structures such as proteins, nucleic acids, and phospholipids. Compared to other types of spectroscopy such as Raman, fluerescence, etc, ^{1}H MRS and IR spectroscopy have better signal to noise ratio.

The main objective of this thesis will be the spectroscopic characterization of ACF, both with NMR and FT-IR. The purpose is not to replace histopathological methods of diagnosis, but to complement them, and to see if these two techniques support the hypothesis that ACF represent putative preneoplastic lesions of the colon.

1 Cancer

1.1 Definitions and clinical features of neoplasia

Neoplasm literally means new growth. A neoplasm could be defined as an uncontrolled proliferation of cells which continues even after the stimulus which evokes it has been removed. Many neoplasms penetrate and destroy adjacent tissues -local invasion- in which case the neoplasm is classified as malignant. Metastasis, the invasion and colonization of distant organs, is usually a follow up to local invasion. Once the neoplasm has invaded distant organs local excision of the primary neoplasm does not cure the patient.

The killing properties of neoplasms are several. Both benign and malignant carcinomas form bulky structures which could affect the functioning of important anatomical structures. They could obstruct the flow of main circulatory streams thus depleting organs of blood circulation. The cells that compose a neoplasm, both benign and malignant, represent transformed cells of the primary organ. Thus, if the primary organ is a gland, the neoplastic cells have the potential to overproduce a specific hormone, which could bring fatal consequences. A protruding polyp into the digestive tract could lead to intestinal infarction or obstruction. Malignant neoplasms also destroy the primary tissue and in doing so they cause bleeding and secondary infections, and have the potential to destroy the function of the organ itself (Cotran *et al.*, 1994).

1.2 The genetic nature of cancer

A genetic basis for cancer has been hypothesized for over half a century. In 1911, Rous induced neoplasms in chickens using a cell free filtrate obtained from avian sarcomas (Rous, P., 1911). That experiment was the landmark that led to the idea that cancer could be induced by discrete genetic elements. Sixty years later, it was discovered that the responsible carcinogenic agent was an RNA virus, the Rous Sarcoma Virus (RSV; Murray and Hunt, 1993). The specific transforming viral sequence of RSV was deduced by comparing the RSV genome, with the genome of the non-transforming Rous-associated virus. The difference between the genomes of these two viruses was discovered to be an extra gene that was isolated and named v-*src* (viral sarcoma). Later it was discovered that the genome of normal cells contains a gene, c-*src*, that is closely related to v-src. This gene encodes a 60 kilodalton phosphoprotein with tyrosine kinase activity called $pp60^{c\text{-}src}$. Subsequently, it has been found that all oncogenes of RNA tumor viruses are, in fact, transduced cellular genes. These viral oncogenes cause transformation because they represent the mutated versions of normal cellular genes, known as proto-oncogenes, which are normally involved in the regulation of important cellular functions such us growth, differentiation, migration, and division (Murray and Hunt, 1993; Alberts *et al.*, 1994).

However, the discovery that cancer would arise from a somatic mutation of a normal cellular proto-oncogene, failed to explain why certain forms of cancer

have an inherited trait, like childhood retinoblastoma, colorectal and breast cancer. Oncogenes act in a dominant fashion, a mutation in only one of the two parental copies of the proto-oncogene is enough to promote their effects. Therefore oncogenes can not be transmitted through the germ line because they perform important functions like differentiation, proliferation, etc., thus perturbing the developmental process (Alberts *et al.*, 1994).

When cancer cells are fused with normal cells, the resultant hybrid assumes a normal phenotype. This suggests that the normal cell is contributing with the genetic information able to suppress malignancy. However these hybrids were found to be unstable. They would randomly lose chromosomes. When the lost chromosome came from the normal parent, the hybrid would revert back to a tumorigenic state. This has been the first evidence that cancer cells often lose growth-regulating information (Weinberg, 1991). These genes were called tumor suppressors or anti-oncogenes because tumorigenicity could be suppressed even in the presence of oncogenes, like *ras*, in the hybrid cells. Obviously, unlike proto-oncogenes, tumor suppressor genes act in a recessive fashion. Both copies have to be altered in order to cancel their growth-controlling effects (Knudson, 1975). Retinoblastoma, is a retinal neoplasm that most of the time appears sporadically, but in some families it follows an autosomal dominant inheritance, affecting children at a very early age. Based on the observation of forty-eight cases, Knudson developed the hypothesis that in those children one mutation was inherited via the germinal cells, while the second mutation occurred in the somatic cells of the child. Knudson also hypothesized that in the non-

hereditary form of this disease, both copies of the gene were mutated in the somatic cells. Indeed, it was found that in the case of the hereditary form of retinoblastoma, the children's karyotype demonstrated a deletion in chromosome 13. The same deletion was found in patients with the non-hereditary form of the disease, supporting the idea that this form of cancer was due to the loss of a gene rather than to the mutation of a proto-oncogene. This tumor suppressor gene was called the retinoblastoma, or *Rb*, gene (Weinberg, 1991).

Many tumor suppressor genes have been discovered and cloned since. A few years after the cloning of *Rb*, a second gene, *p53*, long available in cloned form, was also discovered to be a tumor suppressor gene. *Rb* and *p53* are now known to serve as important check points during cellular division (Livingston *et al.*, 1993; Lane, 1992). *p53* (chromosome 17) was also found to have an important role in the regulation of programmed cell death or apoptosis (Jacks and Weinberg, 1996). Loss of *p53* has been seen in more than 75% of colorectal carcinomas (Fearon and Vogelstein, 1990). Deleted in colon carcinoma (*DCC*) gene (chromosome 18), which is lost in more than 70% of colorectal carcinomas, encodes a protein with significant homology to the cell adhesion family of molecules, suggesting that its mutation might alter the normal cell-cell and/or cell-extracellular matrix interactions. The other important tumor suppressor gene often found mutated in colorectal cancer is *APC* (chromosome 5) which was linked to familial adenomatous polyposis, a hereditary disease in which the patient presents hundreds of polyps, and has a great predisposition for colorectal cancer (Fearon and Vogelstein, 1990).

1.3 The multi-step nature of cancer

From experimental studies, carcinogenesis has historically been divided into three steps: initiation, promotion and tumor progression (Berenblum and Shubik, 1947; Boyd, and Barret, 1990).

a- Initiation:

Tumor initiation occurs as a result of an irreversible genetic damage. This damage is a heritable change, it can be propagated from one cell generation into the next one. However, this alteration by itself is not sufficient to induce malignant transformation, but it does confer the cell with a latent growth advantage over the neighboring ones. Initiation may arise from an inherited or spontaneous mutation or following the exposure to a carcinogen.

b- Promotion:

Promotion is the selective clonal expansion of initiated cells. It is a reversible process and the removal of the promoting agent results in regression. Since the rate of accumulation of mutations is proportional to the rate of cell division, it follows that clonal expansion of the initiated cells would produce cells that are a greater risk of accumulating more mutations.

c- Progression:

Progression is the expression of the malignant phenotype. The additional genetic alterations accumulated during the promotion phase/step, result in increasing genomic instability and malignant transformation. This stage is characterized by the evolution of increasingly aggressive clones exhibiting accelerated growth, invasiveness and metastasis (Boyd and Barret, 1990).

More than half a century ago it was noticed that the incidence of cancer in humans increases very steeply with age (Armitage and Doll, 1954). When the incidence of the most common human cancers is plotted against age, the analysis of the slope suggests that the development of malignant cancer would require around 6 "hits". These hits could represent insults to separate cells, but because now we know that neoplasms are the clonal expansions of a single cell, it is more likely that those hits represent sequential mutations in a single cell and its progeny.

Morphological observations of tumor development are also in accord with the multi-hit hypothesis. In the colon the development from benign polyps to malignant adenocarcinomas has been well established in what is known as the adenoma-carcinoma sequence (Muto *et al.*, 1975). The different morphological types of lesions found in colorectal cancer, have been studied for the presence of different mutations (Fearon and Vogelstein, 1990). It was discovered that the malignant cells within a neoplasm have the same type of mutations found in the benign portion of the lesion, but with the addition of at least one further mutation, absent in the benign cells. This was strong evidence supporting the adenoma-

carcinoma sequence. The addition of mutations onto those already present in the benign adenomas would result in progression to adenocarcinoma. Because colorectal cancer evolves through well-defined morphological stages, it was possible to correlate each stage with the presence of a specific mutation, with the objective of establishing a possible order in which these mutations occur (Figure 1.1). However, after studying thousands of neoplasms, it was concluded that even though the sequence shown in Figure 1.1 is the most likely to occur, the accumulation of mutations is more important than the sequence itself.

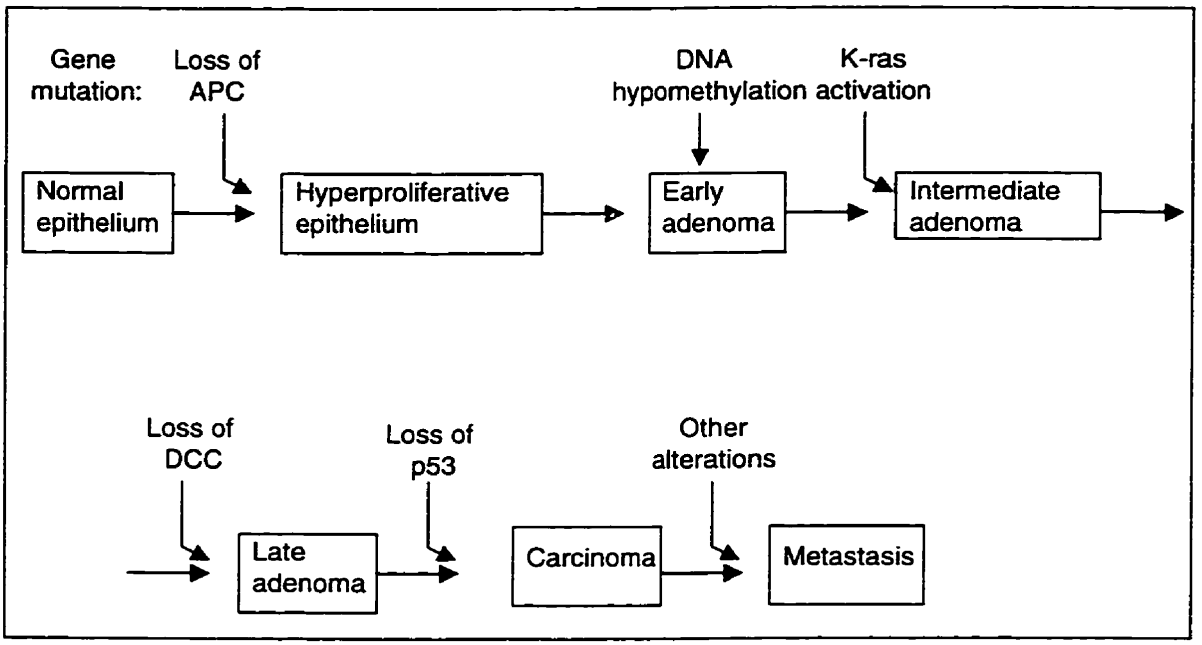

Figure 1.1 Genetic model for colorectal carcinogenesis. Adapted from Fearon and Vogelstein, 1990.

The morphological and epidemiological observations only indirectly support the multi-hit scenario. Better and more direct evidence is provided by gene transfer experiments. Different models have been used to help establish at the molecular level, the concept that carcinogenesis is a multistep process. Transgenic mouse strains carrying individual oncogenes are instructive because with this model it is possible to study the function of these genes in vivo, and, by varying the promoters or enhancers of transcription we can cause the gene of interest to be expressed in specific tissues.

Generally, tissue-specific expression of oncogenes in transgenic mice leads to tumor incidence in the expected tissues with a variable latency and frequency. This could be explained by the necessity for second events before a frank neoplasm is evident (Varmus *et al.*, 1994). If the time in which the carcinomas developed is indeed needed for the appearance of other mutations in proto-oncogenes or anti-oncogenes, by inserting a second oncogene or tumor suppressor gene into the transgenic animal, this lag time should become shorter. With this hypothesis in mind, different crosses were made between different transgenic mice carrying oncogenes and, with the addition of a second oncogene in the genome of the first generation of these double-transgenic mice, the onset of the disease was dramatically reduced (Varmus *et al.*, 1994).

1.4 References

Alberts, B., Bray, D., Lewis, J., Raff, M., Roberts, K. and Watson, J.D. *Molecular biology of the cell*, 3rd. edn. Gerland Publishing Inc., New York, 1994.

Armitage, P. and Doll, R. 1954, The age distribution of cancer and a multi-stage theory of carcinogenesis, Br. J. Cancer, **8**, 1-12 .

Bird, R.P. Observation and quantification of aberrant crypts in the murine colon treated with a colon carcinogen: preliminary findings, Cancer Letts., **37**, 147-151, 1987.

Bird, R.P., Role of aberrant crypt foci in understanding the pathogenesis of colon cancer, Cancer Letts., **93**, 55-71, 1995.

Boyd, J.A., and Barret, J.C. Genetic and cellular basis of multistep carcinogenesis. Pharmac. Ther., **40**, 469-486,1990.

Cotran, R.S., Kumar, V., and Robbins, S.L. *Robbins Pathologic Basis of Disease* W. B. Saunders Company, Philadelphia, 5th ed., 1994.

Fearon, E.R., and Vogelstein, B. A genetic model for colorectal tumorigenesis, Cell, **61**, 759-767, 1990.

Jacks, T., and Weinberg, R.A. 1996 Cell cycle control and its watchman, Nature **381**, 643-644.

Knudson, Jr., A.G. 1975 Mutation and cancer: statistical study of retinoblastoma, Proc. Nat. Acad. Sci. USA, **68**, 820-823.

Lane, D.P. 1992 *p53*, guardian of the genome, Nature 358, 15-16

Livingston, D.M., Kaelin, W., Chittenden, T., and Qin, X., 1993 Structural and functional contributions to the G1 blocking action of the retinoblastoma protein. Br. J. Cancer, **68**, 204-208.

Murray, A., and Hunt, T. *The cell cycle: an introduction*, Oxford University Press, New York, 1993.

Muto, T., Bussey, H.J.R., and Morson, B.C. The evolution of cancer of the colon and rectum, Cancer **36**, 2251-2270, 1975.

Rous, P. A sarcoma of the fowl transmissible by an agent separable from the tumor cells, J. Exp. Med. **13**, 397,1911.

Rous, P., and Kidd, J.G. Conditional neoplasms and subthreshold neoplastic states, J. Exp. Med. **73**, 365-389, 1941.

Varmus, H.E., Godley, L.A., Roy, S., Taylor, I.C.A., Yuschenkoff, L., Shi, Y.-P., Pinkel, D., Gray, J., Pyle, R., Aldaz, C.M., Bradley, A., Medina, D., and Donehower, L.A. Defining the steps in a multistep mouse model for mammary carcinogenesis, Cold Spring Harbour Symp. Quant. Biol., **59**, 491-499, 1994.

Warthin, A.S. Heredity with reference to carcinoma, Arch. Intern. Med. **12**, 546, 1913.

Weinberg, R.A., Tumor supressor genes, Science, **254**, 1138-1146, 1991.

2 Cancer of the colon

2.1 Introduction

Colorectal cancer remains the second leading cause of death due to cancer in North America (Canadian Cancer Statistics, 1997; Landis *et al.*, Cancer statistics 1998). While the etiology of colon cancer is not wholly understood, environmental and genetic factors are clearly involved. The most important environmental factor is probably diet; a high fat, low fiber diet appears to increase the risk of development of colon cancer. Such diets delay the transit time of faecal material through the colon, potentially allowing increased degradation of material by the bacterial flora of the colon to produce mutagenic substances, and increased exposure of the colon mucosa to these mutagens (Cotran *et al*, 1994).

The treatment of this killer disease varies from the simple local removal of a malignant lesion to the removal of sections of the colon, to chemotherapy, and radiotherapy, and often to removal of parts of other organs if the cancer has metastasized. Current screening tests include rectal exam, proctoscopy and colonoscopy. The higher risk population includes individuals over 50 years old, and individuals with a family history of colon cancer or ulcerative colitis (ulcers in the lining of the large intestine).

Diagnosis of Neoplasia of the Colon: The clinical history and physical examination of a patient may give the first indication as to whether or not there is a neoplasm. Some physical indications include weight loss, loss of general well-being, anemia and the presence of blood in urine or feces (Cotran *et al.*, 1994). Further information is given by radiography. At the present time the most accurate way of diagnosing neoplasia is histopatholgy of biopsy samples. The histological diagnosis involves sectioning and staining of a small sample of tissue and the subsequent analysis of the section under the light microscope. However, sampling errors are possible, which are larger the smaller with the pieces of tissue examined. This method is also subjective since it relies upon visual discrimination by a histopathologist.

Diagnostic investigations are followed by an assessment of the stage of the neoplasms. Since the chance of recovery from cancer of the colon (prognosis) depends largely on the stage of the cancer, on whether it is just a cancer *in situ* (a tumor that does not cross the basement membrane of the lining epithelium) or if it has spread to other places, several staging systems have been devised. In general the lower the staging number the less spread the tumor is. One of the most widely used staging systems is the modified Dukes' system (Figure 2.1). Dukes' is a classification for staging colorectal cancer based on the extent of the local spread of the tumor (Dukes' A through C) and in the presence of distant metastasis (Dukes' D). Patients with Dukes' A lesions have a 70-100% chance for 5 years survival following surgical resection. Patients with Dukes' B1 have

65%, 43% for B2 and 15% for C2. Hence the importance of early diagnosis is evident (Cotran, *et al.*, 1994).

Correct diagnosis is very important since treatment of neoplasms is often distressing, life threatening and, sometimes, carcinogenic.

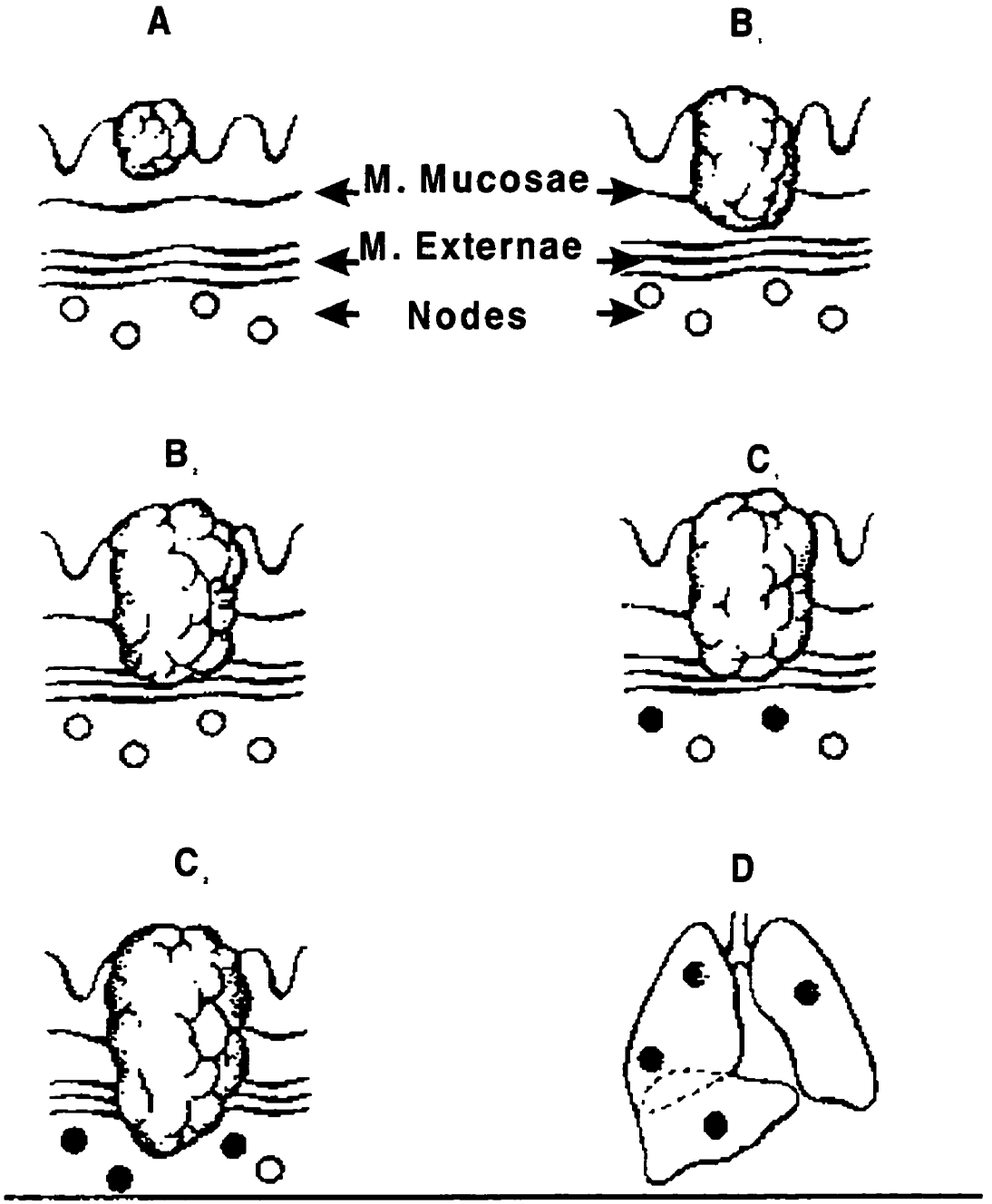

Figure 2.1. Modification of Dukes' classification for pathologic staging of colorectal cancer. This scheme of staging is based on the extent of local spread of the tumor (stages A though C) and the presence of metastasis (stage D). Adapted from Cotran *et al.*, 1994).

2.2 The anatomy and histology of the normal rat colon

The colon is the largest segment of the large intestine. The large intestine extends from the end of the small intestine (ileum) to the anus thus it constitutes the end of the digestive tract. The large intestine has a greater caliber than the small intestine. The caliber of the colon is larger at its beginning (caecum) and it gradually diminishes towards the rectum. Anatomically the large intestine is divided into the caecum, which is the commencement, the colon, and the rectum, ending at the anal canal. The colon is divided into four parts: the ascending, transverse, descending and sigmoid. The colon is about 1.3 meters long in the human (Gray's Anatomy, 1995) and 15 cm. in the rat (Baker *et al.*, 1979)

Histologically, rat and human colons are quite similar (Shamsuddin, 1990). The wall of this organ consists of 4 principal layers of tissues, as depicted in Figure 2.2. The serosa, a thin layer of connective tissue, forms the outer most layer of the colon. The muscularis externa contains smooth muscle cells organized into an internal (closer to the lumen) circular layer and an external longitudinal layer. The submucosa is composed of loose connective tissue containing blood and lymph vessels, nerve fibers, adipocytes, and lymphoid tissue. Lining the lumen of the colon is the mucosa, composed of epithelial cells, a lamina propria rich in lymphocytes, blood and lymph vessels, and a thin layer of smooth muscle known as the muscularis mucosae.

The cells lining the healthy colon are arranged to form deep pits or crypts known as glands of Lieberkün. The lining epithelium consists mainly of goblet

The cells lining the healthy colon are arranged to form deep pits or crypts known as glands of Lieberkün. The lining epithelium consists mainly of goblet

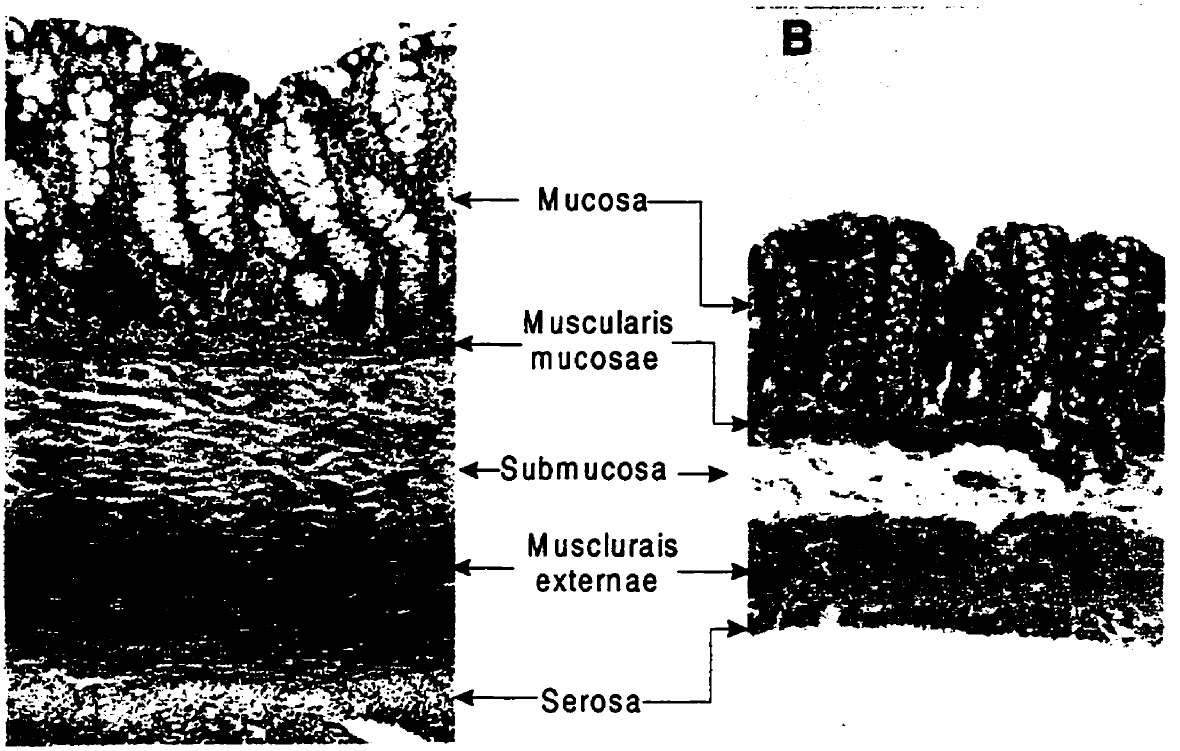

Figure 2.2 Cross section of the colon with its various layers.A, human, magnification: x 30 (adapted from Junqueira *et al.*, 1989). B, rat, magnification: x 40. H&E stain.

cells, absorptive cells, and a small number of enteroendocrine cells. Goblet cells produce acid glycoprotein for the protection and lubrication of the intestinal epithelium. The absorptive cells are tall columnar cells with abundant microvilli on their apex, which considerably increase the surface area of the cells needed for absorption.

the absorption of water and the formation of the fecal mass (Junqueira *et al.*, 1989).

2.3 Cell Proliferation in the healthy rat colon

In the gastrointestinal tract the proliferative process is divided into compartments. At the bottom of the intestinal glands are located the stem cells that give rise to the whole population of cells composing the intestinal epithelium. This zone is known as the stem cell compartment. The cells multiply in the proliferation compartment and migrate via a transitional zone to the surface of the mucosa where they are extruded. In the transitional zone the cells start developing their final mature characteristics. Once they become mature they form the maturation compartment. The distinction among the different zones was made possible by studying the distribution of mitotic figures, and tritiated-thymidine (^{3}HTdR), and bromodeoxyuridine (BUdR)-labelled cells. Perfect longitudinal sections of crypts of the rat descending colon sampled one hour after injection of ^{3}HTdR, which demonstrates cells undergoing DNA synthesis, reveal three regions. At the bottom the crypts have low proliferative indices due to the presence of the stem cells with long cell cycle times. Right above that, is where the labeling indices are the highest and, where the proliferative compartment is found. At the top of the crypts the proliferation indices decline again as the cells leave the cell cycle and are found in the maturation

compartment. The distribution of the ^{3}HTdR labeled cells and mitotic figures indicate that the proliferative compartment is located in the lower half of the crypts in the colon of the rat. The upper half houses the maturation zone while the transitional zone is located between relative crypt cell position 0.4-0.6 (Sunter *et al.*, 1979; Rijke *et al.*, 1979). Regional differences in the size of the proliferative compartment and in the number of labeled cells along the colon have been found (Sunter *et al.*, 1979). In the ascending colon the ^{3}HTdR-labeled cells are indeed located only in the lower half of the crypt, thus confirming the results obtained by others (Rijke *et al.*, 1979). The peak labeling index of 20% was found right next to the bottom of the crypt where a slight depression of this index is found. The depression in the labeling index becomes more obvious in the transverse and ascending colon where the peak labeling of 20% is found near the middle point of the crypt. In the caecum the peak-labeling index, which rises above 30%, is also found next to the crypt bottom (Sunter, *et a.l*, 1979).

There are some discrepancies with respect to the number of cells found in one colonic crypt. In those studies the number of cells per crypt was calculated by multiplying the means of the number of cells in longitudinally sectioned crypts times the number of cells in transversely sectioned crypts, assuming crypts to be perfect regular cylinders with hemispherical bases. Tutton and Barkla working with male Sprague Dawley (S.D.) rats observed a value of 39.5 cells in the crypt circumference and 38.2 cells in length. Their estimation of the crypt cell population was in the order of 1300 cells (Tutton and Barkla, 1976). Rijke *et al.*

observed the crypts to be 32.8 cells in length and 18.9 across, and estimated around 625 cells/crypt (Rijke *et al.*, 1979), while Sunter *et al.* found a crypt cell population of 735 cells, with 42 cells in length and 17.6 across (Sunter *et al.*, 1979). Later, by obtaining complete serial sections across the crypts, McLellan *et al.* found in female S.D. rats that each crypt consisted of 411 cells. (McLellan *et al.*, 1991). The difference in the number of cells per crypt found by the different investigators could be due to several reasons including the strain of the rats, their age, gender, which region of the colon they examined, and the methodology employed in those studies.

2.4 The adenoma-carcinoma sequence

Cancer of the colon is the best studied form of cancer from the morphological and genetic point of view. In the colon, macroscopic and microscopic examination of tumors will reveal that most of them contain contiguous benign and malignant tissues (Muto *et al.*, 1975). This was concluded to be evidence that the adenocarcinoma arose from a previously benign tumor or adenoma. This development from adenomas into adenocarcinoma is referred to as the adenoma-carcinoma sequence.

Small (under 1 cm) adenomatous polyps and villous adenomas are the first recognized manifestations of neoplasia in colorectal epithelium. The adenomatous polyp consists of branching tubules embedded in the lamina

propria that take a pedunculated form. The villous adenoma is composed of finger-like projections of lamina propria covered by epithelium and it often reaches the muscularis mucosa. This type of adenoma is often sessile rather than pedunculated, and they spread through a large surface area. Also, a mixture between adenomatous polyps and villous adenomas can be found. The potential for malignancy depends on the type of adenoma and the size of the lesion. Adenomatous polyps are by far more common than villous adenomas and they also have less malignant potential than the villous adenomas (Muto *et al.*, 1975).

2.5 Cell proliferation in adenomas and carcinomas of the colon

Recalling from the previous section about cell proliferation in the normal colonic mucosa, the proliferative zone is located in the lower portions of the colonic crypts. In human neoplastic tissue the proliferative zone is moved into the upper third of the crypts and the free surface of the colonic mucosa (Deschner *et al.*, 1966). This pattern of cell proliferation was also noticed in the epithelium adjacent to the neoplasms, where there was no microscopic indication of malignancy. This transfer of the proliferative zone to the upper third of the colonic crypt was considered to be one of the first abnormalities towards the development of malignant tissue (Deschner *et al.*, 1966). Similar results were found in colonic tissue of rodents heavily-treated with the carcinogen

dimethylhydrazine (Lipkin, 1974). In this first stage of the development of colon cancer the rate of cytokinesis of cells is still equal to the rate of extrusion, so that there is not an overall accumulation of cells in the colonic crypts. At some point the crypts fail to extrude cells and the rate of cytokinesis becomes larger than the rate of extrusion. This results in a net retention of cells, a phenomenon commonly known as *"hyperplasia"*. One possible sequence of events towards the development of neoplasms is illustrated in Figure 2.3. The larger dark ovals represent thymidine-labelling in DNA-synthesizing cells. In the normal crypt the proliferating cells are found in the lower sections of the crypt (A). In the first phase the proliferative zone moves upwards as the cells fail to inhibit the incorporation of thymidine ^{3}H into their DNA, but the number of cells per crypt still normal (B). In the following stage, the proliferating cells are retained and accumulated in the mucosa (C). Finally, as the cells continue accumulating abnormalities, i.e. mutations, they start to protrude into the colonic lumen in the form of defined neoplastic lesions such as adenomatous polyps and villous papillomas (Lipkin, 1974).

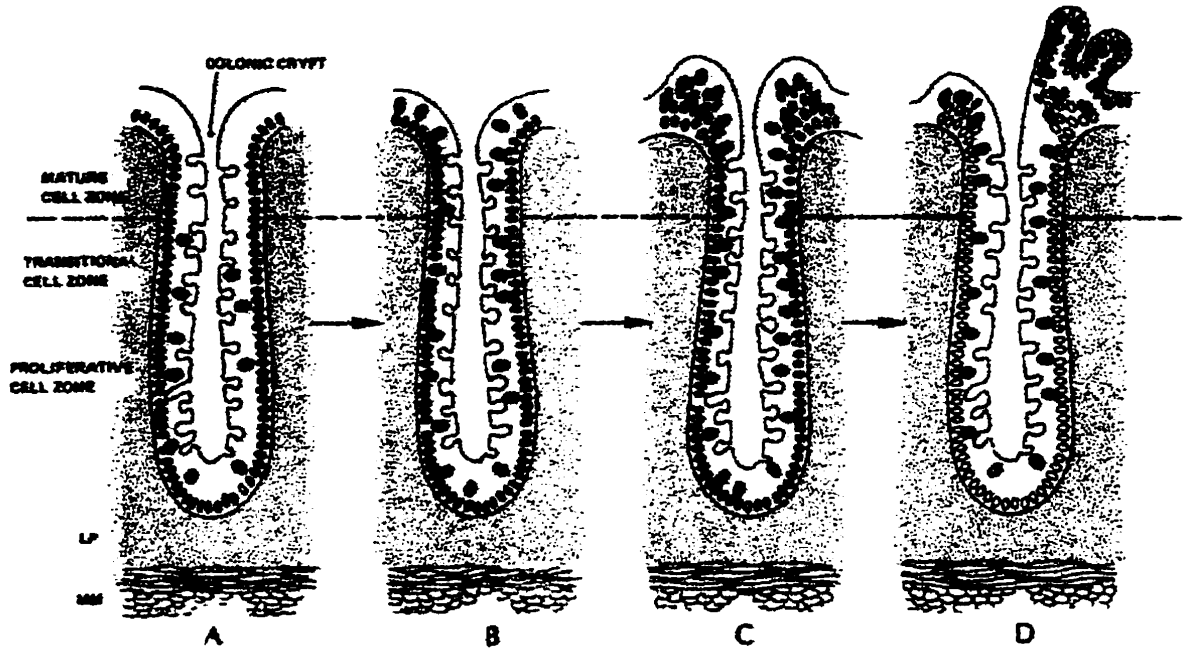

Figure 2.3. Possible sequence of events for the formation of polypoid neoplasms in man and rodent. Dark cells represent thymidine labeled cells that are undergoing DNA synthesis to prepare for cell division. (A) shows the location of proliferating and differentiating cells in a normal colonic crypt. As cells pass from the proliferative zone to the transitional zone, DNA synthesis and mitosis are repressed. The cells leave the proliferative cycle and undergo maturation before they reach the surface of the mucosa. (B) demonstrates how cells fail to repress DNA synthesis and enhance their ability to proliferate. In this early proliferative lesion, the number of cells born equals the number of cells extruded. (C) shows a more advance stage of the prolifeartive lesion. Now the cells developed new properties that allow them to accumulate in the mucosal surface. (D) shows further differentiation of the abnormally retained proliferating cells into a neoplastic lesion. Adapted from Lipkin, 1974.

2.6 References

Baker, H.B., Lindsey, J.R., and Weisbroth, S.H., eds. *The laboratory rat*, Volume I Biology and disease, Academic Press, New York, 1979.

Cotran, R.S., Kumar, V., and Robbins, S.L. *Robbins Pathologic Basis of Disease,* W. B. Saunders Company, Philadelphia, 5th ed., p. 815, 1994.

Deschner, E.E., Lipkin, M., and Solomon, C. Study of human rectal epithlial cells *in vitro*. II. H^3-Thymidine incorporation into polyps and adajecent mucosa, J. Natl. Cancer Inst., **36**, 849-857, 1966.

Gray's Anatomy: the anatomical basis of medicine and surgery, Churchill Livingstone, New York, 1995.

Junqueira, L.C., Carneiro, J., and Kelley, R.O. *Basic Histology,* Appleton & Lange, CA, 6^{th} ed.,1989.

Landis, S.H., Murray, T., Boldenand, S., and Wingo, P.A., Cancer statistics 1998, CA Cancer J. Clin. **48**, 6-29, 1998.

Lipkin, M., Phase 1 and phase 2 proliferative lesions of colonic epithelial cells in diseases leading to colon cancer, Cancer, **34**, 878-888, 1974.

McLellan, E.A., Medline, A., and Bird, R.P. Dose response and proliferative characteristics of aberrant crypt foci: putative preneoplastic lesions in rat colon, Carcinogenesis, **12**, 2093-2098, 1991.

Muto, T., Bussey, H.J.R., and Morson, B.C. The evolution of cancer of the colon and rectum, Cancer, **36**, 2251-2270, 1975.

National Cancer Institute of Canada: Canadian Cancer Statistics 1997, Toronto, Canada, 1997.

Rijke, R.P.C., Plaisier, H.M., and Langendoen, N.J. Epithelial cell kinetics in the descending colon of the rat, Virchows Arch., **30**, 85-94, 1979.

Shamsuddin, A.M., Normal and pathological anatomy of the large intestine. In *Colon Cancer Cells*, M.P. Moyer and G.H. Poste, eds. Academic Press, New York, ch. 2, 1990.

Sunter, J.P., Watson, A.J., Wright, N.A., and Appleton, D.R. Cell proliferation at different sites along the length of the rat colon, Virchows Arch. **32**, 75-87, 1979.

Tutton, P.J.M., and Barkla, D.H. Cell proliferation in the descending colon of dimethylhydrazine treated rats and in dimethylhydrazine induced adenocarcinoma, Virchows. Arch. B Cell Path. **21**, 147-160, 1976.

3 Aberrant Crypt Foci: Preneoplastic Lesions of the colon

3.1 Introduction

As it was previously established, cancer is a multi-step process that requires a lifetime to develop in humans (Armitage and Doll, 1954). In animals, even after a long treatment with a carcinogen, carcinomas rarely develop before a long span of time and usually intermediate lesions precede them (Rous and Kidd, 1941).

According to the adenoma-carcinoma sequence, malignant carcinomas arise from benign adenomas, which in turn arise from even smaller and less traumatic lesions. In line with this idea it would be reasonable to find the first neoplastic lesion which begins the sequence of events. Indeed, dysplastic crypts were recognized as early neoplastic lesions both in humans and animals (Chang, 1984; Jass *et al.* 1984). However, there was still missing a methodology to quantify the altered crypts and to study them more closely. It was not until three years later that a simple method was developed for the characterization of the dysplastic crypts. The method consisted of removing the colons of rodents previously treated with a specific colon carcinogen such as azoxymethane (AOM) or 1,2-dimethylhydrazine (DMH), cutting them open along the longitudinal medial axis, and fixing them flat between two pieces of filter paper in 10%

formalin. After a minimum of 24 hours the unsectioned colons were stained with 0.2% methylene blue in buffered saline or buffered formalin for 5-15 minutes. The colons were then placed mucosal side up on top of a microscopic slide for their topological observation under a light microscope (Bird, 1987). With this methodology, focal lesions were revealed in the colons of mice, consisting of one to several clusters of large crypts, slightly more elevated than the adjacent mucosa, more darkly stained, and with atypical features in the size of their lumen and nuclei. These altered crypts, named aberrant crypt foci or ACF, were found to have an elliptical shape and a slit-like lumen rather than the circular shape found in normal crypts (Bird, 1987). Some foci exhibit severe dysplastic changes while others show only mild atypia (Bird *et al.*, 1989). The fact that some ACF exhibit dysplasia, a feature that was related to the development of colon cancer (Konishi *et al.*, 1982), is strong evidence that ACF are indeed putative preneoplastic lesions.

ACF were also noticed, using the above-mentioned methodology, in the human colon (Roncucci *et al.*, 1991; Pretlow *et al.*, 1991). According to Roncucci and co-authors, ACF show variable features ranging from almost normal to marked dysplasia, even within the same colon. They also found that the degree of dysplasia was more marked in patients with familial polyposis, a hereditary autosomal dominant disease in which the wall of the colon becomes literally covered with polyps, than in patients with colorectal carcinoma (Roncucci *et al.*, 1991). More recently, a thorough histological study of human ACF was carried out (Di Gregorio *et al.*, 1997). In that study a large number of ACF were

collected from 24 surgical resections from 24 patients with colorectal cancer. ACF were easily detected from the normal crypts in colons stained with methylene blue, because of their larger size and irregular luminal shapes. Crypt multiplicity (number of crypts per focus) was found to range from 2 to 150 crypts per ACF. Taking into account nuclear features such as size, shape, number of mitoses, and polarity, the authors divided the ACF into three groups. In the first group (group A) the only difference between normal and aberrant crypts was the size of the nucleus. Most of the ACF investigated fell in this category (70%) and were considered the "typical" ACF. The intermediate group (20%; group B) had features similar to those found in hyperplastic polyps: enlarged and crowded (overlapped) nuclei, with less than three mitotic figures and mucin depletion, but they did not present dysplasia and stratification (nuclei did not lean against the cellular base). In the third group (10%; group C) the nuclei were large, crowded and stratified, with loss of polarity, more than three mitotic figures, presence of mucin depletion and mild dysplasia. Mucin depletion was present in ACF of the intermediate and dysplastic groups. A decrease in sulfomucin production and an increase in sialomucin production in the goblet cells of the colon, was correlated with neoplastic transformation (Filipe, 1975; Griffioen *et al.*, 1989). Group A was found to have a median number of 28 crypts per focus (7-150). The median of 45 (28-150) for group B was found to be significantly higher than both groups A and C which had a median of 21(10-34).

3.2 Are ACF preneoplastic lesions?

If ACF truly represent putative preneoplastic lesions of the colon, they could be used as the end points in the study of the effects of diets, chemical treatments, and environmental factors on the carcinogenic process. They could also serve to shed light on the understanding of the first steps of carcinogenesis itself, for instance by revealing which are the first oncogenes or tumor supressor genes that start the series of events leading to the formation of a tumor.

The first line of evidence comes from the histological appearance of ACF. As mentioned before, ACF exhibit dysplasia, a feature that precedes the development of colon cancer (Konishi *et al*, 1982). The degree of dysplasia found in ACF was correlated to crypt multiplicity, i.e. the higher the number of aberrant crypts per focus, the higher the degree of dysplasia (Thorup, 1997), and to the progression time of the disease (McLellan *et al.*, 1991a). Di Gregorio and co-workers found that the larger ACF had a higher probability of being hyperplastic, but they could not correlate the histology of the two more advanced B and C groups of ACF with crypt size (Di Gregorio *et al.*, 1997). They did however notice an anatomical distribution of ACF from group B similar to that of hyperplastic polyps while the more dysplastic crypts of group C had an anatomical distribution similar to that of adenomatous polyps. Their conclusion was that ACF from group A could evolve into either ACF of group B or C, with group B ACF being the precursors of hyperplastic polyps, and group C ACF

being the precursors of adenomatous polyps raising the possibility that more than one population of ACF exists.

The formation of ACF after a single dose of AOM requires a minimum of 8 days in the more sensitive strains of mice (McLellan *et al.*, 1988), and 2 weeks in SD rats (McLellan *et al.*, 1991b). The latter study also showed that the total number of lesions per colon increased with time from 13 at the second week to a high of 160 at the forty-first week post AOM treatment. It could be concluded that (1) not all ACF develop at the same time, and (2) a heterogeneous population of aberrant crypts exist.

The number of ACF per colon was shown to increase with an increasing dosage of carcinogen, linking the formation of ACF to the exposure to a carcinogen (Bird *et al.*, 1989). Feeding rodents with a dimethyl hydrazine (DMH) and AOM inhibitor prior to their exposure to these chemical carcinogens resulted in a significantly lower number of ACF (McLellan and Bird, 1991). Colon cancer promoters such as diets rich in fat content have been shown to enhance the growth of ACF (McLellan and Bird, 1988).

In the rodent models, most of the ACF were found in the distal portion of the colon (McLellan and Bird, 1988; Pretlow *et al.,* 1990), a site where also most of the tumors are also found (Wiebecke, 1973). A possible explanation for this difference in ACF and tumor location could be that cell proliferation in the distal portion of the colon is slower than in the proximal portion of it (Sunter *et al.*, 1979). Therefore, cells in the distal portion of the colon are exposed for longer

times to carcinogens that might be present in the large intestine, than cells in the ascending portion of the colon.

Carter *et al.* (1994) reported a correlation between the distribution of intestine-associated lymphoid tissue and tumors and a lack of significant colocalisation between ACF and tumors. Based on those findings it was concluded that lymphoid nodules have a carcinogenic promotional role and ACF have little, if any, malignant potential in their mouse model. In that study the mice were repeatedly treated with DMH and the animals were all sacrificed at the same time (24 weeks) after they received their final DMH treatment. In doing so, the researchers studied only one "window" of time, several monthss after the 8 days in which ACF in mice have first been reported to appear (McLellan *et al*, 1988). This creates the speculation that after 24 weeks, many of the ACF developed into the tumors seen by the authors, which would support the preneoplastic nature of ACF. Other investigators have demonstrated an extensive infiltration of lymphocytes in the majority of human colon carcinomas and that such infiltration was associated with improved survival rather than carcinogenic promotional role (Di Georgio, 1992). The mice utilized by Carter *et al.* (1994) were exposed to repeated treatments of DMH. This methodology is not commonly employed. Multiple AOM exposure results in a lag period before the ACF start to grow between weeks 14-28 in SD rats exposed to 4 AOM injections (Bird, 1995). At the later time points, ACF growth occurs mainly in the proximal segment of the colon. In contrast, in rats exposed to single AOM injections, ACF growth is more rapid and their distribution is mainly located in the distal portion of the colon.

3.3 Cell proliferation in ACF

In SD rats, 19 weeks after being treated with a single injection of the carcinogen DMH, ACF were found to contain from 1.2 to 5.3 times more cells than in the normal neighboring crypts. The ^{3}HTdR labeling index also revealed a higher mean value in the aberrant crypts than in the normal crypts (McLellan *et al.* 1991b). A similar result was also found in F344 rats where ACF and colon tumors were also found to have a similar increase in their proliferative rate (Pretlow *et al.*, 1994). In this work the rats were treated with a single injection of AOM and the ACF were studied at different time periods after the carcinogen treatment. In each time period the ACF not only showed an increase in the numbers of cells per crypt with respect to the normal crypts, but also the cells in the aberrant crypts incorporated more bromodeoxyuridine (BUdR), as detected by immunohistochemistry, than their normal counterparts. In humans, cell proliferation in ACF was also found to be higher than in normal colonic crypts. Both the number of cells per crypt and the BUdR labeling index (percentage ratio of BUdR-labeled cells/ total cells in the crypt) were significantly higher in aberrant crypts than in normal crypts (Roncucci *et al.*, 1993). The nuclei in the aberrant crypts were shown to contain a higher number of nucleolar organizer regions than the nuclei of the normal crypts, but less than those of adenomas and adenocarcinomas (Bird, 1995). The nucleolar organizer regions indicate an

increase in the cellular activity due to an increase in protein synthesis, and that was found to be associated with neoplastic changes.

3.4 The molecular biology of ACF

Another road that can be taken towards the investigation of the putative preneoplastic nature of ACF, would be to look for the presence of known molecular markers that characterizes cancer of the colon.

As it was previously mentioned, the type of mucus production is indicative of colon cancer development (Filipe, 1975; Griffioen *et al.*, 1989). Goblet cells normally produce sulfomucin but they produce more sialomucin during malignant transformation of the colon. Thorup (1997) found an association between the decrease in sulfomucin production with crypt multiplicity and degree of dysplasia.

Enzyme histochemical studies have demonstrated an altered hexosaminidase activity in human colonic carcinomas (Brattain *et al.*, 1977); and in rodents, aberrant crypts have decreased hexosaminidase activity with respect to the normal crypts (Pretlow *et al.*, 1990).

The expression of different growth factors, cytokines, and phosphorylated cellular tyrosine (P-tyr), all previously associated with malignant transformation, has been studied in ACF. The transforming growth factor α (TGF-α) is a cytokine frequently detected in carcinomas expressing large amounts of the epidermal growth factor receptor (DiMarco *et al.*, 1989). However, positive TGF-

α immunostaining was only found in normal crypts but not in ACF, regardless of the crypt multiplicity and degree of dysplasia (Thorup, 1997; Bird, 1995). P-tyr immunoexpression was described both in ACF and normal crypts by Thorup (1997); however, Bird found a decrease in the expression of P-tyr in ACF. These findings demonstrate the heterogeneity of the ACF population. Another line of evidence supporting the preneoplastic nature of ACF comes from the study of the genetic make-up of these lesions. Because colon carcinogenesis evolves through a series of well-defined morphological steps, it was possible to establish a genetic model for this disease (Fearon, and Vogelstein, 1990). According to this model, one of the first chromosomal alterations to occur involves the k-*ras* proto-oncogene. Unfortunately, Fearon and Vogelstein did not study the genetic alterations in ACF. Working with SD rats, Stopera and Bird found significant expression of *ras* oncogene in ACF both at the mRNA (*in situ* hybridization) and protein (immunohistochemistry) levels with respect to the normal crypts (Stopera and Bird, 1992). Later, Smith *et al.* (1994) found, at the DNA level, the *ras* oncogene in 13% of the ACF taken from colonectomy specimens, and the *APC* tumor suppressor gene in 4.6% of the ACF. They also found the *ras* oncogene in only 1% of the normal mucosa samples, and in 45% of tumors evaluated. However, there was no mention of the percentage of *APC* found in normal crypts, and the only three ACF found to bear the *APC* mutation came from the same patient. Dolara *et al.* (1997) have found ACF in patients with a low risk of colon cancer. They argue that since *ras* mutations have been reported in human and experimental ACF with a low frequency, and, because *ras* mutations are

detected at earlier stages of colon carcinogenesis, there is a problematic correlation between ACF and carcinogenesis. Although genetic alterations occur according to a preferred sequence, it is the accumulation of mutations what determines the tumor biologic properties. Hence, although *ras* mutations are not found, that absence does not mean that other genetic alterations, i.e. *APC*, DNA hypomethylation, etc., are not present. In fact, some adenocarcinomas have been shown to express only the wild type form of the *ras* proto-oncogene.

In a more recent publication the nature of the genetic alterations of the *ras* oncogene demonstrated a better-than-average agreement between the *ras* mutations found in the ACF and the ones found in the adenocarcinomas of the same patient (Shivapurkar *et al.*, 1997). This result supports the idea that the adenocarcinomas have evolved from the clonal expansion of the ACF. The analysis showed the presence of *ras* in 23% of the ACF and 30% of the adenomas and adenocarcinomas. They also found mutations to the tumor suppressor *p53* in only one out of 23 ACF and in 10 tumors out of 13 patients with colorectal carcinoma. This finding confirms the idea that mutations to *ras* may represent one of the earliest events in colon carcinogenesis, while *p53* represents one of the last ones (Fearon and Vogelstein, 1990). However, the fact that a few adenomas and adenocarcinomas express only the wild type form of *ras* supports the belief that it is the accumulation of mutations that is the important phenomenon, and that mutations to the *ras* proto-oncogene are the most likely, but not necessarily the single first event in colorectal carcinogenesis.

In summary, the evidence described above supports the hypothesis that ACF represent preneoplastic lesions of the colon. ACF were shown to exhibit the genotypic and phenotypic characteristics commonly found in neoplastic tissues.

3.5 References

Armitage, P. and Doll, R. The age distribution of cancer and a multi-stage theory of carcinogenesis, Br. J. Cancer, **8**, 1-12, 1954.

Bird, R.P. Observation and quantification of aberrant crypts in the murine colon treated with a colon carcinogen: preliminary findings, Cancer Letts., **37**, 147-151, 1987.

Bird, R.P., McLellan, E.A., and Bruce, RW.R. Aberrant crypts, putative precancerous lesions, in the study of the role of diet in the aetiology of colon cancer, Cancer Surveys, **8**, 189-200, 1989.

Bird, R.P., Role of aberrant crypt foci in understanding the pathogenesis of colon cancer, Cancer Letts., **95**, 55-71, 1995.

Brattain, M.G., Kimball, P.M., and Pretlow, T.G. Ǝ-hexosaminidase isoenzyme in human colonic carcinoma, Cancer Res., **37**, 731-735, 1977.

Carter, J.W., Lancaster, H.K., Hardman, W. E., and Cameron, I.L. Distribution of intestine-associated lymphoid tissue, aberrant crypt foci, and tumors in the large bowel of 1,2-dimethylhydrazine-treated mice, Cancer Res., **54**, 4304-4307, 1994.

Chang, W.W.L. Histogenesis of colon cancer in experimental animals. Scand. J. Gastroenterol. **19**, 27-43, 1984.

Di Giorgio, A., Botti, C., Tocchi, A., Mingazzini, P., and Flammia, M. The influence of tumor lymphocytic infiltration on long term survival of surgically treated colorectal cancer patients, Int. Surg., **77**, 256-260, 1992.

Di Gregorio, C., Losi, L., Fante, R., Modica, S. Ghidoni, M., Pedroni, M., Tamassia, M.G., Gafa, L., Ponz de Leon, M., and Roncucci, L Histology of aberrant crypt foci in the human colon. Histopathology, **30**, 328-334, 1997.

Di Marco, E., Pierce, J.H., Fleming, T.P., Kraus, M.H., Molloy, C.J., Aaronson, S.A., and Di Fiore, P.P. Autocrine interaction between TGF alpha and the EGF-receptor: quantitative requirements for induction of the malignant phenotype. Oncogene, **4**, 831, 1989.

Dolara, P., Caderni, G., Lancioni, L., Giannini, A., Anastasi, A., Fazi, M., and Castiglione, G. Aberrant crypt foci in human colon carcinogenesis, Cancer Detection and Prevention, **21**, 135-140, 1997.

Fearon, E.R., and Vogelstein, B. A genetic model for colorectal tumorigenesis, Cell, **61**, 757-767, 1990.

Filipe, M.I. Mucous secretion in rat colonic mucosa during carcinogenesis induced by dimethylhydrazine. A morphological and histochemical study, Br. J. of Cancer, **32**, 60-77, 1975.

Griffioen, G., Bosman, F.T., Verspaget, H.W, de-Bruin, P.A., Biemond, I., and Lamers, C.B. Mucin profiles and potential for malignancy of human colorectal adenomatous polyps, Cancer, **63**, 1587-1591, 1989.

Jass, J.R. Strudley, I., and Faludy, J. Histochemistry of epithelial metaplasia and dysplasia in human stomach and colorectum Scand. J. Gastroenterol., **19**, 109-130, 1984.

Konishi, F. and Morson, B.C. Pathology of colorectal carcinomas:a colonoscopy survey, J. Clin. Pathol., 35, 820-841, 1982.

McLellan, E. A., and Bird, R.P., Aberrant crypt foci: potential preneoplastic lesions in the murine colon, Cancer Res., **48**, 6187-6192,1988.

McLellan E.A., Medline, A., and Bird, R.P. Sequential analyses of the growth and morphological characteristics of aberrant crypt foci: putative preneoplastic lesions, Cancer Res., **51**, 5270-5274. 1991a.

McLellan E.A., Medline, A., and Bird, R.P. Dose response and proliferative characteristics of aberrant crypt foci: putative preneoplastic lesions in rat colon, Carcinogenesis, **12**, 2093-2098, 1991b.

McLellan, E.A., and Bird, R.P. Effect of disulfiram on 1,2-dimethylhydrazine- and azoxymethane- induced aberrant crypt foci, Carcinogenesis, **12**, 969-972, 1991.

Pretlow, T.P., O'Riordan, M.A., Kolman, M.F., Jurcisek, J.A. Colonic aberrant crypts in azoxymethane-treated F344 rats have decreased hexosaminidase activity, Am. J. Pathol., **136**, 13-16,1990.

Pretlow, T.P., Barrow, B.J., Ashton, W.S., O'Riordan, M.A., Pretlow, T.G., Jurcisek, J.A., ans Stellato, T.A. Aberrant Crypts: putative preneoplastic foci in human colonic mucosa, Cancer Res., **51**, 1564-1567, 1991.

Pretlow, T.P., Cheyer, C., and O'Riordan, M.A. Aberrant crypt foci and colon tumors in F344 rats have similar increases in proliferative activity. Int. J. Cancer, **56**, 599-602, 1994.

Rous, P. and Kidd, J.G. Conditional neoplasm and subthreshold neoplastic states. J Exp. Med., **73**, 365-389, 1941.

Roncucci, L., Stamp, D., Medline, A., Cullen, J.B., and Bruce, W.R., Identification and quantification of aberrant crypt foci and microadenomas in the human colon, Human Pathology, **22**, 287-294, 1991.

Roncucci, L., Pedroni, M., Fante, R., DiGregorio, C., and Ponz de Leon, M. Cell kinetic evaluation of human colonic aberrant crypts. Cancer Res., **53**, 3726-3729, 1993.

Shivapurkar, N., Huang, L., Ruggeri, B., Swalsky, P.A., Bakker, A., Finkelstein, S., Frost, A., and Silverberg, S. K-ras and p-53 mutations in aberrant crypt foci and colonic tumors from colon patients, Cancer Letts., **115**, 39-46, 1997.

Smith, A.J., Stern, H.S., Penner, M., Hay, K., Mitrri, A., Bapat, B.V., and Gallinger, S. Somatic *APC* and K-ras codon 12 mutations in aberrant crypt foci from human colons, Cancer Res., **54**, 5527-5530, 1994.

Sunter, J.P., Watson, A.J., Wright, N.A., and Appleton, D.R. Cell proliferation at different sites along the length of the rat colon, Virchows Arch. B.Cell Pathol., **32**, 75-87, 1979.

Stopera, S.A., and Bird, R.P. Expression of ras oncogene mRNA and protein in aberrant crypt foci, Carcinogenesis, **13**, 1863-1868, 1992.

Thorup, I. Histomorphological and immunohistochemical characterization of colonic aberrant crypt foci in rats: relationship to growth factor expression, Carcinogenesis, **18**, 465-472, 1997.

Wiebecke, B., Krey, U., Lohrs, U., and Eder, M. Morphological and autoradiographical investigations on experimental carcinogenesis and polyp development in the intestinal tract of rats and mice. Virchows Arch. Abtr. A. Pathol. Anat., **306**, 179-193, 1973.

4 Hypothesis and objectives

This thesis is based on three hypotheses:

1. Cancer of the colon is a multi-step process.
2. ACF represent an early event in the genesis of cancer of the colon.
3. Biochemical changes precede morphological changes associated with colon cancer, and ^{1}H MRS and FT-IR spectroscopy can detect them.

The objectives of this work will be:

1. To explore the use of ^{1}H MRS and FT-IR spectroscopy in characterizing ACF of the rat colon.
2. To see if ^{1}H MRS and FT-IR spectroscopy can determine the preneoplastic nature of ACF.

5 ^{1}H Magnetic Resonance Spectroscopy

5.1 Basics of nuclear magnetic resonance spectroscopy

There are several advantages that make nuclear magnetic resonance (NMR) spectroscopy a valuable tool in the study of biological systems. One of the most attractive characteristics of this spectroscopic technique is its non-destructive nature, thus keeping the structural integrity of tissues intact. NMR spectroscopy allows the continuous monitoring of a single system thus providing a direct link between physiological processes and tissue biochemistry. It also allows the detection of unknown compounds in a tissue of interest since all tissue constituents are observed simultaneously. In addition NMR can also be used as a quantitative method of analysis to compare the concentration of specific metabolites in different biological systems. This section will include a brief description of the theory behind NMR, followed by the application of proton magnetic resonance spectroscopy (^{1}H MRS) in the study of cancer of the colon. Since ^{1}H MRS will exclusively be used in this work, emphasis will be placed on this nucleus.

5.1.1 The magnetic properties of the nuclei

All nuclei possess charge and mass. Many nuclei also possess angular momentum or spin. The angular momentum is a fundamental requirement for the NMR phenomenon to be observed. The angular momentum determines the number of states a nucleus may assume. In the absence of an external magnetic field, these states have the same energy. In the presence of an external static magnetic field B_0 the possible orientations represent slightly different energy levels. A nucleus may assume $m = 2I + 1$ spin states orientations with respect to B_0, where m is the magnetic quantum number, a discrete spin variable that could take values between I, (I-1), (I-2), ... $-I$. I is the spin quantum number and it can take values of 0,1/2, 1, 3/2 and so forth. A nucleus with $I = 0$ has no spin and therefore no magnetic moment, while a spinning charged nucleus ($I \neq 0$) has a magnetic moment μ associated with it. This magnetic moment is represented as a vector parallel to the angular momentum. Therefore for nuclei with $I = 1/2$ (^{1}H, ^{19}F, ^{13}C, and ^{31}P) there are two possible energy levels: $m = +1/2$ parallel (aligned with) to the external field and $m = -1/2$ antiparallel to the external magnetic field. The spins parallel to the magnetic field have a lower energy state. The difference between the two energy levels (ΔE) is proportional to the strength of the external magnetic field and μ

$$\Delta E \propto \frac{\mu B_0}{I} \qquad (1)$$

The distribution of the spins into the two populations is given by the Boltzmann distribution, which can be expressed with sufficient accuracy by

$$\frac{N_+}{N_-} = 1 + \frac{2\mu B_0}{k T} \qquad (2)$$

where N_+ and N_- represent the spin populations of the lower and upper energy states respectively, T is the absolute temperature and k is the Boltzmann constant. At equilibrium, the lower energy level (+1/ 2) is slightly more occupied, differing from unity by only 10^{-5} or 10^{-6}, depending upon μ and B_0.

When nuclei with spins of 1/ 2 such as protons, are placed in a static magnetic field B_0, their magnetic moment experience a torque (aligning force) causing them to precess, about the magnetic field direction (conventionally the z axis). The number of times per second the nuclei precess is termed the *Larmor precession frequency* and is particular to each nucleus(ω_0) (Fig. 1-a). The fundamental NMR equation correlates the Larmor frequency with the magnetic field strength

$$\omega_0 = \gamma B_0, \qquad (3)$$

where γ, the gyromagnetic ratio, is a constant characteristic of a given nucleus that defines the magnitudes of the nuclear magnetic moments with respect to the nucleus' spin number

$$\gamma = 2\pi\mu / hI, \tag{4}$$

h = Planck's constant.

As it can be seen in (3), the Larmor frequency at which the nuclei precess is proportional to the strength of the magnetic field B_0: the larger the field, the higher the frequency at which the nuclei precess. The ω for ^{1}H at 8.7 Tesla (T) is 360 MHz while at 11.7T it is 500 MHz.

5.1.2 The nuclear magnetic resonance experiment: The pulse Fourier transform method

The excess of individual spins in the lower energy state is extremely small but enough to result in a net magnetization M_0 along the axis of the external magnetic field (Figure 5.1-a). If we place ourselves in the rotating frame of the precessing nuclei, M_0 could be seen as a stationary vector. This means that in this frame there is no B_0 field present (Figure 5.1-b; Chen and Hoult, 1989).

Lets us now consider the introduction of another magnetic field B_1 in the form of a radiofrequency pulse (rf pulse) perpendicular to B_0, along the x-axis, for a short moment of time (μs) and at the Larmor frequency of the nucleus of interest. In the rotating frame, B_1 would also be stationary. The magnetization will experience a torque, due to B_1, and rotate towards the *y*-axis (Figure 5.1-b).

Generally by applying our B_1 pulse for just the right amount of time, the magnetization can be flipped by 90° onto the y-axis. The magnetization generated along the y-axis can be detected by induction of a voltage in a receiver coil of the probe that surrounds the sample. The receiver coil can only detect a flux of magnetization that passes through the coil. Protons can be visualized as tiny magnets that have an associated magnetic field. As the protons precess, at some points their magnetic fields will pass through the coil inducing a voltage. In order to understand this process, it is better to go back and position ourselves in the laboratory frame. Now we can see the vector M precessing around B_0, the z-axis. This process is illustrated in Figure 5.1-c. The receiver coil can only detect signals on the x, y plane. When M is on (1), the receiver coil will not register a voltage. As M passes by (2) the flux of magnetization passes through the receiver coil axis and this is illustrated as a positive signal. When M passes by (3) the flux is now perpendicular to the receiver coil and therefore the signal goes back to zero. At (4) the flux passes through the receiver coil but in the opposite sense, resulting in a negative induced voltage. When plotted against time, it can be seen that the voltage oscillates at the Larmor frequency. In this way "the presence of freely precessing nuclear magnetization can be detected by induction of a voltage in a receiving coil" (Chen and Hoult, 1989). According to Faraday's Law of Magnetic Induction, the magnitude of the voltage depends on the amount of net magnetization, which is proportional to the concentration of the nuclei of interest in the sample. However, as M precesses around B_0, its component on the x, y

plane decays, due to the transverse relaxation caused by spin-spin interaction. This is captured by the receiver coil as a decaying signal in time. This period of time, called the *transverse relaxation time constant* (T_2), can be measured and is specific to each nucleus. The decaying signal recorded as a function of time is termed the *free induction decay* (FID). The Fourier transformation of the FID (time domain spectrum) performs a time-to-frequency transformation of the data and the *frequency domain spectrum* is obtained (Figure 5.2).

After the magnetization M_0 is tipped toward the *xy* plane, it returns to the *z* axis. The mechanism by which this "relaxation" process takes place, is called the longitudinal relaxation time, represented by T_1. Because it involves the transfer of energy from the excited protons to the surrounding protons it is also known as the *spin-lattice* relaxation process (Silverstein and Webster, 1998).

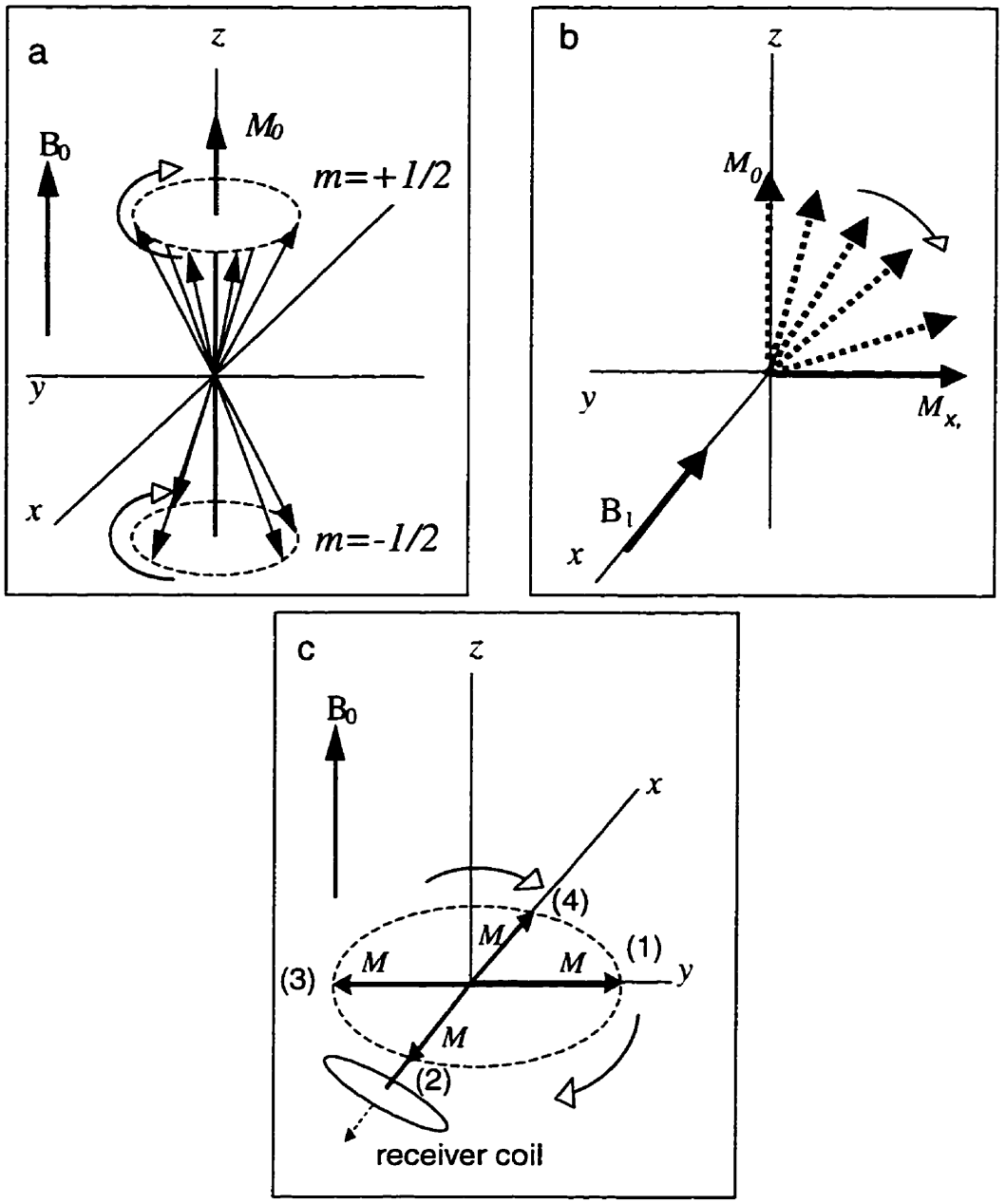

Figure 5.1. Basics of NMR spectroscopy. *a*, precession of nuclei of spin 1/2 around the external magnetic field B_0. The vector *M* represents the net magnetization. *b*, during an rf pulse (B_1) in the rotating frame, the bulk magnetization *M* is tipped into the *x*-*y* plane. *c*, the NMR signal is detected by the receiver coil (see text for more detailed explanation; *a*-b adapted from Macomber, 1988).

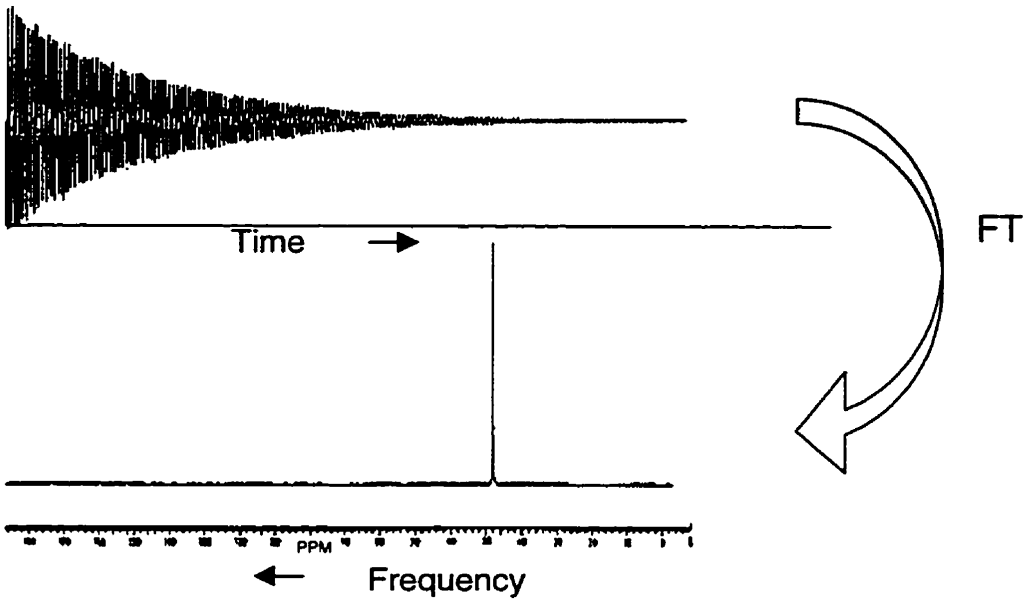

Figure 5.2. Free induction decay (time domain) (above) and transformed NMR spectrum (frequency domain). The application of Fourier transformation transforms the signal from the time domain to the frequency domain resulting in the NMR spectrum (adapted from Silverstein and Webster, 1998).

5.1.3 Spin-spin coupling

Magnetic nuclei are coupled, and transmit information to each other through the intervening chemical bonds between them. This coupling between nuclei also affects the magnetic field experienced by the nuclei and hence their positions in the spectra. This coupling between nuclei is termed spin-spin or J-coupling. Two coupled nuclei of I = 1/ 2 will split each other's resonance lines to a doublet. There is an equal probability of finding each other's spin to be oriented with (+1/ 2) or against (-1/ 2) B_0. If an hydrogen proton has n equivalent coupled neighbors of spin 1/ 2, that proton will resonate as a multiplet of n + 1 component resonance lines. The intensities of each one of those peaks are determined by a binomial distribution and could be illustrated by the Pascal triangle (adapted from Macomber, 1988):

n	n+1	Intensity ratio	Multiplicity
0	1	1	singlet
1	2	1 1	doublet
2	3	1 2 1	triplet
3	4	1 3 3 1	quartet
4	5	1 4 6 4 1	quintet

The CH_2 and CH_3 resonances of an ethyl group are split into multiplets by the spin-spin coupling between them. The CH_2 resonance is a quartet due to the

coupling to the three protons found in the CH_3 group. The CH_3 resonance will be split into three peaks due to the presence of two protons in the CH_2 group. Spin states and statistical weights for the CH_2 and CH_3 groups are shown in Figure 5.3.

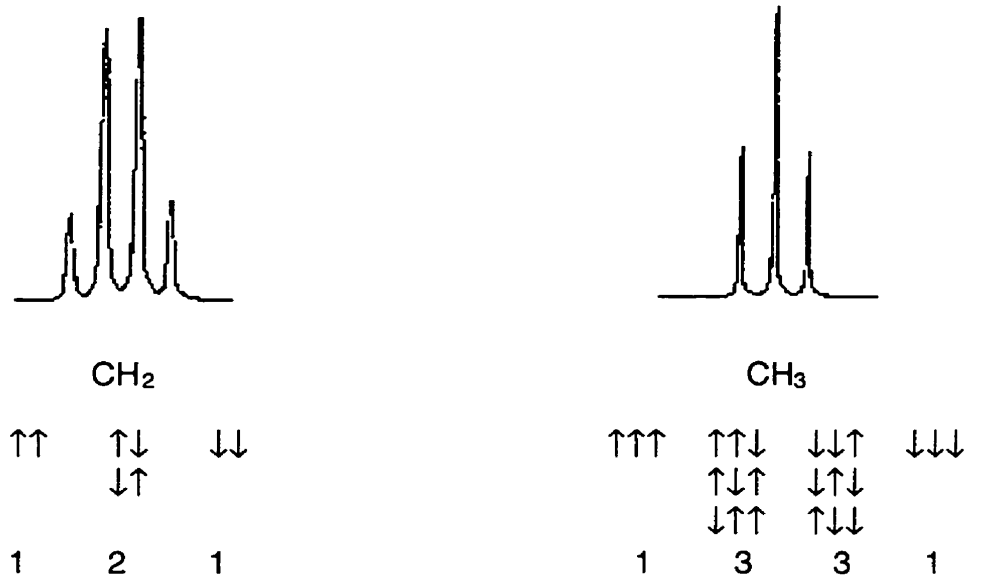

Figure 5.3. Energy levels of the three and four spin states of the methylene and methyl groups respectively that produce the triplet and quadruplet shown in the figure.

5.1.4 The chemical shift

We previously considered that the resonance frequency of a nucleus is directly proportional to the applied magnetic field B_0. If this was the only magnetic field the nuclei experience, then they would absorb energy at the same

frequency and not much information would be obtained. Fortunately, in addition to the external magnetic field, nuclei also experience small magnetic fields generated by their neighbors, either in the same molecule or in an adjacent molecule and by inhomogeneities of the external magnetic field itself. In this way not all the hydrogen nuclei experience the same B_0. The different nuclei within the sample have a specific frequency that depends on the type of nuclei and on the chemical environment that nuclei are found and therefore they will resonate at a characteristic frequency. The magnetic field induces orbital currents in the electronic clouds that surround the nuclei, which results in small local magnetic fields opposite to the applied magnetic field. The nuclei are in this way partially shielded from the magnetic field and need higher magnetic fields to resonate. The greater the shielding of the nucleus, the lower the frequency at which it will resonate (by convention, the farther to the right in the spectrum). Nuclear shielding is proportional to the magnetic field strength. Because of this, the spacing between peaks is also proportional to the magnetic field. As a consequence in MRS there is no natural scale unit. The parts per million (ppm) scale is the most commonly used. The zero point ($\delta = 0$) is also arbitrarily defined. An arbitrary substance is usually used as a reference to which all the resonating peaks in the sample are referred to, and the displacement from this "internal" reference is what is known as chemical shift (δ). The resulting spectrum gives information about the different chemicals present with each peak located at a characteristic position along the frequency axis. The spectrum also gives information about how much of each biochemical is present in the sample.

The areas of the NMR peaks are proportional to the number of nuclei present. As a result, by calculating the area under each peak and comparing it to the area of the chemical shift reference substance, which concentration is known *a priori*, the relative concentration of different substances can be obtained.

Appendix I lists the chemical shifts of many metabolites identified in normal human blood ^{1}H MR spectra. Tables such as these are extremely valuable in the assignment of the different resonance. Many different biochemical compounds share the same type of chemical bonds, resulting in an overlap of different metabolites in the same region of the spectrum. This makes peak identification difficult. This task becomes even more difficult when we are dealing with tissues. In tissues the molecules are more restricted in their motion. The lesser the mobility of the molecules, the broader the NMR peaks. Broad peaks superimpose each other, thus reducing the overall resolution of the spectrum. One way to overcome this problem would be to obtain perchloric acid or other extracts of the biopsies. Signal resolution is superior in extracts due to the increased rate of motion of the metabolites, and assignments can be made more rigorously. However, the results obtained with this technique cannot be completely extrapolated to the spectrum of the tissue biopsy from which the extraction was made because of the destructive action of the acid on the tissue.

5.1.5 Limitations of NMR

NMR machines are large, expensive to maintain and expensive to buy. To maintain the coil's superconductivity, liquid helium and liquid nitrogen are

placed around the coil. Regular maintenance of the magnet increases the overall cost of the experiment.

The most important limitation of NMR, however, is its lack of sensitivity, which can be expressed in terms of signal-to-noise ratio (S/N). Its detection ranges from 0.1 to 0.5mM for ^{1}H (Van Den Thillart, and Van Waarde, 1996). Thus, large quantities of material are required to obtain significant signal-to-noise ratios. MRS is also limited by the length of time the acquisition of a single spectrum may take, from several seconds to several minutes, even hours. The longer the time the greater the chances of metabolic degradation in the case of tissue biopsies (*ex vivo*). ^{1}H became one of the most popular nuclei due to its high detection sensitivity and its high natural abundance in living tissues. With high concentrations, rapid measurements result in better resolution and S/N.

Inspection of an NMR spectrum reveals that the baseline is not completely flat. The continuous oscillation of the baseline represents the background noise. This noise is generated by the electronic circuits within the instrument and it does not represent a problem as long as the spectral signals are strong enough to be differentiated from the noise (Macomber, 1988). The goal in an NMR experiment is to maximize this differentiation.

The S/N depends on a number of variables.

1. Strength of the magnetic field. Because the precessional frequency of a nucleus is directly proportional to the strength of the magnetic field, so is the difference in the frequency between two different nuclei. Therefore the stronger the magnetic field, the greater the separation between signals. Also,

the stronger the magnetic field, the larger the separation between the spin states of the nuclei, which results in a larger population of nuclei in the lower state, enhancing the intensity of the NMR signal (equation 2).

2. Number of acquisitions, or scans, acquired during a NMR experiment. The S/N improves by adding the data obtained in one acquisition to those obtained in subsequent acquisitions. The more acquisitions the better the S/N

$$\frac{S}{N} = \left(\frac{S}{N}\right)_1 \times \sqrt{n}\,, \qquad (5)$$

where n is the number of acquisitions and $(S/N)_1$ is the ratio after a single scan. However the acquisitions must be repeated only after the protons in the sample are brought back to equilibrium. The *time delay* employed between acquisitions will be set according to the estimate of the longitudinal relaxation time T_1.

3. The volume of sample. The larger the volume, the larger the S/N. This is dependent on the design of the spectrometer. Usually, a minimum of 0.4 ml of sample in a tube of 5 mm outer diameter is required in ^{1}H NMR. For ^{31}P NMR volumes between 10-20 ml are required. Improvements in the diameter of the bore allows for the use of much larger volumes, so that it is possible to obtain spectra from animals and humans (Gadian, 1982).

4. The nucleus to be studied (The relative sensitivities of the most common nuclei are listed in Table 1).

5. The design of the spectrometer.

6. The length of time used to monitor the FID signal (*acquisition time*). The resolution of the signal is directly dependent on the acquisition time. But the acquisition time can not be too long because more noise than signal would be obtained due to the decay in the signal.

7. The width of the spectral lines. Broader line widths result in lower peak heights and therefore lower S/N.

8. The relaxation times T_1 and T_2.

9. The concentration of the nuclei of interest.

Table 5.1. Nuclei of major interest in NMR

Nucleus	Spin	$\gamma \times 10^{-8}$	Resonance frequency at 1T (MHz)	Abundance (%)	Relative sensitivity at constant field[1]
^{1}H	1/2	2.6752	42.577	99.98	100
^{2}H	1	0.4107	6.536	0.0156	1.5×10^{-4}
^{13}C	1/2	0.6726	10.705	1.1	1.6×10^{-2}
^{14}N	1	0.1933	3.076	99.6	1.0×10^{-1}
^{15}N	1/2	-0.2711	4.315	0.36	3.7×10^{-4}
^{19}F	1/2	2.5167	40.055	100.0	83.0
^{23}Na	3/2	7.0761	11.262	100.0	9.3
^{31}P	1/2	1.1305	17.235	100.0	6.6
^{35}Cl	3/2	2.1820	4.1717	75.4	3.5×10^{-1}

[1] Relative sensitivity is the NMR sensitivity of a nucleus relative to that of an equal number of protons, multiplied by the percentage of natural abundance (Adapted from Gadian, 1982).

5.2 ^{1}H MRS in cancer of the colon

Over the past twenty years, nuclear magnetic resonance (NMR) spectroscopy has become a powerful tool in the research and diagnosis of cancerous tissue. The advent of improvements in the development of new NMR technology, better tissue-bound water suppression, and arrival of higher magnetic fields, allowed the NMR spectroscopic study of cancer cells (Block *et al.*, 1977) and tissues (Mountford *et al.*, 1982).

Lipid signals were shown to dominate the one-dimensional ^{1}H MR spectra of cancer cells and solid tumor biopsies. Characteristic resonances due to methyl ($-CH_3$), methylene ($-CH_2$), and olefinic (-CH=CH-) groups arise at 0.9, 1.3 and 5.3 ppm respectively. The methylene region (1.3 ppm) in the ^{1}H MR spectrum could actually be resolved in at least four components, with a relatively narrow signal component in the spectra of cell lines with metastatic potential (Mountford *et al.*, 1984a). A long transverse relaxation (T_2) value (400-800 ms) was also found in the protons resonating at 1.33 ppm, in rat mammary adenocarcinoma cells with metastatic potential. This long T_2 value was not found in nonmetastatic cells (Mountford *et al.*, 1984b). For a single, homogeneously broadened resonance, the T_2 transverse relaxation time is inversely proportional to the width of the peak at half of its height. Narrow peaks imply longer T_2 values, and they are frequently related to less viscous solutions and more mobile molecules. The resonance at 1.3 ppm associated with the long T_2 value was found to come from the methyl groups of proteolipid-bound fucose. When the metastatic cells were

pre-treated with fucosidase, the resonance at 1.3 ppm remained but its intensity was reduced, and its T_2 value was less than 350 ms thus confirming that the resonant signal was indeed coming from fucose (Wright *et al.*, 1988). Biochemical studies had shown that malignant cells have an increase in the amount of fucolipids bound to their membranes (Hakomori, 1989). The highly tumorigenic cells also demonstrated stronger resonances at 3.2 ppm ($^{+}N(CH_3)_3$) (Lean *et al.*, 1992). The peak at 3.2 ppm has been assigned to the head group of choline-containing metabolites. Choline metabolites are known to be essential components of membrane phospholipids, and their increased presence in the highly tumorigenic cells could be due to the higher membrane turnover associated with transformed cells (Ruiz-Cabello and Cohen, 1992).

These *in vitro* experiments led to the ^{1}H MRS study of human cancer tissue biopsies. Human ovarian and colon cancer biopsies demonstrated long T_2 values in 45 out of 47 tumor biopsies studied (Mountford *et al.*, 1986). The long T_2 values found for the peak at 1.3 ppm resembled those of the metastatic cells, suggesting their potential to spread to the surrounding organs. Long term follow-up confirmed those results. Many of the patients with long T_2 values with no metastasis at the time of surgery and long T_2 component, developed metastasis thereafter, while none of those with short T_2 values at the time of surgery had metastases thereafter (Smith *et al.*, 1990). Another spectral characteristic of biopsies was the presence of a stronger resonance in the tumors at 3.2 ppm, found to be almost absent in the spectra of normal colonic mucosa (Smith *et al.*, 1990). The intensity of this peak was correlated to the

stage of the tumor increasing from Dukes' stages A through C and diminishing in Dukes' D. Dukes' is a classification for grading colorectal cancer based on the extent of the local spread of the tumor (Dukes' A through C) and in the presence of distant metastasis (Dukes' D). It was found that the ratio of intensities 3.2/ 0.9 ppm, was always >1 for tumors and <1 for normal mucosa. However considerable overlap existed in the range of values for individual samples and it was not possible to differentiate between Dukes' B, C and D tumors.

In another study the ratio between the peaks at 3.2 ppm and 0.9 ppm (methyl CH_3 groups) was used to differentiate between cancer and normal tissue, and more than two fold difference between these two groups was found (Lean *et al.*, 1993). However there was extensive overlap in the values observed for each of the groups under study. This large overlap was the result of the presence of altered lipid profiles in those tissues. That problem was solved by reducing the lipid resonances. In this way the investigators were able to separate malignant from normal colonic samples (Lean *et al.*, 1993). The presence of mobile lipids in those tissue samples could have been the consequence of sampling errors. The colonic wall is a heterogeneous tissue and it is quite possible that some of the tissue biopsies included fragments of the underlying submucosal tissue. The presence of submucosa in colonic biopsies has been correlated to broad lipid resonances at 1.3 ppm (Brière *et al.*, 1995), and may be due to the adipocytes present in this layer of the colon. Adipocytes are large cells that store mobile lipids in a vesicle that occupies most of the cellular cytoplasm, squeezing the nucleus to a thin slit against the cell membrane. The trygliceride content of the

submucosa would also increase the resonance at 0.9 ppm thus artifactually decreasing the 3.2/ 0.9 ppm ratio value.

Moreno *et al.* (1993) working with *ex vivo* tissue biopsies of colonic tumors and normal mucosa, confirmed the overlap seen in the 3.2/ 0.9 ppm ratio and they also attributed it to the presence of submucosal contamination in the biopsies. In that study, it was noticed that the peak resonating at 3.4 ppm was highly discriminant between the normal and cancerous tissues, with the tumor biopsies presenting a higher intensity of this peak. The peak was assigned to taurine; its area in relation to the area of the creatine peak (3.0 ppm) show significant discrimination between tumors and normal colon mucosa, without significant overlap. Taurine is the product of methionine and cysteine catabolism, and has been assigned many functions such as a neurotransmitter and modulator of the central nervous system. Taurine is mainly present in highly metabolic tissues such as the retina, and it has also been proposed to play a role in the protection of the cellular membrane by mechanisms that include detoxification, antioxidation and osmotic regulation (Wright, *et al.*, 1986). High concentrations of taurine were also found in acid extracts of malignant astrocytomas compared to the levels of the benign form in this disease (Peeling and Sutherland, 1992).

Decreased inositol levels, high levels of lactate, aspartate and glutamate were also reported in ^{1}H MR spectra of human colon tumor biopsies with respect to the levels observed for normal mucosa (Moreno and Arús, 1996).

The studies mentioned above show the ability of ^{1}H MRS to detect significant differences in the spectra of tumors and normal tissues. The *ad hoc* approach

utilized for the analysis of the ^{1}H MR spectra of the studies cited before, has allowed the characterization of many possible malignant markers, but not one has become the "magical" diagnostic marker for colorectal cancer. With the analysis of single parameters such as peak heights, peak areas, and peak ratios important diagnostic and biological information may be lost. Rather than relying on individual markers, pattern recognition algorithms have successfully been used for the analysis of ^{1}H MR spectra. These multivariate statistical methods involve considering all the variables found in a spectrum simultaneously and equally important. Multivariate analyses were successfully used for the classification of different types of cancer, including thyroid, brain, cervical, prostate, and colon (Somorjai *et al.*, 1995; Nikulin *et al.*, 1995; Hahn *et al.*, 1997; Bezabeh *et al.*, 1996). Multivariate analysis gave 100% correct classification of control versus cancerous human colon tissues (Bezabeh *et al.*, 1996). The diagnostic regions included the peaks at 3.2 and 3.4 ppm which is consistent with the previous reports described earlier in this chapter.

5.3 ^{1}H magnetic resonance spectroscopy study of normal, preneoplastic (ACF) and neoplastic tissue of the rat colon

5.3.1 Materials and Methods

i. *MRS specimens*

Pathogen free, Sprague-Dawley male rats (Charles River, Montreal; n=32), four weeks old were injected s.c. with azoxymethane (Sigma Chemical Co., St. Louis, MO)/saline (15 mg of drug/ kg body weight in 0.07 cc) at seven days intervals for four weeks. Ten animals that served as controls were injected with the saline vehicle. The animals were killed in groups by CO_2 asphyxiation at the 12th, 14th, 16th, and 18th week following the first injection. Following euthanasia the colons were removed, flushed with isotonic saline and cut open. ACF (n=32), mucosa (AOM-M; n=31), and tumors (n=33) from azoxymethane-treated rats as well as normal mucosa samples (control; n=33) from controls were obtained under a dissecting microscope. We did not attempt to classify the ACF according to size, since the individual lumina of the crypts were not easily identified in all suspected ACF, and the time factor did not allow to go back and check thoroughly. Immediately after dissection, the samples were placed into a vial, frozen in liquid nitrogen and stored at –80 °C until use.

The samples were positioned for MRS in a glass capillary (SMI Capillaries-D, American Dade, Miami, FL) filled with phosphate buffered saline (PBS; Sigma Chemical Co., St. Louis, MO) in D_2O according to Kuesel *et al.* (1992; Figure 5.4). The capillaries were then closed in one end with a teflon plug and inserted

into a 5-mm NMR tube containing the chemical shift reference substance. Para-aminobenzoic acid (PABA; Aldrich Chemical Co., Milwaukee, WIS., 99%; 0.5 mmol/L in phosphate-buffered saline/D_2O solution) was used as a chemical shift reference and quantitation standard, and shifts were expressed with respect to sodium 3-(trimethylsilyl)propanesulfonate (TSP) at 0.0 ppm.

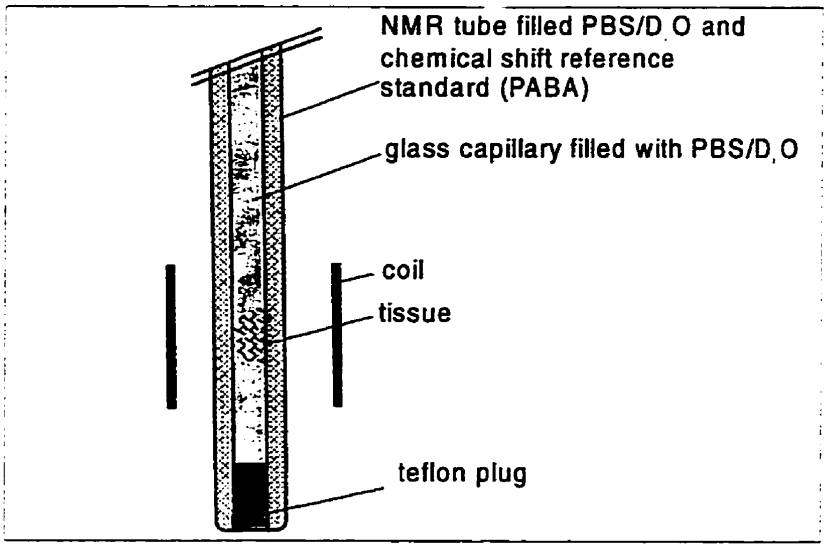

Figure 5.4. Schematic of tissue specimen in a capillary inside an NMR tube. Adapted from Kuesel *et al.*, 1992.

ii. Histological assessment

Following ^1H MRS, all the samples were weighed (control: 0.012 gms. ± 0.005; AOM-mucosa: 0.014 ± 0.005; ACF: 0.008 ± 0.003; tumor: 0.006 ± 0.003; mean ± S.D.) and fixed in 10% buffered formalin, and sections of 5 μm were cut and

stained with hematoxylin and eosin (H&E). The histological assessment was performed blindly by a histopathologist (C.L.) and by an instructor of human histology (L.M.). After a first assessment by the histopathologist, the origin of the tissue and the result of microscopic evaluation by the present author were presented to him, and he was allowed to perform a second assessment. The degree of agreement between the three assessments and the evaluation by origin of tissue were measured with a *kappa statistic* (κ) with a 95% confidence interval (c. i.). In addition the degree of agreement between the assessment by the instructor of human histology and the two assessments by the histopathologist were also measured.

iii. Peak assignments

Resonances of the ^{1}H MR spectra of colon tissue biopsies, were assigned *via* ^{1}H MR spectra of tissue extracts, comparison with chemical shift values of compounds found to be relevant in previous studies, and literature values.

a. Tissue extractions

The method used for the tissue extractions is a modified version of Folch's procedure (Folch's, 1956), and is described in detail in Appendix II. The choice of this method is based on its more gentle treatment of the tissues relative to the acid procedure, with less possibility of hydrolizing polymeric material.

b. Isolated molecules

Creatine, phosphorylcholine, L-glutamic acid, L-glutamine, and taurine were obtained from Sigma Chemical Co., St. Louis, MO. For the ^{1}H MRS analysis the compounds were dissolved in PBS/ D_2O. The ^{1}H MR spectra of these biochemicals are shown in Appendix III.

iv. ^{1}H MRS Experiments

One-dimensional ^{1}H MR spectra of tissue biopsies, extracts and related compounds (640 acquisitions, $\pi/2$ pulse 7 μs, repetition time 2.41 s, spectral width 5000 Hz, 4K data points), were obtained on a Bruker AM 360 spectrometer at 25 °C, without sample spinning, and with low power presaturation of the water signal (20 dB attenuation below 0.2 W).

v. Changes in time

The time elapsed from the moment the tissue samples were thawed until the end of the one-dimensional ^{1}H MRS experiment was measured to be approximately forty minutes. In order to analyze post-mortem changes in the metabolism of the tissues, for a few samples, two consecutive spectra were taken so that after the second spectrum the total time elapsed was around fifty-four minutes (960 scans) or one hour and eight minutes (1280 scans).

vi. Statistical analysis

The one-dimensional FIDs were zero-filled to 8K and Fourier-transformed after multiplication with a Lorentz-Gauss window function (Bruker parameters: GB 0.25, LB -1). Peak heights and areas were determined with the spectrometer software (DISNMR89). The peak heights at 0.90, 1.33, 2.00, 2.24, 2.34, 3.00, 3.20, and 3.40 ppm, and the areas under the peaks at 3.00, 3.20 and 3.40 ppm were calculated per unit mass of tissue. The spectra were analyzed by comparing those heights and areas per unit mass of tissue using MANOVA and a Duncan test ($p \leq 0.01$; Statistica version 4.5).

vii. *Multivariate analysis*

The original one-dimensional FIDs were Fourier-transformed and the magnitude spectra automatically normalized so that the area under the region of interest equaled one, using software developed in-house. The spectra were later partitioned into a training set (16 per class) and a test set (17 control mucosa, 15 AOM-mucosa, 16 ACF, 17 tumor). Only the 0.5-4.5 ppm region of each spectrum was used in order to avoid the spectral artifacts created by suppression of the water peak. Different numbers of subregions, ranging from 1-10, were tested for optimal classification using a genetic algorithm developed in-house (Appendix IV; Nikulin *et al.*, 1995). The optimal set of eight subregions gave the best overall classification accuracy. Linear Discriminant Analysis, made more robust by cross-validating with the Leave-One-Out method, was used to

test the accuracy of the classification based on the eight best attributes (Somorjai *et al.*, 1995).

5.3.2 Results

i. Influence of time on tissue catabolism

Figure 5.5 shows the spectra of a tumor after forty minutes (a) and fifty three minutes (b). Figure 5.6 shows the spectra of a mucosa sample after 40 minutes (a) and one hour and eight minutes. In both cases no significant changes in the spectra between the two times can be seen.

ii. Tissue extractions

Epithelial cells of the colon do not naturally contain lipid droplets in their cytosol. Most of their lipids are found in the form of various cellular membranes. In the membranes, the lipids are restricted in their motion, causing their MR signals to be broadened beyond high resolution detection. A representative spectrum of a lipid phase extract with its correspondent biopsy, is shown in Figure 5.7. It is obvious from this figure that the two spectra are very different. The lipids extracted from the tissues are free from restrictions in motion, and therefore peaks that are absent in the tissue biopsies will be present in the lipid phase of the extractions. As a result, the spectrum of the extracted lipid phase does not aid in the assignment of the ^{1}H MR peaks of the colon tissue biopsies.

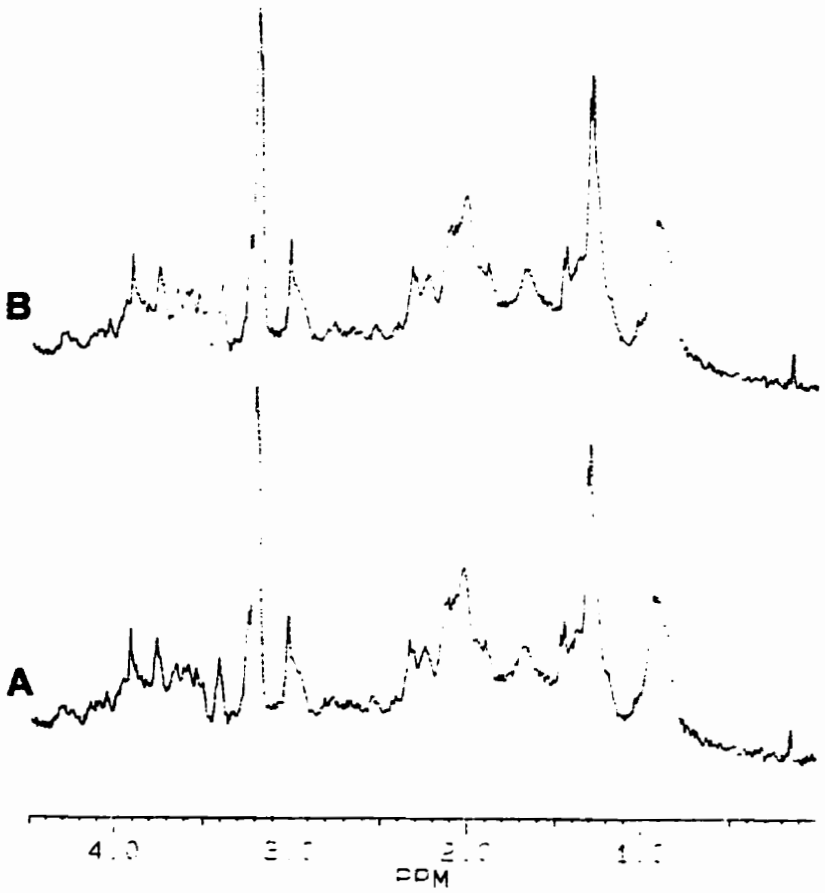

Figure 5.5. ^{1}H MR spectra of rat colon tumor after 40 minutes (A) and 53 minutes (B) from the moment the tissue was thawed.

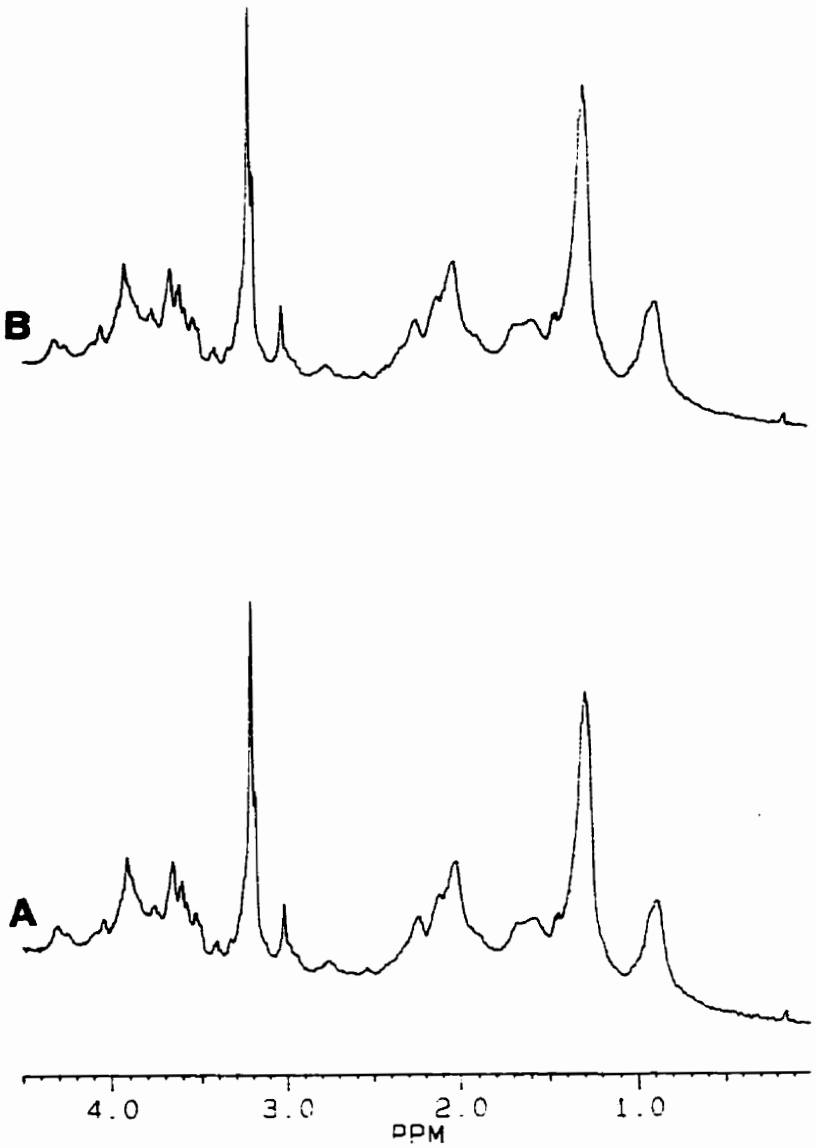

Figure 5.6. ^{1}H MR spectra of rat colon mucosa after 40 minutes (A) and 68 minutes (B) from the moment the tissue was thawed.

A representative spectrum of each of the upper, water-soluble extract and the corresponding tissue biopsy, is shown in Figure 5.8. Most of the resonating peaks found in the tissue biopsies are seen in the upper water-soluble phase.

It can be observed in Figures 5.7 and 5.8 that the intensity height ratio between the peaks resonating at 1.3 and 0.9 ppm is larger in the organic phase. This ratio in the biopsies and water-soluble phase is roughly equal. This suggests a low mobile-lipid contribution to the spectra of the tissue biopsies.

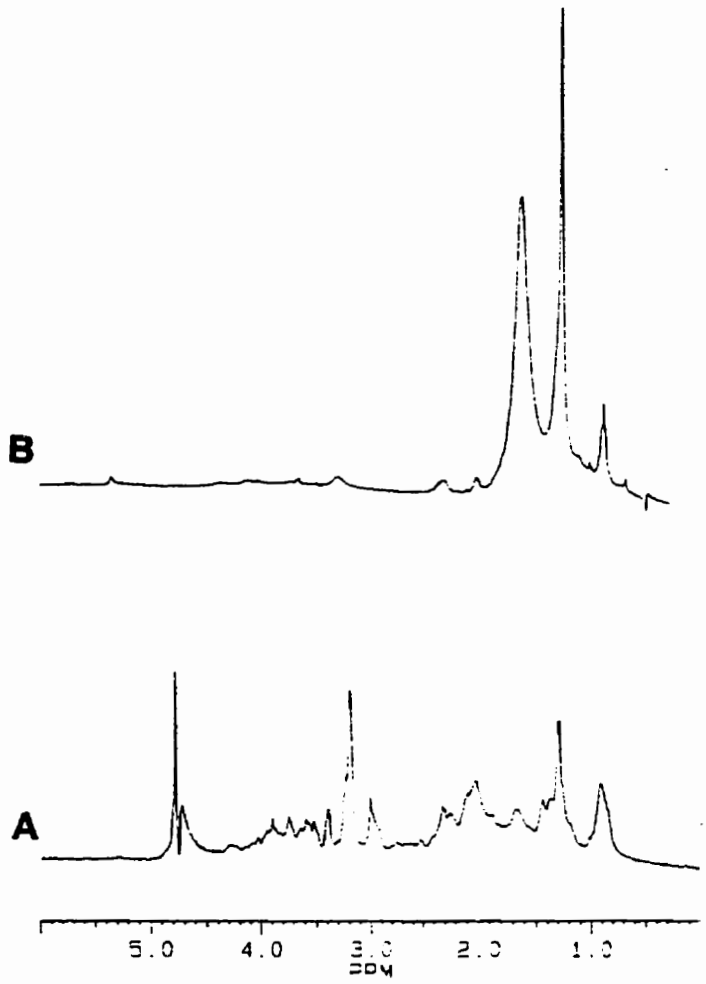

Figure 5.7. ^{1}H MR spectra of rat colon tumor biopsy (A) and its lipid phase extract.

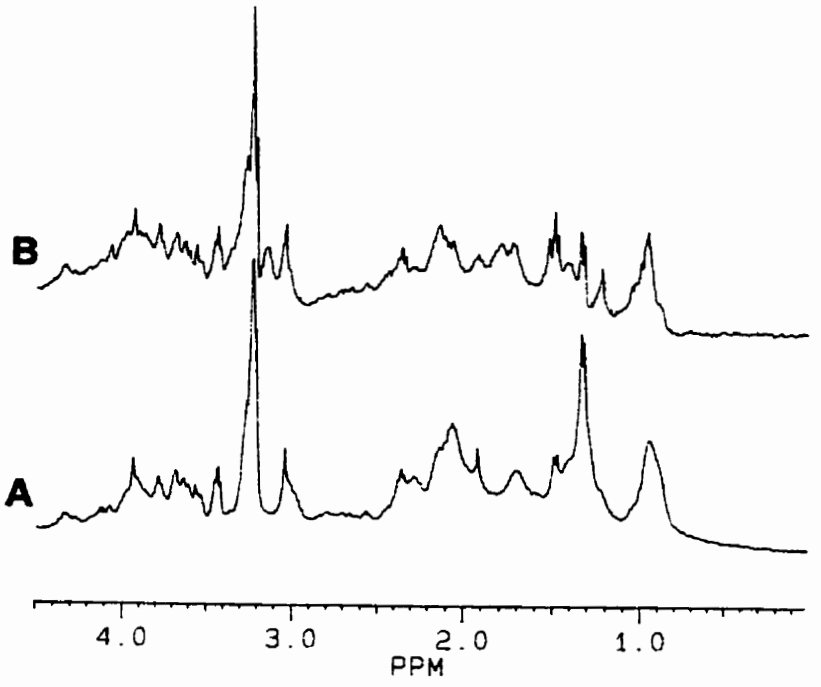

Figure 5.8. ^{1}H MR spectra of rat colon tumor biopsy (A) and its water-soluble phase extract (B).

iii. ^{1}H-MR Spectral characteristics of colon tissue

Figure 5.9 shows the class-averages of the ^{1}H-MR spectra for (A) tumors, (B) ACF, (C) mucosa from AOM-treated rats, and (D) control mucosa. The four spectra are dominated by resonances at 0.9, 1.3, 2.0, and 3.2 ppm, assigned in

part to amino acids, lactic acid, glutamic acid and choline-containing compounds, respectively. Comparison of the four spectra in the region 2.20-2.45 ppm, suggests that this region is particularly sensitive to tissue types. Comparing the intensities of the peaks at 2.24 and 2.34 ppm, the peak at 2.34 ppm is noticeably higher in the average tumor spectrum. The ACF spectrum showed these two resonances to be almost equal, while for the control and AOM-treated mucosa samples, the intensity of the peak at 2.24 ppm is higher. A statistical analysis of the 2.24/2.34 peak ratio (Table 5.2) confirms the qualitative analysis. The peak intensity ratios for ACF and tumor, and separately for the two mucosas, were not significantly different ($p \leq 0.671$, $p \leq 0.197$ respectively). However, the peak ratio for ACF and tumor spectra were significantly smaller from those of the two mucosa sample types ($p \leq 0.0001$; Figure 5.10). One possible candidate for the peak resonating at around 2.34 ppm is glutamic acid. This is based on three lines of evidence. The tables in appendix I show that the γ-CH_2 group of glutamic acid has a chemical shift around 2.36 (Table 1) and 2.35 (Table 2) ppm. The spectrum of isolated glutamic acid demonstrates a multiplet between 2.30-2.36 ppm (Appendix III). Lastly, colon samples spiked with glutamic acid, show an increase in the intensity of the peak at around 2.34 ppm (Figure 5.11).

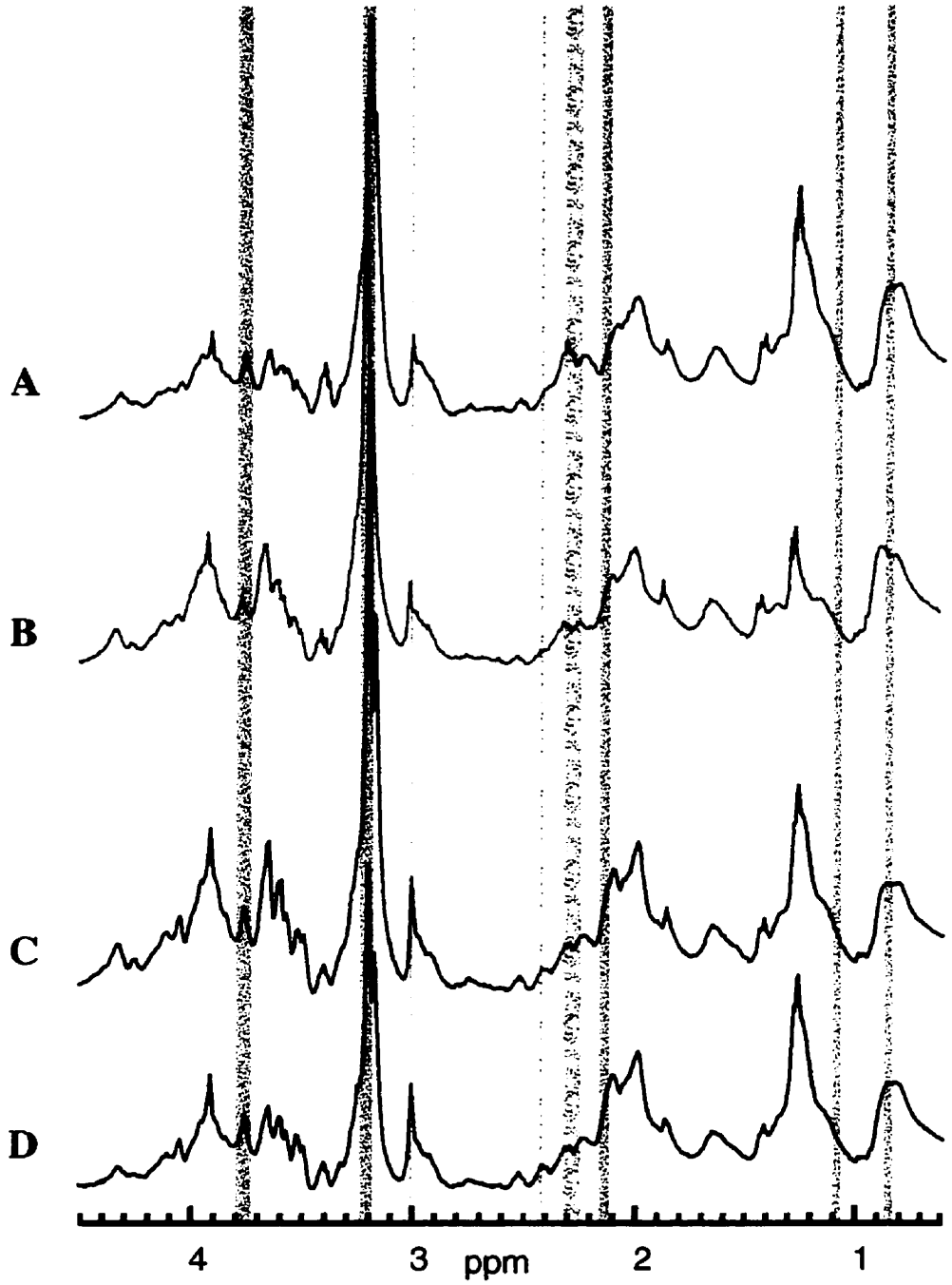

Figure 5.9. Class averages of ^{1}H MR spectra of rat colon tissue. (A) tumor, (B) ACF, (C) AOM-mucosa, (D) control mucosa. The grey areas are the optimal discriminatory subregions as determined by multivariate analysis.

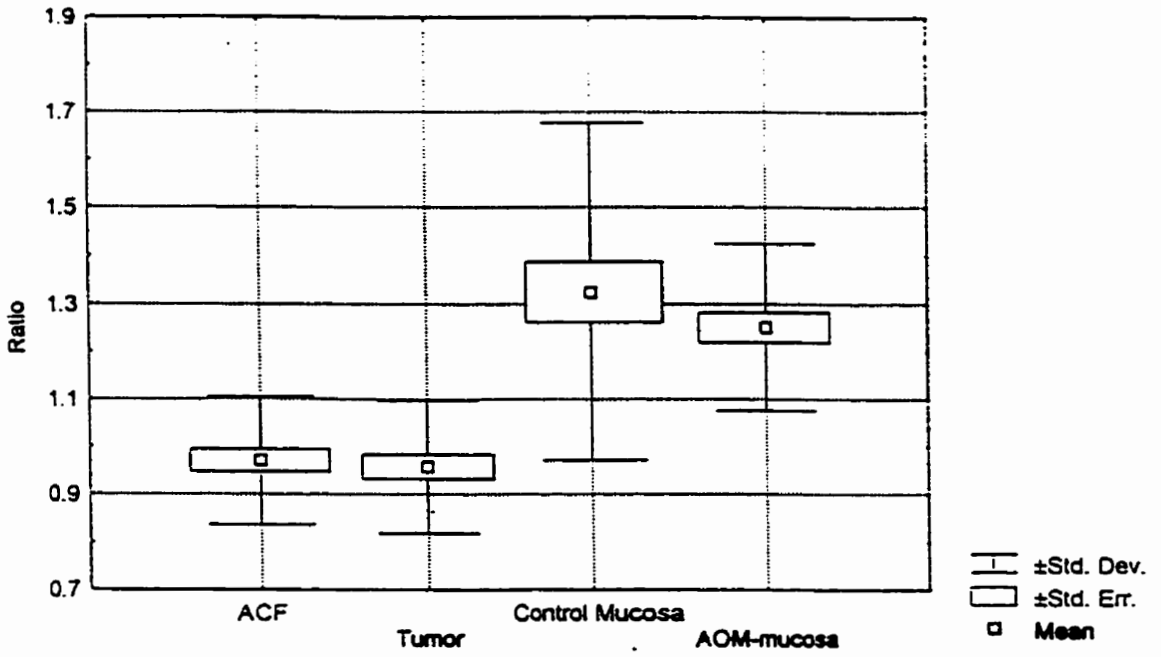

Figure 5.10. Mean, standard deviation and standard error of the 2.24/2.3 ppm resonance intensity ratio.

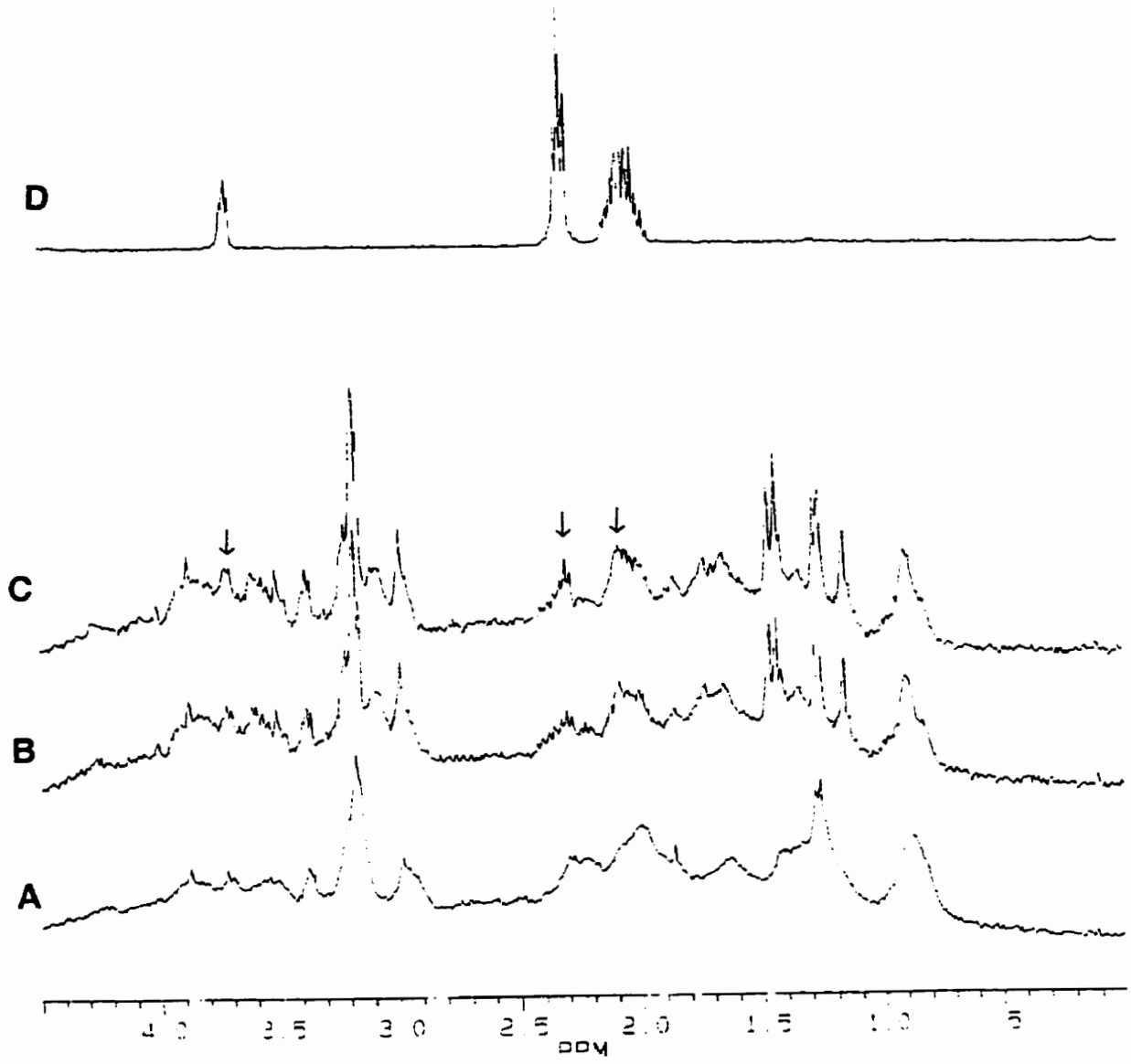

Figure 5.11. ^{1}H MR spectra of rat colon tumor biopsy (A), its water-soluble extract (B), the water-soluble extract spiked with glutamate (C), and of isolated glutamate (D). The arrows indicate the change in the intensity of the peaks due to glutamate.

A summary of the statistical analysis of the intensities of the four dominant resonances, and those at 2.24, 2.34, and 3.40 ppm is shown in Table 5.2. In every case, the intensities of the peaks in the tumor spectra were significantly different from those of the control mucosa. Only at 3.20 ppm was the resonance intensity for the tumor samples not significantly different from that of the AOM-treated mucosa ($p \leq 0.013$). In comparing ACF and tumors, only four peak intensities (1.33, 2.24, 2.34, and 3.40 ppm) were significantly different. None of the peaks in the ACF spectra was statistically different from the respective peaks in the normal and AOM-treated mucosa samples.

The statistical comparison of the areas corresponding to the peaks at 3.4, 3.2 and 3.0 ppm is shown in Table 5.3. None of these areas was found to be statistically different in comparing ACF and tumors. However, the tumors were significantly different from both of the mucosa classes. The ACF were also significantly different from both of the mucosa classes (AOM and normal), except for the area of the peak at 3.0 ppm, in which case only ACF and AOM-mucosa were statistically different.

Table 5.2. Means and standard deviations of resonance intensities per unit mass.

Peak	Control	AOM-M	ACF	Tumor
0.90 ppm	10.02 ± 7.6	11.56 ± 7.46	25.67 ± 25.85	40.75 ± 45.53[1]
1.33 ppm	24.4 ± 27.55	20.03 ± 21.18	33.83 ±37.72	93.34 ± 124.1[2]
2.00 ppm	16.23 ± 18.79	14.88 ± 9.39	27.22 ± 26.41	43.93 ± 50.31[1]
2.24 ppm	6.39 ± 5.99	6.40 ± 4.22	11.93 ± 11.42	25.24 ± 28.44[2]
2.34 ppm	5.11 ± 5.12	5.13 ± 3.22	12.61 ± 12.82	29.24 ± 38.59[2]
3.00 ppm	13.83 ± 18.3	12.87 ± 12.61	21.42 ± 22.24	38.93 ± 47.65[1]
3.20 ppm	43.84 ± 77.67	62.75 ± 46.62	129.31 ± 53.06	168.60 ± 261.84[3]
3.40 ppm	5.27 ± 4.9	4.97 ± 3.7	12.53 ± 12.80	28.47 ± 36.84[2]
2.24/2.34	1.32 ± 0.35	1.25 ± 0.17	0.97 ± 0.13[1]	0.94 ± 0.15[1]

$p \leq 0.01$

[1] Significantly different from AOM- and control mucosa

[2] Significantly different from ACF, AOM- and control mucosa

[3] Significantly different from control mucosa

Table 5.3. Means and standard deviations of the resonance areas per unit mass.

Area	Control	AOM-M	ACF	Tumor
3.00 ppm	29.61 ± 22.20	26.99 ± 9.1	56.77 ± 44.14[2]	83.64 ± 67.4[1]
3.20 ppm	66.26 ± 59.43	81.55 ± 30.59	156.88 ± 107.54[1]	202.03 ± 79.20[1]
3.40 ppm	9.77 ± 6.74	8.81 ± 4.06	21.18 ± 16.50[1]	31.55 ± 28.15[1]

$p \leq 0.01$

[1] Significantly different from AOM- and control mucosa

[2] Significantly different from AOM-mucosa

[3] Significantly different from control mucosa

[4] Significantly different from ACF, AOM- and control mucosa

iv. Multivariate Analysis

The results of the multivariate analysis of the spectra are shown in Tables 5.4 and 5.5. The overall accuracy for the training and test sets was 89.1% and 81.5% respectively. No control or AOM-treated mucosa samples were assigned in the tumor class, and no tumor sample was assigned to either mucosa class. The only misclassified tumor sample was assigned to the ACF class. The few misclassified ACF samples were assigned to the mucosa groups. Misclassified samples of the AOM-treated mucosa class were assigned to either the ACF or control mucosa classes, and misclassified control mucosa samples were assigned as either ACF or AOM-treated mucosa.

Figure 5.9 illustrates the averaged magnitude spectra of the four classes, reduced to the region of analysis. The eight discriminatory subregions are shown as gray areas in Figure 5.9. Analysis of the discriminatory regions reveals that three of the diagnostic subregions include the three resonances of glutamic acid, and the three resonances of glutamine. Given the low lipid content of the colon samples utilized for this work, amino acids are the main contributors for the 0.83-0.87 and 1.07-1.11 ppm diagnostic subregions. Amino acids that resonate in this region of the spectrum include valine, leucine, and isoleucine. However, we cannot ignore the fact that some lipid molecules may also be contributing to these subregions. The subregion between 3.00-3.01 ppm can be assigned to creatine. The assignment of the 3.19-3.25 ppm subregion is less straight forward. In the literature, this peak has been assigned to choline groups (Lean *et al.*, 1992); however, analysis of the spectrum of isolated taurine, reveals a

contribution of this compound. We shall assign this peak to both taurine and choline. Since taurine has been indicated to be a discriminant marker of malignancy in previous studies (Moreno *et al.*, 1993; Brière *et al.*, 1995; Bezabeh *et al.*, 1996) it is possible that the discriminatory characteristics of this subregion could also be due to its taurine content.

Table 5.4. Classification accuracy for the training set.

Desired Class	Assigned Class					
	Control	**AOM-M**	**ACF**	**Tumor**	**%Correct**	**n**
Control	**12**	2	2	0	75	16
AOM-M	1	**14**	1	0	87.5	16
ACF	1	0	**15**	0	93.8	16
Tumor	0	0	0	**16**	100	16

Numbers on the diagonal indicate the cases where the ^{1}H MRS classification agrees with the histological one. Off-diagonal numbers denote misclassifications.

Table 5.5. Classification accuracy for the test set.

Desired Class	Assigned Class					
	Control	**AOM-M**	**ACF**	**Tumor**	**%Correct**	**n**
Control	**12**	5	0	0	70.6	17
AOM-M	2	**11**	2	0	73.3	15
ACF	1	1	**14**	0	87.5	16
Tumor	0	0	1	**16**	94.1	17

Numbers on the diagonal indicate the cases where the ^{1}H MRS classification agrees with the histological one. Off-diagonal numbers denote misclassifications.

v. Histological Assessment

Figure 5.12 shows a number of ACF as seen under the dissecting microscope. Figures 5.13-14 show examples of 5 μm thick, H&E sections of normal and AOM-treated mucosa, ACF, and tumors. Table 5.6 describes the histological assessment of most of the biopsies utilized. The missing biopsies were used to obtain tissue extracts. None of the biopsies was shown to contain submucosa or muscularis contamination. In his first analysis, the pathologist classified correctly only two out of 15 ACF dissected. The instructor of human histology meanwhile, diagnosed correctly 11 of the 15 ACF. For the second trial, the pathologist was trained for the morphology of ACF. In this case 14 of the 15 ACF were correctly classified. In order to measure the degree of agreement among the three diagnoses, the diagnostic labels given by the instructor of human histology and the pathologist had to be translated into the four classes of treatments, i.e. tumor, ACF, AOM-mucosa, and control. The conversion was done in favor of the pathologist and the instructor of histology according to the following rules:

- If the diagnosis was normal + ACF, the conversion was either ACF or AOM-mucosa in accordance to the specific tissue.
- If the diagnosis was ACF and the correspondent biopsy comes from a tumor, the conversion was tumor.

With these rules it was found that the amount of agreement (κ) was higher between the first diagnosis of the pathologist and the origin of the tissues (κ = 0.483, 95% c. i. (0.360, 0.605)) than between the instructor of histology and the

origin of the tissues (κ = 0.428, 95% c. i. (0.283, 0.573)). As expected, the best agreement was found for the second trial of the pathologist (κ = 0.536, 95% c. i. (0.392, 0.605)). The amount of agreement was higher between the instructor of histology and the first diagnosis of the pathologist (κ = 0.437, 95% c. i. (0.315, 0.559)) than with the second diagnosis (κ = 0.416, 95% c. i. (0.278, 0.554)).

The overall diagnostic accuracy of the instructor histology with respect to the origin of the tissues was 68.85%. The pathologist had an overall accuracy of 75.41% in the first trial and 85.25% in the second trial. However, these numbers were calculated using the two rules described before.

Figure 5.12. Topographic view of unstained, unmodified rat colon. The tip of the forceps and the open arrows point to a few ACF present in the field of view. Scale bar = 1mm.

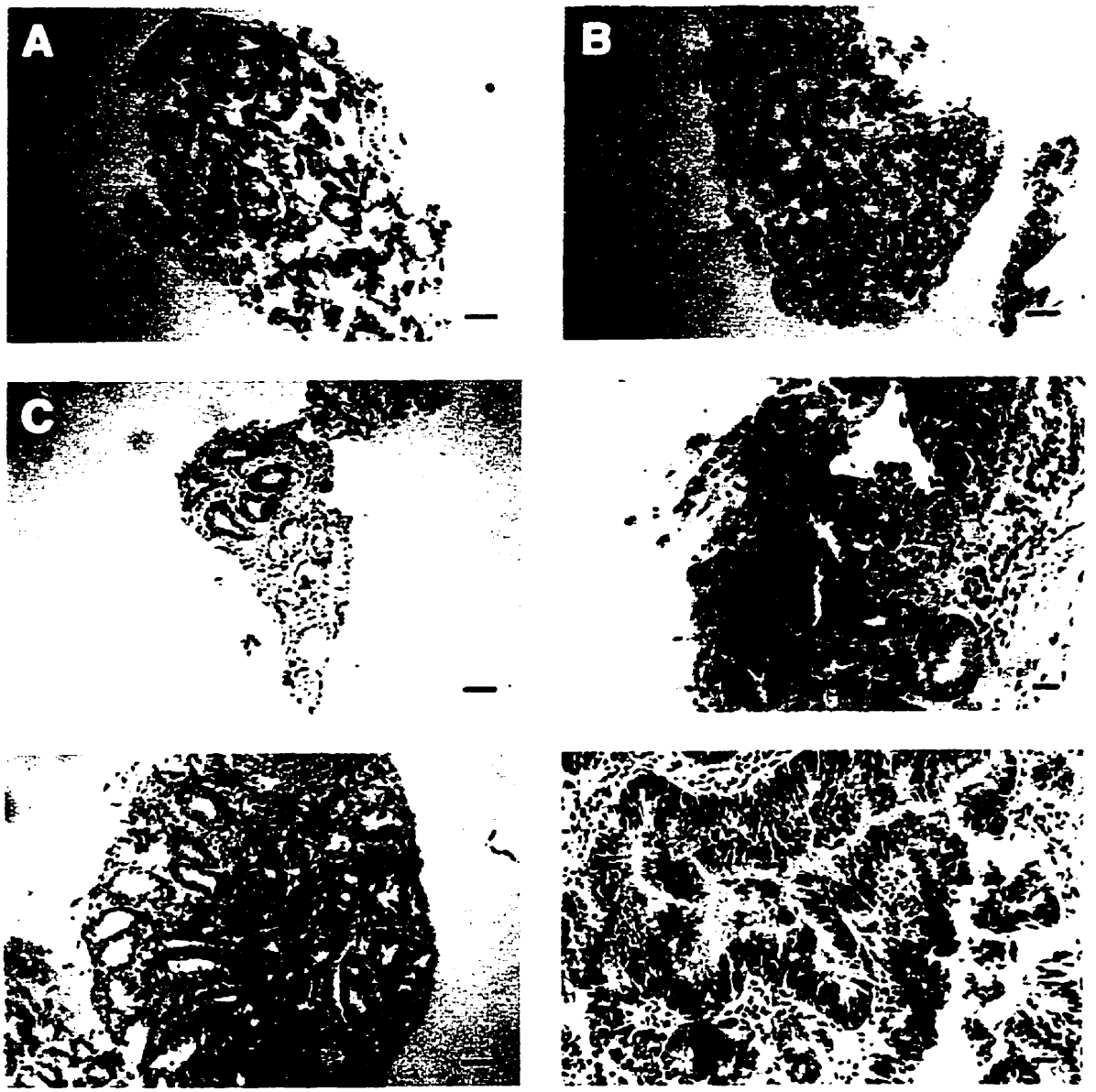
A
B
C

Figure 5.13. (from previous page) (**A**) Photomicrograph of normal control mucosa. Scale bar = 50 μm. (**B**) Photomicrograph of morphologically normal mucosa from a carcinogen (AOM) treated rat. The samples were obtained by gently scarping the colonic surface with a glass slide. Note the histological similarity between the two photomicrographs. Scale bar = 50 μm. (**C**) Transverse section of an ACF consisting of five aberrant crypts. Note the thicker epithelial lining, and the presence of deeply stained (hyperchromatic), larger nuclei, compared with the normal-looking crypts at the bottom of the section. This slide was diagnosed by the histopathologist in his first assessment as normal mucosa. Scale bar = 100 μm. (**D**) Transverse section on an ACF. Note the more basophilic cytoplasm and elongated nuclei with respect to the normal crypts. Scale bar = 2 0 μm. (**E**) Transverse section of an ACF consisting of more than ten crypts. Scale bar = 50 μm. (**F**) Adenocarcinoma with severe epithelial atypia. Note the irregular architecture of the crypts, the hyperchromatic, elongated, stratified nuclei, and the virtual lack of secretory vacuoles. Scale bar = 50 μm. H&E stain.

Table 5.6. Histological assessment

Vial #	Origin of Tissue	Histopathologist #1	Histopathologist #2	Histology instructor
1	T	dysplasia	dysplasia	normal
2	ACF	normal	ACF	ACF
3	T	dysplasia	dysplasia	microadenoma
4	Z	hyperplasia	normal	normal + ACF
5	Z	hyperplasia	normal	normal + ACF
6	C	normal	normal	normal + ACF
7	C	normal	normal + ACF	normal
8	T	dysplasia	dysplasia	adenoma
9	ACF	normal	normal	normal
10	T	dysplasia	dysplasia	adenoma
11	z	hyperplasia	normal	normal + ACF
12	Z	hyperplasia	normal	ACF
13	ACF	dysplasia	ACF	ACF
14	Z4	normal	normal	ACF
15	ACF	normal	normal + ACF	normal + ACF
16	Z	hyperplasia	normal + ACF	normal + ACF
17	ACF	normal	ACF	ACF
18	T	dysplasia	dysplasia	microadenoma

19	C	normal	normal +ACF	ACF
20	C	normal	normal	normal + ACF
21	C	normal	normal + ACF	normal + ACF
23	Z	normal	normal + ACF	ACF
24	C	normal	normal + ACF	ACF
25	Z	normal	normal + ACF	normal
26	T	dysplasia	dysplasia	ACF
27	T	malignant carcinoma	malignant carcinoma	adenoma
28	Z	normal	normal	normal
29	T	dysplasia	dysplasia	adenoma
30	T	dysplasia	dysplasia	ACF
31	C	normal	normal + ACF	normal + ACF
32	ACF	normal	normal + ACF	ACF
33	C	normal	normal	normal
34	C	normal	normal	normal + ACF
35	C	normal	normal + ACF	normal
36	T	malignant carcinoma	malignant carcinoma	adenoma
37	T	malignant carcinoma	malignant carcinoma	adenoma
38	Z	normal	normal	normal
39	T	malignant carcinoma	malignant carcinoma	adenoma
40	Z	normal	normal + ACF	normal

41	T	normal	mild dysplasia	normal
42	Z	normal	normal + ACF	some ACF
43	T	normal	mild dysplasia	some ACF
44	C	normal	normal + ACF	ACF
45	T	malignant carcinoma	malignant carcinoma	adenoma
46	T	dysplasia	mild dysplasia	ACF
47	Z	normal	normal + ACF	normal
48	T	atypia	atypia	ACF
49	Z	normal	normal + ACF	ACF
50	T	dysplasia	dysplasia	ACF
51	ACF	normal	normal + ACF	normal
52	ACF	normal	normal + ACF	normal
53	ACF	normal	normal + ACF	ACF
54	C	normal	normal + ACF	ACF
55	ACF	normal	normal + ACF	normal
56	ACF	hyperplasia	normal + ACF	ACF
57	ACF	normal	normal + ACF	ACF
58	ACF	normal	normal + ACF	ACF
59	ACF	normal	normal + ACF	ACF
60	ACF	normal	normal + ACF	ACF

C= control; T= tumor; Z= AOM-mucosa.

5.3.3 Discussion

The results obtained in the present study support the hypothesis that ACF represent preneoplastic lesions. This conclusion is based primarily on two factors. Firstly, comparison of peak heights and areas by MANOVA shows the strong rank order relationship between the ACF and the two mucosa classes as well as between the ACF and the tumors. The mean peak height for rat ACF and tumors at 0.90, 2.00, 2.24, and 3.2 ppm, were not significantly different, whereas the peak heights at 1.30, 2.34 and 3.40 ppm were significantly different. Spectra of rat ACF showed a closer relationship with the two classes of mucosa samples, since none of the mean peak height values obtained was significantly different. However, when the areas under those peaks were compared, the ACF appeared to be closer in content to the tumors, with none of the peak areas for ACF and tumors found to be significantly different. Secondly, multivariate analysis has clustered each tissue type into a separate group. The few misclassified samples demonstrate that these tissue types are related to one another. Most of the misclassifications were found between the control and AOM-mucosa groups which are histologically indistinguishable . No mucosa sample classified in the tumor class but a few of them did so in the ACF class. ACF samples were mainly assigned to their own group (93.8% in the training set and 87.5% in the test set). The only misclassifications were found in the mucosa groups. No ACF sample was misclassified in the tumor group. These data shows that a relationship exists between mucosa samples and ACF; however,

there are enough spectral features to separate the ACF into their own independent class. The tumor samples comprise the more homogeneous class. Only one tumor misclassified; it was assigned to the ACF class.

In a previous study (Lean *et al.*, 1993), the 3.2/0.9 peak ratio was used as a measure of malignancy, but no significant differences were found between human colon control and tumor samples. Submucosal contamination of mucosa samples has been offered as an explanation of the large spectral variations (Moreno *et al.*, 1993). More recently, the presence of intense -"broad"- lipid resonances in mucosal samples was reported to occur with submucosal contamination (Brière *et al.*, 1995). The presence of such broad resonances would obscure neighboring resonances, making it difficult, if not impossible, to compare contaminated and pure mucosa samples. None of the mucosa samples in the present study gave rise to a broad lipid resonance. This is likely due to the present sampling procedure, by which the mucosa samples were carefully separated from the rat colons by gently scraping with a glass slide under a dissecting microscope enabling us to monitor the tissue samples closely. The histological analysis of the tissue samples confirmed that none of the samples assessed was contaminated with submucosa.

In a previous study the resonance at 3.40 ppm was found to be a discriminant peak between perchloric acid extracts of colonic human mucosa and tumor samples (Moreno *et al.*, 1993). This study supports that finding, since the mean peak height of the resonance at 3.40 ppm was significantly higher in tumors than in ACF and the two mucosa classes. The peak at 3.40 ppm has previously been

assigned to taurine. This peak is present in the aqueous phase of the tissue extractions and the spectrum of isolated taurine support this assignment.

We have also reported that the ratio of intensities 2.24/2.34 ppm is a useful diagnostic marker to differentiate between ACF and normal samples. Note that in the tumor and ACF spectra this ratio is <1, while in the AOM-mucosa and normal mucosa the ratio is >1. A statistical comparison of this ratio resulted in a significant difference between ACF and tumor vs. AOM- and normal mucosa ($p \leq 0.0001$); however, there was overlap among the range of values found for the four classes of samples.

Although not useful for diagnostic purposes, the overlap found for all the features under study further supports the relationship among tumors, ACF, AOM-treated and normal mucosa, and their use as comparison groups.

In addition to proceeding with the traditional analysis of ^{1}H-MRS peak heights and areas, pattern recognition algorithms were applied to classify spectra. In this analysis, the classification scheme is known as a priori, since first the program is trained with representative data, and then based on this training, an unknown set of data are assigned to known classes. This method was previously used with great success in the classification of thyroid biopsies (Somorjai *et al.*, 1995) and human colon tissue (Bezabeh *et al.*, 1996). The optimal set of eight diagnostic subregions was determined with the aid of genetic algorithms (see Tables 4 and 5). These eight best attributes enabled the classification of the spectra, using Linear Discriminant Analysis, with an accuracy of 89.1% for the training set and 81.5% for the validation set. The few misclassifications are possibly indicative of

the continuous relationship among the four classes; for example, control and AOM-treated mucosas were found to be closely related. The ACF biopsies appeared to be a group to themselves with only three misclassifications out of thirty-three, while the tumor group was found to be the most homogeneous, with only one spectrum out of thirty-three assigned to a different class, namely ACF.

From the analysis of the diagnostic subregions (Table 6), it is worth noting that three of the diagnostic subregions include the three resonances of glutamate, and the three resonances of glutamine. The amino acid analysis of colon tissue revealed increased levels of glutamate and aspartate in the tumors as compared to the levels found in the normal mucosa (Okada *et al.*, 1993). High levels of these two amino acids were also found in ^{1}H MRS of perchloric acid extractions of human colon tumors (Moreno *et al.*, 1996). *In vitro* studies of tumor mitochondria indicate that glutamine is avidly taken up by the tumors and serves as an essential component of tumor metabolism. Glutamine serves as one of the most important precursors of tumor proteins, and purine nucleotides. Glutamine also serves as a major energy source for neoplasms of different tissues. The main pathway of glutamine catabolism in tumors is its conversion into glutamate. Prominent levels of activity by glutaminase, the first enzyme in the hydrolysis of glutamine, activity levels were described in human liver hepatomas (Matsuno and Goto, 1992). Glutamate is also taken up exogenously by the tumors (Okada *et al.*, 1993). Glutamate can the be catabolized in the tumor mitochondria to supply it with ATP (Matsuno and Goto, 1992). The

findings reported here provide more evidence that glutamine and glutamate play key roles in tumor metabolism.

5.3.4 Conclusion

Several biochemical characteristics of the ACF, detected by ^{1}H MRS, suggest that these lesions are an early event in the development of colon carcinogenesis. The application of pattern recognition algorithms to classify the different classes of colon tissues supports this conclusion, since ACF samples were grouped between the normal tissue samples and the tumors. Diagnostic regions included mainly resonances due to glutamate and glutamine. The multivariate analysis yielded a better and more objective classification accuracy than the conventional histopathological analysis.

5.4 Future perspectives

In this chapter I have shown that ^{1}H MRS was able to detect changes in the biochemistry of the different classes of tissues utilized that correlate with the progression of colon cancer. By combining magnetic resonance imaging (MRI) and *in vivo* ^{1}H MRS, it should be possible to diagnose colon cancer non-invasively. However, the diagnostic potentials of *in vivo* ^{1}H MRS and MRI of the colon are

hampered by artifacts caused by the peristaltic movements of the colon, the motions due to respiration, and the presence of fat. In addition, in the case of *in vivo* ^{1}H MRS, in general a voxel of a minimum size of approximately 1 cm^3 is needed to obtain good signal-to-noise ratio. Because of the peristaltic movements and the contour of the colon, it becomes a difficult task to fix a voxel just in the mucosa. Advances have been made to reduce many of the drawbacks mentioned before. Technical progress in the development of endoscopic MRI instruments should increase the signal-to-noise ratio by placing the rf coils closer to the tissue of interest. The results obtained in combination with improved MRI technology could very well serve one day for the diagnosis and staging of colon cancer.

5.5 References

Bezabeh, T., Smith, I.C.P., Krupnik, E., Somorjai, R.L., Kitchen, D.G., Bernstein, C.N., Pettigrew, N.M., Bird, R.P., Lewin, K.J., Brière, K.M. Diagnostic potential for cancer *via* ^{1}H magnetic resonance spectroscopy of colon tissue, Anticancer Res., **16**, 1553-1558, 1996.

Block, R.E., Maxwell, G.P., Prudhomme, D.L., and Hudson, J.L. High resolution proton magnetic resonance spectral characteristics of water, lipid, and protein signals from three mouse cell populations, J. Natl. Cancer Inst., **58**, 151-156, 1977.

Bovey, F.A. Nuclear magnetic resonance spectroscopy, Academic Press, San Diego, 1988.

Brière, K.M., Kuesel, A.C., Bird, R.J.P., and Smith, I.C.P. ^{1}H MR visible lipids in colon tissue from normal and carcinogen-treated rats, NMR Biomed. **8**, 33-40,1995.

Chen, C-N., and Hoult, D. Biomedical magnetic technology, Adam Hilger, Bristol, 1989.

Gadian, D.G. Nuclear magnetic resonance and its applications to living systems, Clarendon Press, Oxford, 1982.

Hakomori, S. Aberrant glycosylation in tumours and tumour associated carbohydrate antigens, Adv. Cancer Res., **52**, 257-331, 1989.

Hahn, P., Smith, I.C.P., Leboldus, L., Littman, C., Somorjai, R.L., and Bezabeh, T. The classification of benign and malignant human prostate tissue by multivariate analysis of ^{1}H magnetic resonance spectra, Cancer Res., **57**, 3398-3401, 1997.

Kuesel, A.C, Kroft, T., Saunders, J.K., Prefontaine, M., Mikhael, N., and Smith, I.C.P. A simple procedure for obtaining high-quality NMR spectra of semiquantitative value from small tissue specimens: cervical biopsies, Magn. Reson. Med., **27**, 349-355, 1992.

Lean, C.L., Mackinnon, W.B., Delikatny, J.E., Whitehead, R.H., and Mounford, C.E. Cell-surface fucosylation and magnetic resonance characterization of human malignant colorectal cells, Biochemistry, **31**, 11095-11105, 1992.

Lean, C.L., Newland, R.C., Ende, D.A., Bokey, E.L., Smith, I.C.P., and Mountford, C.E. Assessment of human colorectal biopsies by ^{1}H MRS: correlation with histopathology. Magn. Reson. Med., **30**, 525-533, 1993.

Macomber , R.S. NMR spectroscopy: basic principles and applications, Harcourt Brace Jovanovich, San Diego, 1988.

Matsuno, T. and Goto, I. Glutaminase and glutamine synthetase activities in human cirrhotic liver and hepatocellular carcinoma, Cancer Res., **52**, 1192-1194, 1992.

Moreno, A., Rey, M., Montane, J.M., Alonso, J., and Arús, C. ^{1}H NMR spectroscopy of colon tumors and normal mucosal biopsies; elevated taurine levels and reduced polyethylenglycol absorption in tumors may have diagnostic significance, NMR Biomed., **6**, 111-118, 1993.

Moreno, A., and Arús, C., Quantitative and qualitative characterization of ^{1}H NMR spectra of colon tumors, normal mucosa and their perchloric acid extracts: decreased levels of myo-inositol in tumours can be detected in intact biopsies, NMR Biomed., **9**, 33-45, 1996.

Mountford, C.E., Grossman, G., Reid, G., and Fox, R.M. Characterization of transformed cells and tumours by proton nuclear magnetic resonance spectroscopy, Cancer Res., **42**, 2270-2276,1982.

Mountford, C.E., Mackinnon W.B., Bloom, M., Burnell, E.E., and Smith I.C.P. NMR methods for characterizing the state of the surface of complex mammalian cells, J. Biochem. Biophys. Methods, **9**, 323-330, 1984a.

Mountford, C.E., Wright, L.C., Holmes, K.T., Mackinnon, W.G., Gregory, P., and Fox, R.M. High resolution proton magnetic resonance analysis of metastatic cancer cells, Science, **226**, 1415-1418, 1984b.

Mountford, C.E., May, G.L., Williams, P.G., Tattersall, M.H.N., Russell, P., Saunders, J.K., Holmes, K.T., Fox, R.M., Barr, I.R., and Smith, I.C.P. Classification of human tumours by high resolution magnetic resonance spectroscopy, The Lancet, **1**, 651-653, 1986.

Nikulin, A., Brière, K.M., Friesen, L., Smith, I.C.P., and Somorjai, R.L. Genetic algorithm-guided optimal attribute selection: a novel preprocessor for classiffying MR spectra, Proc. Soc. Magn. Reson., **3**, p.1940, 1995.

Okada, A., Takehara, H., Yoshida, K., Nishi, M., Miyake, H., Kita, Y., and Komi, N. Increased aspartate and glutamate levels in both gastric and colon cancer tissues, Tokushima J. Exp. Med., **40**, 19-25, 1993.

Peeling, J., and Sutherland, G., High resolution ^{1}H NMR spectroscopy study of extracts of human cerebral neoplasms, Magn. Reson. Med., **24** , 123-136, 1992.

Ruiz-Cabello, J. and Cohen, J.S. Phospholipid metabolites as indicators of cancer cell function, NMR Biomed. **5**, 226-233, 1992.

Silverstein, R.M. and Webster, F.X. *Spectrometric identification of organic compounds*, John Wiley & Sons, Inc., New York, 1998.

Smith, I.C.P. , Princz, E.J., and Saunders, J.K. Magnetic resonance spectroscopy in cancer research, J. Can. Assoc. Radiol., **41**, 32-38, 1990.

Somorjai, R.L., Nikulin, A., Pizzi, N., Jackson, D., Scarth, G., Dolenko, B., Gordon, H., Russell, P., Lean, C.L., Delbridge, L., Mountford, K.E., and Smith, I.C.P. Computerized consensus diagnosis: a classification strategy for the robust analysis of MR spectra. I. Application to ^{1}H spectra of thyroid neoplasms, Mag. Reson. Med., **33**, 257-263, 1995.

Van Den Thillart, G., and Van Waarde, A. Nuclear magnetic resonance spectroscopy of living systems: applications in comparative physiology, Physiol. Reviews, **76**, 799-837, 1996.

Wright, C.E., Tallan, H.H., and Yong, Y.L. Taurine: biological update, Ann. Rev. Biochem., **55**, 427-453, 1986.

Wright, L.C., May, G.L., Gregory, P., Dyne, M., Holmes, K.T., Williams, P.G., and Mountford, C.E., Inhibition of metastatic potential by fucosidase: an NMR study identifies a cell surface metastasis marker, J. Cell. Biochem., **37**, 49-59, 1988.

6 Fourier transform infrared Spectroscopy

6.1 Basics of Fourier transform infrared spectroscopy

Infrared (IR) radiation refers to that part of the electromagnetic spectrum between the visible and microwave regions. IR spectroscopy is the study of molecular structure by means of the interaction of light of wavelengths 0.75-1000 μm (10-13300 cm^{-1}) with matter. IR radiation is absorbed and converted by an organic molecule into energy of molecular vibration. Since each vibrational energy change is accompanied by a number of rotational energy changes, IR spectrum appears as bands rather than discrete lines. The frequency or wavelength of absorption depends upon the nature of the bonds (e.g. C-H, P=O, N=H etc.), the type of vibration (e.g. stretching, bending) and the strength of the bonding interactions. For complex mixtures, such as tissues, each infrared active species contributes to the infrared spectrum, the relative contribution of each species depending upon its concentration. The infrared spectrum of tissue therefore provides information that reflects structural and biochemical aspects of the tissue. Abnormal biochemical processes, such as the formation of ACF or tumor development, should be reflected in changes in the infrared spectrum of the tissue.

In the IR region of the electromagnetic spectrum, the practical unit for wavelength is the micrometer, μm (10^{-6} meters). The wavelength is a property of radiation but not of the molecule. The energy and frequency are properties in common between radiation and molecules. Since the frequency (υ) in Hz in the infrared portion of the spectrum is inconveniently large, the wavenumber ($\bar{\upsilon}$) is more commonly used. The wavenumber is proportional to the frequency and wavelength of light (λ)

$$\upsilon = \bar{\upsilon} c = \frac{c}{\lambda}$$

where c is the velocity of radiation (2.998 x 10^{10} cm/second in a vacuum). The wavenumber will also be referred to as the "frequency in cm^{-1}".

The IR region of the electromagnetic spectrum is divided into three regions characterized by absorptions from distinct types of vibrational transitions. The far-IR region (10-400 cm^{-1}) contains the vibrations of bonds between metal atoms and both inorganic and organic ligands (Skoog, 1985). Of greatest practical use is the mid-IR region (400-4000 cm^{-1}). The mid-IR can be subdivided into the 1300-4000 cm^{-1} and the 1000-1300 cm^{-1} regions. The higher frequency subregion is called the functional group region. Characteristic stretching vibrations of important functional groups such as O-H, N-H and C=O are found here. The 1000-1300 cm^{-1} region is characterized by a multitude of low and mid intensity bands arising from interacting vibrational modes. This region of the IR spectrum gives rise to a unique pattern of bands for every molecular

species hence is also known as the "fingerprint" region. Subtle changes in the molecular environment, such as conformational changes, can be detected in the mid-IR. In fact, the strength of absorptions from biological materials in the mid-IR hampers the potential of this spectral region to be used in *in vivo* diagnosis.

Pathlengths greater than 15 μm result in a complete absorption of the IR beam. Given this drawback, recently there has been interest in the near-IR region (4000-13300 cm^{-1}). This region is characterized by the absence of sharp peaks and an abundance of overtones (multiples of a given frequency) and combination tones (sum of two or more other vibrations; Schrader, 1995). Absorptions in the near-IR region usually arise from groups containing light atoms. Thus X-H vibrations (e.g. C-H, N-H, O-H) are seen in the near IR, but C-O and P-O groups are not. The reduced absorption in the near-IR region (compared to the high information content of the mid-IR), allows for greater pathlengths to be utilized. This offers the possibility of studies aimed at non-invasive measurements of biomolecules (Carney *et al.*, 1993).

There are two types of molecular vibrations: stretching and bending. A stretching vibration is a rhythmical movement along the bond axis such that the interatomic distance is increasing or decreasing. Stretching vibrations could involve movement towards the same direction with respect to the central atom, in which case they are called *symmetrical stretching vibrations*; or could involve movement in an opposing direction, *asymmetrical stretching vibration.* A bending vibration involves a change in the angle of the bonds without changing the interatomic distances. They could be sub-divided into twisting (out-of-plane

bending), rocking (in-plane bending), scissoring (in-plane bending), and wagging (out-of-plane bending) vibrations (Figure 6.1). In general, stretching vibrations give rise to more prominent IR absorptions than bending ones. Asymmetric vibrations require more energy than symmetric vibrations and therefore they absorb IR radiation at higher wavenumbers.

Only those vibrations that result in a change in the dipole moment of the molecule give rise to an IR band. In other words, only when there is a change in the electric charge distribution within a molecule, the infrared radiation can be coupled with the molecular vibration. In this way homonuclear diatomic molecules such as H_2 which have zero dipole moment for any bond length, are inactive in the infrared, while strong polar groups such as O-H tend to dominate an IR spectrum.

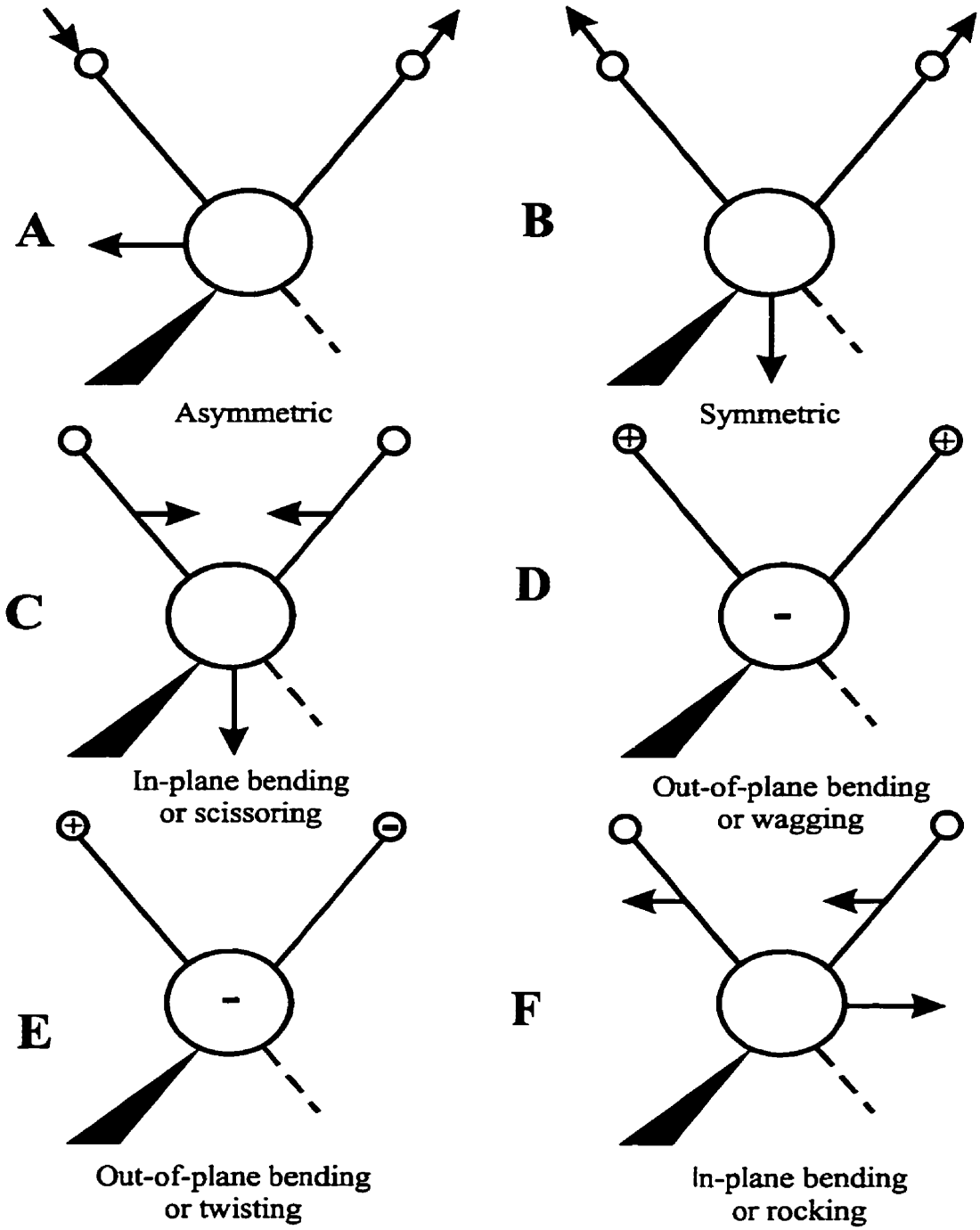

Figure 6.1. Vibrational modes for a CH2 group, including the stretching (A and B) and bending (C, D, E, F) vibrations. "+" and " -" indicate movement perpendicular to the plane of the page. The arrows indicate movement in the plane of the page (Adapted from Silverstein and Webster, 1998).

6.2 Instrumentation: The Fourier transform spectrometer (Michelson interferometer)

A schematic diagram of a Fourier transform (FT) IR apparatus is shown in Figure 6.2. The Michelson interferometer consists of two mirrors: one fixed mirror (FM) and a second moving mirror (MM) placed at 90^0 angle to the first. Between the mirrors there is a beam-splitter, a half-reflecting mirror that splits the incoming beam from the source into two equal parts. The two resulting beams are reflected at the MM and the FM. Following reflection at these mirrors, the two beams recombine at the beam splitter which then sends half the radiation back to the IR source, and the other half pass through the sample before being focused onto the detector. When the two mirrors are equidistant from the beam splitter, the pathlength of the two reflecting beams are equal and will recombine constructively for all the frequencies present in the original IR beam, and the pathlength difference (retardation) will be zero. By moving the MM away from the equidistant point, the two beams will recombine at the beam splitter out-of-phase, and destructive interference occurs, the retardation will be greater than zero. "The plot of detector response as a function of retardation is an interferogram" (Colthup *et al.*, 1990). The interferogram (time domain) is then Fourier transformed into the more familiar frequency domain. A single scan of the movable mirror produces a complete single beam spectrum of the sample. The spectrum is ratioed against a background spectrum, giving rise to the intensity versus frequency spectrum of the sample. A background spectrum is

one generated without a sample present. This serves to remove factors dependent on the instrument function such as the source, the efficiency of the beam splitter, the MM, and the FM, the atmospheric absorbances in the beam path, and the detector response. Since the MM is moved by a motor controlled by the computer, one scan can be measured in a fraction of a second. This is important since a large number of scans are necessary to reduce the noise level. The fast acquisition time allows the measurement of a large number of scans, which are averaged by the computer, reducing the level of noise by the square root of the number of scans. (Silverstein and Webster, 1998, Colthup *et al.*, 1990)

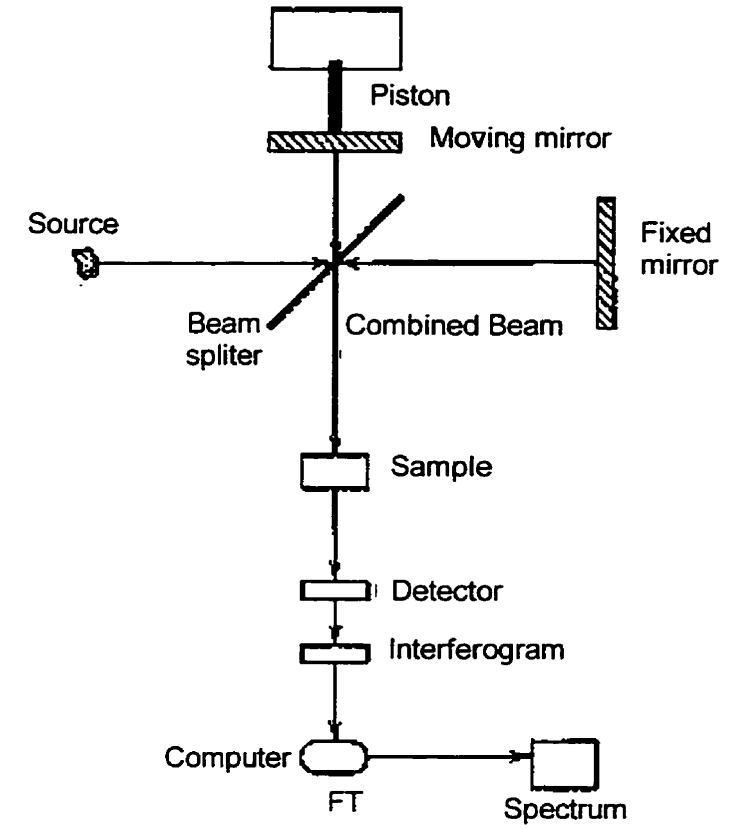

Figure 6.2. Schematic representation of an FT-IR spectrometer (adapted from Silverstein and Webster, 1998).

6.3 Advantages and limitations of IR spectroscopy

High quality spectra can be obtained very rapidly (3-5 minutes) and sample preparation is usually not required. Only a small amount (10-100 μg) of sample is required. IR spectroscopy is a sensitive and specific technique. The IR instrumentation is relatively low cost.

Two major factors limit the IR spectroscopy study of biological samples. The first major limitation when dealing with biological samples is the strong absorption from tissue-bound water molecules which overlap many areas of interest to biological spectroscopists such as the protein carbonyl amide I band. One way to solve this problem is through partial dehydration of the samples. Another is the use of deuterated water (^2H_2O or D_2O) as a solvent. The strong O-D absorption is shifted to a lower wavenumber thus unmasking the absorptions normally found under the O-H band (Mathies, 1995). This "water problem" has been partially resolved with the development of digital subtraction routines. The second major problem is related to the fact that IR spectroscopy is characterized by overlapping spectral bands due to chemical groups which absorb at similar frequencies. This limitation has been partially resolved with the development of band narrowing techniques. Mathematical procedures such as Fourier self-deconvolution, or second derivatives of the spectra, allow the separation of individual subcomponents that strongly overlap in the spectra of biomolecules (Mantsch *et al.*, 1986).

6.4 Infrared band assignments

Infrared spectra of tissues show that tissues can be described as being a mixture of proteins, lipids, nucleic acids and carbohydrates. It is the concentration of these molecules and/ or the presence of characteristic species of those molecules, which make the IR spectra of different tissues different in the infrared spectra. The assignment of infrared bands has been done by first obtaining the infrared spectra of isolated compounds. Then it becomes a simple matter of comparing the feature bands of an unknown sample with those of the individual pure compounds. The table in Appendix V lists the frequency values in the mid-IR of functional groups found in biological compounds. This table has been designed from empirical IR studies on simple organic compounds and from isolated/ synthetic biological species. The table shows the complexity of an IR spectrum. Appendix V also shows that functional groups from different macromolecules "share" the same spectral bands. Methylene groups from proteins and fatty acids absorb at the same frequency. However by studying the ratio of methylene bands to methyl bands it is possible to tell if lipids or proteins dominate the sample. Furthermore, the presence or absence of other bands may offer hints about the molecular composition of an unknown. Infrared band assignments in this thesis will be done by comparing with assignments found in the literature and in Appendix V. However, in order to help with the assignment of the different bands to be found in the IR spectra of colon biopsies, IR spectra of tissue extracts will first be examined. This will facilitate the identification of the

spectral features arising from biochemical species of the colon. The method used for the extractions is a modified version of the Folch's method (Folch *et al.*, 1957). This method is described in Appendix II.

6.4.1 The organic phase

The organic phase is composed of chloroform-soluble lipids (Figure 6.3). This is obvious in the IR spectra of the organic phase due the dominant absorptions in the region 2800-3000 cm^{-1} assigned to CH_3 and CH_2 asymmetric (2956 and 2922 cm^{-1}) and symmetric (2874 and 2852 cm^{-1}) stretching vibrations of acyl chains and side chains of amino acid residues of proteins (not shown). The ratio of the intensities of the CH_2 and CH_3 absorptions provides an indication of the relative proportions of CH_2 and CH_3 groups in the sample. The higher the ratio, the greater the proportion of CH_2 groups relative to CH_3 groups. In turn, this provides an indication of the relative lipid and protein contents of tissues. A high CH_2:CH_3 intensity ratio indicates a relatively high lipid content, while a low CH_2:CH_3 intensity ratio indicates a relatively high protein content. This is easily understood when one considers that lipid acyl chains typically contain 13-17 CH_2 groups for every CH_3 group, while protein side chains contain almost equal numbers of CH_2 and CH_3 groups. As expected, the CH_2:CH_3 ratio in the organic phase is very high as compared to that of the aqueous phase.

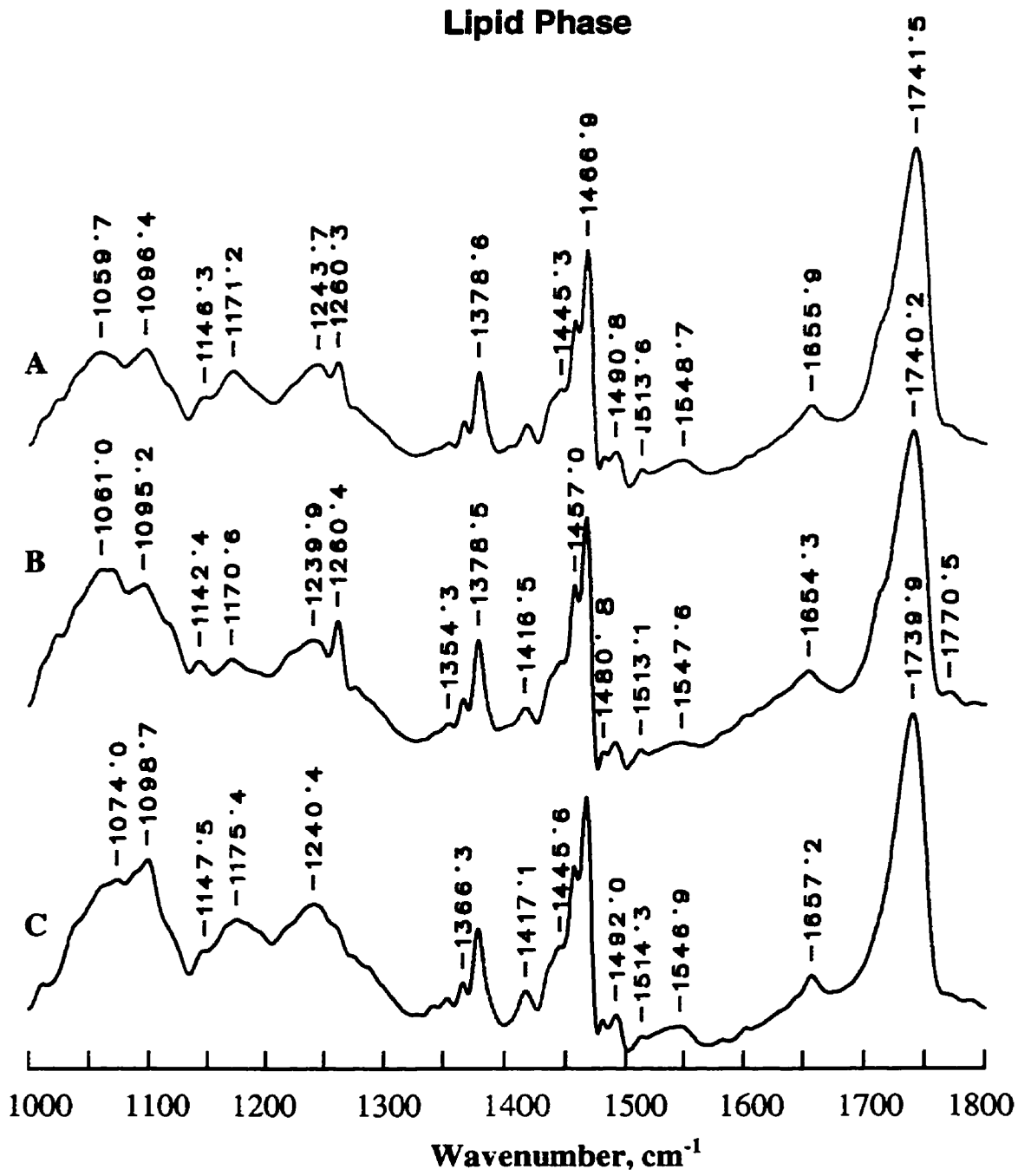

Figure 6.3. Class averages of FT-IR spectra of rat colon extract: (A) tumor (B) AOM-mucosa (C) control mucosa.

The region between 1800-2800 cm^{-1} is devoid of absorptions due to biological species and therefore this region will not be shown in subsequent spectra.

The next strong absorption in the spectra of the organic layer is found at 1740 cm^{-1} due to the stretching vibrations of the ester C=O groups. This absorbance is characteristic of lipids and is not present in the spectra of the aqueous phase.

The small absorption seen at ~1655 cm^{-1} has been assigned to the asymmetric vibrations of the NH^{+}_{3} found in the head group of phosphatidylethanolamine (Lewis and McElhaney, 1996), while the NH^{+}_{3} asymmetric vibration of phosphatidylcholine head group gives rise to a band at around 1480 cm^{-1} (Jackson and Mantsch, 1992).

Absorptions at 1456 and 1468 cm^{-1} arise from the CH_3 asymmetric bending and CH_2 scissoring vibration respectively. Again, as in the stretching region of these two functional groups, it can be observed that the CH_2 band is more predominant than the CH_3 band.

The weak band at 1417cm^{-1} is due to the C-H in-plane bending vibration of $C{=}CH_2$ groups, while the sharp band at 1378 cm^{-1} found in the lipid layer is due to the acyl chain CH_3 symmetric bending vibration.

The other characteristic vibrations found in the IR spectra of lipids include the asymmetric (1229-1258 cm^{-1}) and symmetric (1000-1100 cm^{-1}) from the PO_2^{-} stretching vibrations from the phosphodiester bonds of phospholipids, and the C-O stretching (1150-1200 cm^{-1}) of the acyl chains (Wong *et al.*, 1991a).

6.4.2 The aqueous phase

In the aqueous phase, the CH_3 and CH_2 asymmetric (2956 and 2922 cm^{-1}) and symmetric (2874 and 2852 cm^{-1}) stretching vibrations of acyl chains and side chains of amino acid residues of proteins are roughly equal in their intensities given that proteins have almost equal numbers of CH_2 and CH_3 groups. The same is true for the CH_2 rocking vibration and the CH_3 asymmetric bending vibration.

The absorption at 1717 cm^{-1} (Figure 6.4) is attributed to the C=O stretching vibration of nucleic acids (Fabian *et al.*, 1995).

The strongest absorptions in the water layer, arise from the C=O stretching (the so-called amide I absorption) and N-H bending (amide II) vibrations of the amide linkages in proteins. The position of the both the amide I and amide II absorptions is dependent upon hydrogen bonding interactions. Since each major class of secondary structure found in proteins has a characteristic hydrogen bonding pattern, this gives rise to characteristic amide I and amide II frequencies. Thus, α-helical secondary structure give rise to absorptions in the 1650-57 cm^{-1} region of the spectrum, while absorptions between 1630-40 cm^{-1} are characteristic of more strongly hydrogen bonded β-sheet secondary structures. The secondary protein structures from the extracts were not determined for a number of reasons. During the extraction procedure the protein's secondary structures are no doubt significantly perturbed by the treatment, making it difficult to relate to their real structural conformation in the tissues.

treatment, making it difficult to relate to their real structural conformation in the tissues.

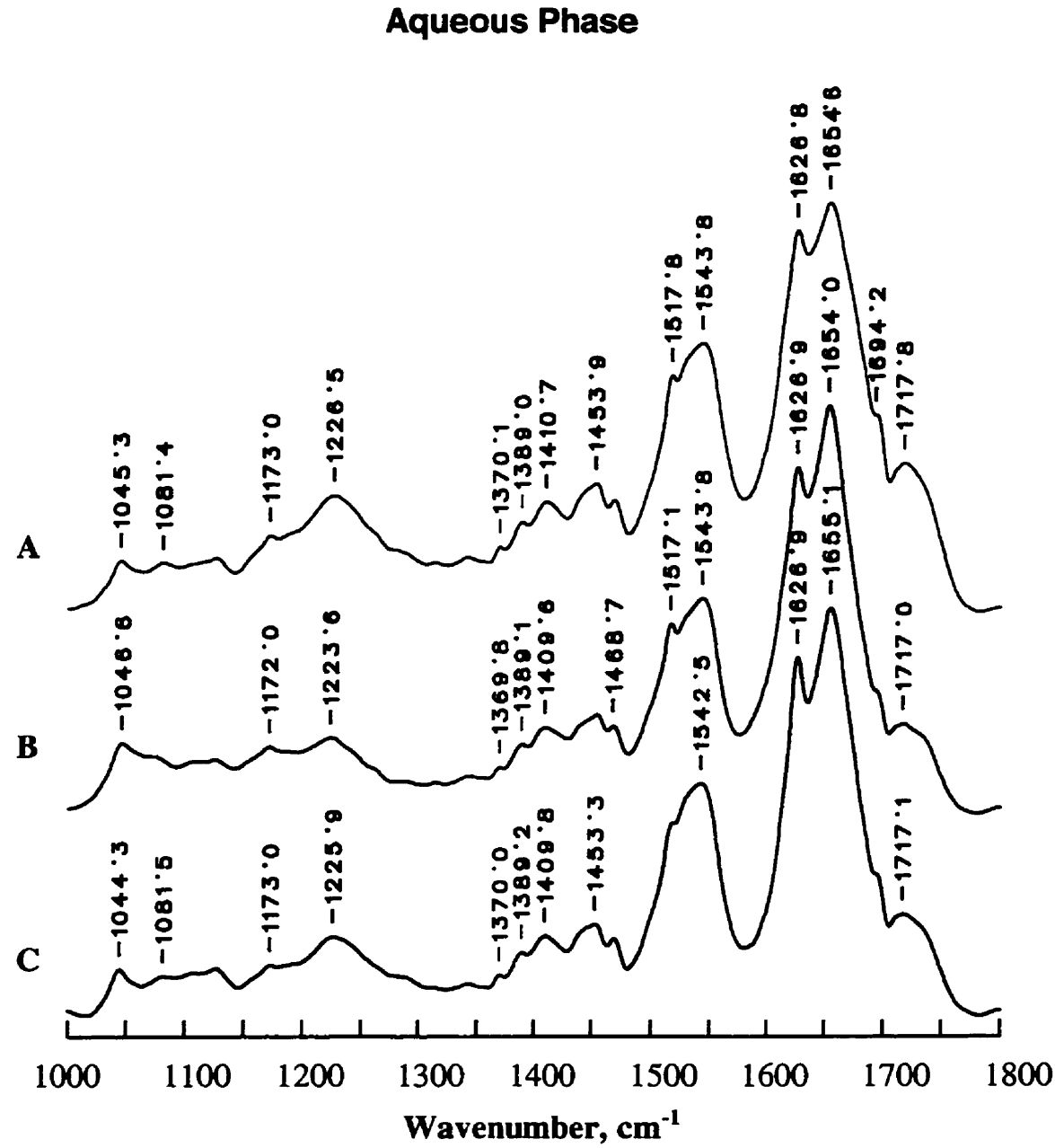

Figure 6.4. Class averages of FT-IR spectra of rat colon tissue extract: (A) tumor (B) AOM-mucosa (C) control mucosa.

In addition, the extraction includes all the proteins found in the tissue samples, cytosolic and membrane-bound. Hence an average of the total protein content is observed.

The sharp absorption at 1517 cm^{-1} in the aqueous-phase spectra arises from tyrosine side chains.

The broad absorption in the aqueous phase centered at around 1400 cm^{-1} is attributed to the COO^- symmetric stretching absorption, arising predominantly from acidic amino acid side chains.

Absorbances from the asymmetric and symmetric stretching PO_2^- vibrations of nucleic acid phosphodiester bonds are found at 1225 and 1080 cm^{-1} respectively.

Other absorptions in the aqueous phase include the small band at 1150-1175 cm^{-1}. This band has been assigned to the C-O stretching of C-OH groups found in serine, tyrosine, and threonine residues of proteins, and carbohydrates (Wong *et al.,* 1991a). The band at ~1044 cm^{-1} due to the C-O stretching vibration of C-O-C groups found in DNA and RNA deoxyribose and ribose groups, and of C-OH groups of the amino acids serine and threonine (Wong *et al.,* 1991a, Fabian *et al.*, 1995).

From this analysis of the important bands found in an IR spectrum, and the assignments found in the literature, we can now start to tackle the analysis of the more complex IR spectra of tissues.

6.5 Infrared spectroscopy in cancer of the colon

IR spectroscopy is a powerful tool for the study of biological systems. Each compound will have a complex and characteristic spectrum. The shapes and positions of the resulting spectral peaks are influenced by nearby molecular components and the environment. Therefore, IR spectroscopy is very sensitive to changes in chemical structure, conformation and environment. IR spectroscopy has been used to determine the gross secondary structure of macromolecules such as proteins (i.e. α-helix, β-sheet content; Jackson and Mantsch, 1995), lipid phase transitions, the interaction of lipids with proteins, and so on.

IR spectroscopy has been applied to the study of cultured cell lines (Rigas and Wong, 1992; Schultz *et al.*, 1996), and biological tissues. The application of IR to the study of biological tissues is a more recent event and includes the examination of Alzheimer's disease plaques (Choo *et al.*, 1993), infarcted rat heart tissue (Liu *et al.*, 1996), and different types of cancers such as breast tumors (Fabian *et al.*, 1995), liver (Wong *et al*, 1991a), cervix (Wong *et al.*, 1991b), human basal cell carcinoma, (Wong *et al.*, 1993a) and colorectal cancer (Wong and Rigas, 1990; Rigas *et al.*, 1990; Wong *et al.*, 1993b).

In recent years, IR spectroscopy has been applied to the study of malignancy. The main differences between malignant and normal tissues, were found in three regions: the PO_2^- symmetric and antisymmetric stretching bands including the C-

O stretching band (1000-1260 cm^{-1}), the amide I band (1640-1700 cm^{-1}), and the C-H stretching bands (2800-3000 cm^{-1}).

The phosphodiester region

The main differences between cancerous and normal tissues and cell lines were found in this region of the spectrum. The PO_2^- asymmetric stretching band in colorectal carcinomas was shown to be split into two at 1241 and 1223 cm^{-1}. Normal tissue samples did not show such a splitting. The band at 1240 cm^{-1} has been assigned to non-hydrogen-bonded form of PO_2^-, while the band at 1223 represents the hydrogen-bonded form (Rigas *et al.*, 1990). As a result, spectra of different types of cancer, including colorectal cancer, showed extensive hydrogen bonding of the phosphodiester groups of nucleic acids, and a decrease in the hydrogen bonding of the C-O groups of proteins (Rigas *et al.*, 1990; Wong *et al.*, 1991a). The band at 1240 has also been assigned to the asymmetric PO_2^- stretching absorption of RNA molecules (Wong *et al.*, 1991b). An alternative explanation of the difference in their IR spectra would be that more DNA is present in tumors than in normal tissue.

The symmetric PO_2^- stretching band peaks at around 1082 cm^{-1} in normal tissues. In malignant tissues this band has been demonstrated to be shifted to 1086 cm^{-1} (Rigas *et al*, 1990).

The band at 1154-1171 cm^{-1} has been previously assigned to the C-O stretching of proteins. This is a relatively weak band. However, it was also found to be different both in its shape and in its spectral position, between

normal and cancerous tissues. In normal samples this band peaks at 1164 cm^{-1}, while in malignant samples it does at 1173 cm^{-1} (Rigas *et al.*, 1990). The lower frequency component band represents the hydrogen-bonded C-O groups. Therefore, malignant tissues display a decrease in the hydrogen bonding of C-O groups of proteins (Rigas *et al.*, 1990).

The amide I band

The amide I absorption is conformationally sensitive and it has been used to predict protein secondary structure (Jackson and Mantsch, 1995). Since the tissues contain a mixture of different proteins, this band represents the average of the total tissue protein content. The secondary structures of tumor proteins are largely α-helices. In leukemic cells an increase in the shoulder at 1635 cm^{-1}, which implies a greater proportion of β-sheet secondary structure, has been noted (Schultz *et al.*, 1996). Similar results were obtain in murine liver tumor tissue (Wong *et al.*, 1991a). In colorectal cancer, contradictory results have been found. In a first report, adenocarcinoma cell lines and colorectal tumors displayed a relatively larger amount of β-sheet with respect to α-helix than in normal tissue (Rigas and Wong, 1992). Later the same investigators reported a smaller contribution of β-sheet secondary structure in colorectal tumors than in the normal mucosa (Wong *et al.*, 1993b).

The C-H stretch region

CH_2 and CH_3 groups of lipids and proteins are found in this region of the IR spectrum. In malignant colorectal tissues, the intensity of the asymmetric CH_3 band was found to be decreased and the symmetric CH_2 band to be increased with respect to the normal mucosa (Rigas *et al*, 1990). Similar results were found in murine liver tumors (Wong *et al.*, 1991a) and basal cell carcinomas (Wong *et al.*, 1993a).

Only one group reported investigations in malignant colonic tissues (Wong *et al*, 1993b). The results of those investigations consisted in analyzing each spectrum and subjectively comparing them with the spectra of normal colonic tissues. No statistical data were provided in those studies.

Attempts were also made to analyze microtome sections of colorectal tumors and normal mucosa (Wong and Rigas, 1990). For that study the samples were embedded in OCT compound (Optimal Cutting Temperature). However the OCT compound gave rise to broad absorbance that hampered the overall spectra of the tissue samples. As a consequence, the authors obtained mid-infrared spectra of fresh-frozen cryostat sections. The only difference between malignant and normal tissue they reported was a shift in the asymmetric PO_2^- stretching bands from 1082 cm^{-1} 1086 cm^{-1}.

At this point it is useful to describe briefly how the spectra of cryostat sections were obtained. Slides of fresh-frozen tissue samples obtained from surgical biopsies were cut in a cryostat (10 μm thick) and placed on top of barium fluoride

window. Then the mid-IR spectra of the sections were obtained in the same manner as the tissue biopsies. Therefore, it is fair to conclude that the tissue sections included layers of the colon other than just mucosa. The same group of investigators reported later that the connective tissue present in the colonic submucosa gives rise to distinctive spectra which could contaminate the features of the tissue sample of interest (Wong *et al.*, 1993b). This may be the reason why they only show one "...representative infrared spectrum ..." rather than an average spectrum of all the spectra taken.

Spectral contamination due to the presence of connective tissue could hamper interpretation the IR spectra, as was found to be true in the study of the central nervous system and breast cancer (Jackson *et al.*, 1995).

6.6 FT IR spectroscopy of normal, preneoplastic (ACF) and neoplastic tissue of the rat colon

6.6.1 Materials and methods

i. Tissue preparation

Specific pathogen-free male Sprague-Dawley rats (Charles River, Que.) were injected subcutaneously with azoxymethane (AOM, 15 mg/kg body weight, n=15) or with the equivalent volume of isotonic saline (n=10) at seven day intervals for four weeks. The animals were euthanised with CO_2 12 weeks after the first injection and the colons removed and flushed with isotonic saline to remove fecal material.

For macroscopic studies, epithelial samples from control (n=46) and treated (n=43) rats were obtained by gently scraping the colonic mucosa with a glass slide. ACF (n=45) from azoxymethane treated rats were located with the aid of a dissecting microscope and removed by micro-dissection. Grossly-visible colonic tumors (n=42) in azoxymethane treated animals were also removed for analysis. All samples were stored at –80° C until use.

For infrared microscopic studies, the saline-flushed colon was flash frozen in liquid nitrogen and mounted on a cryotome. From each colon a series of 15 μm sections was cut and allowed to air dry on a CaF_2 window. After spectroscopic measures, the sections were stained with hematoxilin and eosin and subjected to histological analysis.

ii. Infrared spectroscopy

In the macroscopic studies, a small volume of tissue (1 mm^3) was placed between a pair of CaF_2 windows, one of which contained a 10 mm well etched on one surface. The windows were mounted in a Harrick demountable cell and placed in a Digilab FTS40A Fourier transform infrared spectrometer equipped with a liquid nitrogen-cooled mercury-cadmium-telluride detector. For each sample, 256 interferograms were recorded, signal averaged and Fourier transformed to generate a spectrum with a nominal resolution of 2 cm^{-1}.

For microscopic studies, spectra were acquired from 15 μm sections of rat colon using a Digilab UMA 300 infrared microscope equipped with a narrow band mercury-cadmium-telluride detector and attached to a Digilab FTS60 Fourier transform infrared spectrometer. Areas of interest in the sections were isolated from surrounding tissue using a variable aperture (Figure 6.5). Spectra were acquired from seven distinct tissue types: mucosal epithelium (control mucosa n=48; AOM-mucosa n=55), submucosa (n=83) and mucularis externae (n=83) from both control and azoxymethane-treated rats and from tumors (n=37). For each sample, 256 interferograms were collected, signal averaged and Fourier transformed to generate spectra with a nominal resolution of 4 cm^{-1}. Fourier self-deconvolution was performed using software developed in-house with a half width of 13.5 cm^{-1} and a resolution enhancement factor of 1.7.

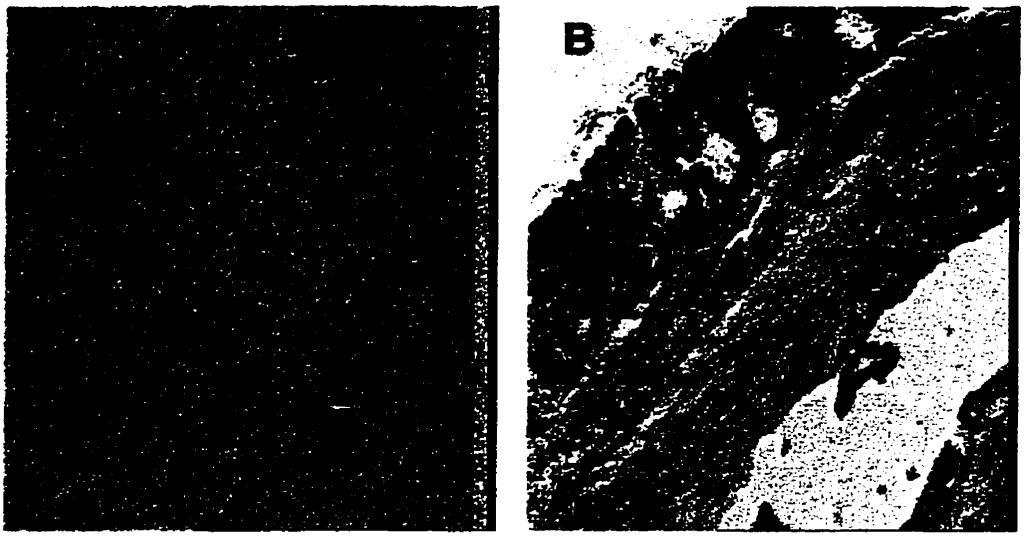

Figure 6.5. Cryostat section of AOM-treated colon tissue, unstained (A) and H&E stained (B). Magnification: x 30. The rectangles delineate the regions from which the spectra were taken.

iii. Statistical analysis

Prior to statistical analysis, all spectra were normalized with respect to area between 1000-1800 cm^{-1}. To remove baseline variations and to enhance any weak spectroscopic features, Savitsky-Golay second derivative spectra were calculated using a 21 data point interval.

A genetic algorithm was applied to the data set to determine the spectral subregions that were most useful diagnostically (Nikulin *et al.*, 1995). Classification was performed using a linear discriminant analysis algorithm

6.6.2 Results and Discussion

i. FT-IR microscopy of colonic cryostat sections

One of the major problems encountered in the spectroscopic study of most organs is sample heterogeneity. This heterogeneity is an obvious consequence of the presence of a number of types of tissue in the organ, each tissue having different morphological, structural and chemical properties. For measurements employing relatively large volumes of tissue ($1mm^3$), the problem of heterogeneity can be difficult to surmount, and the resulting spectrum is the average of the spectra of the different tissue types present. Variations in the relative proportions of the tissues present between samples will result in spectral variations which may be mistaken for biochemical changes associated with the disease process.

With organs such as the colon that are composed of relatively distinct layers of different tissues, the problem of heterogeneity may be overcome in principle by careful dissection of the individual layers, or by careful scraping to remove surface layers. However, the possibility of contamination from underlying layers always exists. Both in ^{1}H-magnetic resonance and FT-IR spectroscopic studies, connective tissue contamination has made it difficult to achieve the correct interpretation of the spectra obtained (Jackson *et al.*, 1995; Bezabeh *et al.*, 1996). To assess the degree of contamination, the spectral characteristics of each of the layers of the colon must be obtained. This may be achieved by the technique of infrared microscopy. An infrared microscope consists essentially of a beam condenser and a variable aperture. The beam condenser concentrates

the infrared light into a narrow beam, which is then directed onto a thin section of tissue. The area of the tissue that is of interest is isolated from the remainder of the tissue with the variable aperture, such that the infrared beam only passes through this area. In this way, spectra of individual layers of tissue in the colon can be obtained.

Class average (mean) spectra of control mucosa, muscularis externae and submucosa obtained using this microscopic method are shown in Figure 6.6. The spectra are complex and exhibit absorptions from all of the major organic species present in each tissue, including lipids, proteins and nucleic acids. Despite this complexity, it is possible to assign many of the absorptions to

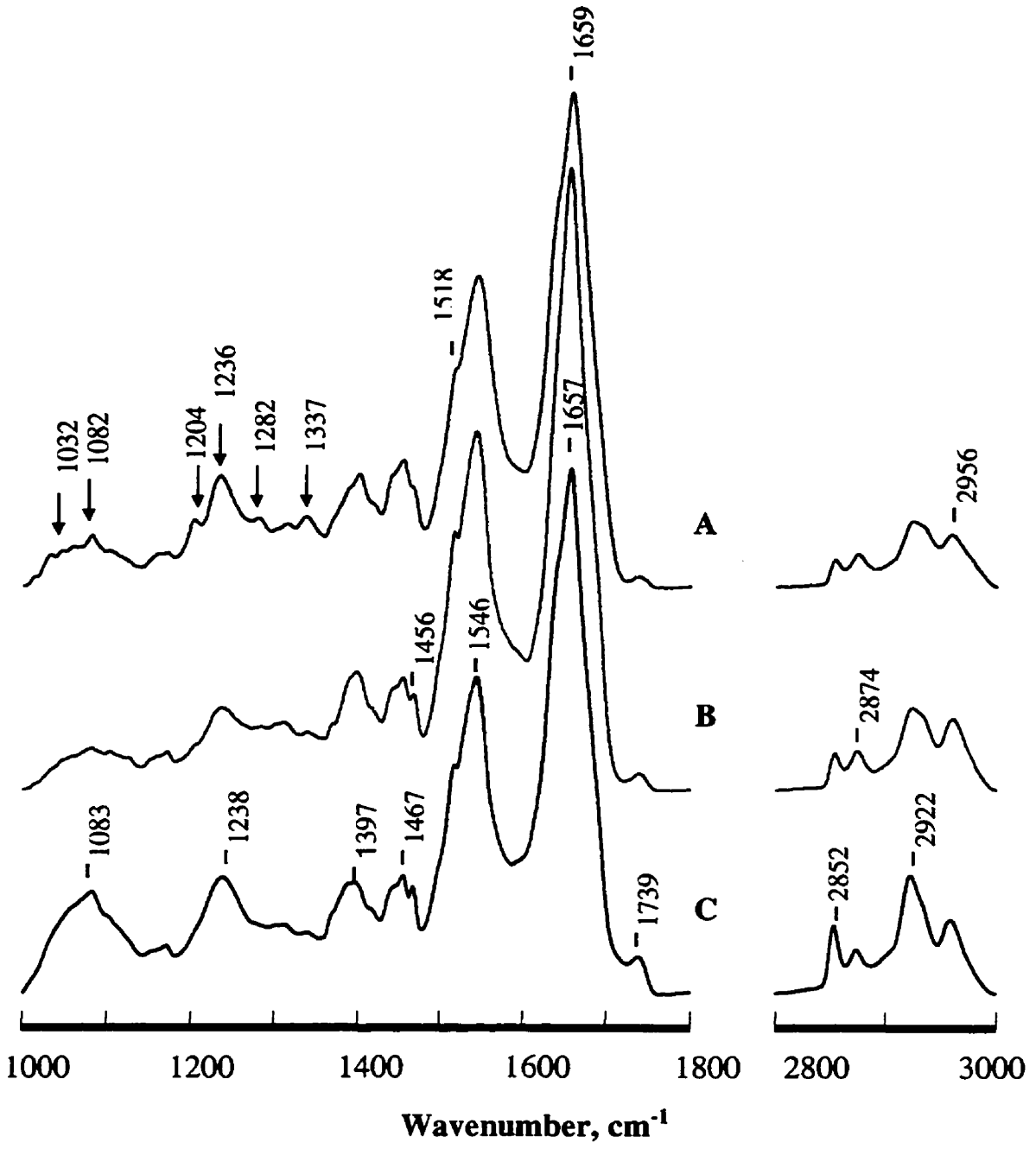

Figure 6.6. Class average FT-IR spectra of cryostat sections of rat colon tissue: (A) submucosa (B) muscularis (C) control mucosa. Arrows indicate characteristic collagen absorptions.

particular functional groups within the various classes of biomolecules present. In the region between 3000-2800 cm^{-1} four characteristic absorptions assigned to CH_3 and CH_2 asymmetric (2956 and 2922 cm^{-1}) and symmetric (2874 and 2852 cm^{-1}) stretching vibrations of lipids and protein are seen.

The ratio of the intensities of the CH_2 and CH_3 absorptions provides an indication of the relative proportions of CH_2 and CH_3 groups in the sample. In Figure 6.6 the CH_2:CH_3 ratio decreases in the order mucosa > submucosa > muscularis externae. This progression can be directly related to the composition of each tissue. The colonic epithelium consists of tightly packed columnar cells whose main function is absorption of water, plus goblet cells that produce a protective acid glycoprotein secretion. The submucosa is composed primarily of fibrous proteins such as collagen deposited in a ground substance, with a few cells embedded in the fiber matrix. Finally, the muscularis externae is composed of fusiform smooth muscle cells rich in contractile proteins such as myosin and actin. The greater CH_2:CH_3 ratio in epithelial tissue is related to the presence of a high proportion of cellular elements, resulting in a relatively strong absorption from membrane lipids. The mucularis externae exhibits the lowest CH_2:CH_3 ratio due to the extremely high protein content of the muscle cells.

The weak absorption at 1740 cm^{-1} is assigned to the ester C=O stretching vibration of phospholipids. The intensities of the ester C=O stretching band decreases in the order mucosa > submucosa > mucularis externae, confirming the relatively high phospholipid content of mucosa. In addition to the absorption at 1740 cm-1, a weak feature is seen at 1717 cm^{-1} which is assigned to the C=O

stretching vibration of nucleic acid bases. This feature is absent in spectra of submucosa and muscularis externae. The absence of this feature in spectra of these tissues can be attributed to the abundance of extracellular matrix and contractile proteins, absorptions from which dominate the spectra.

The strongest absorptions in all spectra arise from the C=O stretching (the so-called amide I absorption) and N-H bending (amide II) vibrations of the amide linkages in proteins. The position of both the amide I and amide II absorptions is dependent upon hydrogen bonding interactions. Since each major class of secondary structure found in proteins has a characteristic hydrogen bonding pattern, this gives rise to characteristic amide I and amide II frequencies. Thus, α-helical secondary structure gives rise to absorptions in the 1650-57 cm^{-1} region of the spectrum, while absorptions between 1630-40 cm^{-1} are characteristic of more strongly hydrogen bonded β-sheet secondary structures. The amide I maxima for control mucosa and the muscularis externae are seen at 1657 cm^{-1}, indicating that the proteins present in both tissues are predominantly α-helical. A weak shoulder at 1636 cm^{-1} indicates the presence of some β-sheet proteins in both tissues.

Interestingly, in the spectra of submucosa tissue the amide I maximum is increased to 1659 cm^{-1}, while the shoulder at 1636 cm^{-1} is increased slightly in intensity compared to that in the spectra of the muscularis externae and mucosa. In addition, the width of the amide I absorption in the muscularis externae and the submucosa spectra is reduced compared to that in the mucosa spectra. These differences are indicative of differences in the nature of the proteins

present. The increased amide I frequency seen in the submucosa indicates that the predominant secondary structural elements in this tissue are characterized by hydrogen bonds weaker than those seen in standard α-helical structures. It has previously been shown that an absorption at 1659-61 cm^{-1} in a number of tissues may be attributed to the presence of collagen triple helices (Jackson *et al.*, 1995). In addition, a pronounced absorption at 1636 cm^{-1}, attributed to formation of collagen cross-links, was seen in these tissues. We therefore attribute the increased amide I frequency and the increased intensity at 1636 cm^{-1} in spectra of submucosa to the presence of collagen fibers in this tissue.

A reduction in the width of individual infrared absorption bands is usually the result of increased motional restriction of the species giving rise to the absorption. In this case the reduced width of the overall protein absorption profile in the muscularis externae and the submucosa is a consequence of a different distribution of the structures, i.e. the predominance of organized structural and contractile proteins present in the tissues, compared to the mainly unorganized cytosolic proteins of the mucosa. As expected given the large amounts of highly ordered contractile proteins present in the smooth muscle cells of the muscularis externae, this tissue exhibits the narrowest amide I absorption.

The sharp absorption at 1515 cm^{-1} in all three spectra arises from tyrosine side chains. The intensity of this absorption is significantly greater in the muscularis externae than in the other two tissues, indicating a much greater tyrosine content in the proteins of which the muscularis is composed.

The spectral region between 1000-1500 cm^{-1} is the most complex. Absorptions at 1468 and 1456 cm^{-1} arise from the CH_2 scissoring and CH_3 asymmetric bending vibration respectively. The broad absorption centered at around 1400 cm^{-1} is attributed to the COO^- symmetric stretching absorption, arising predominantly from acidic amino acid side chains. The difference in the profile of this complex absorption between the three tissue types again reflects the different protein compositions of the tissues. Broad absorptions between 1000-1100 and 1200-1300 cm^{-1} arise from the PO_2^- symmetric and asymmetric stretching vibrations of nucleic acid phosphodiester groups respectively. These nucleic acid phosphodiester absorptions are reduced in intensity in spectra of the muscularis externae, reflecting the increased protein:nucleic acid ratio in this tissue.

The 1000-1350 cm^{-1} region of the spectrum of the submucosa differs significantly from spectra of mucosa and mucularis externae, exhibiting a series of absorptions at 1031, 1082, 1204, 1236, 1282 and 1337 cm^{-1}. These absorptions have been attributed to vibrations arising from the peptide backbone and carbohydrate moieties of type I collagen, and indicate the presence of a significant connective tissue matrix in the submucosa (Jackson *et al.*, 1995).

The band between 1150-1175 cm^{-1}, previously assigned to the C-O stretching of proteins, carbohydrates and acyl chains, in colonic tissue is mainly due to proteins and carbohydrates. In the organic phase it can be seen that the ratio between the C=O stretching band and the C-O band is >1. However in the IR spectra of these cryostat sections it can be seen that the ratio between these two

peaks is <1. Therefore the contributions to this band by the acyl chains can be considered minimal.

It is apparent from this discussion that it is relatively straightforward to distinguish between the different layers of the colon using infrared spectroscopy based upon the nature of the proteins present and the amount of phospholipids and nucleic acid. Thus, the muscularis externae is characterized by narrow protein absorptions (indicative of highly motionally restricted proteins), elevated tyrosine content and relatively low phospholipid and nucleic acid content. The submucosa is characterized by a high collagen content. Finally, the mucosa is characterized by a relatively high phospholipid content, motionally unrestricted proteins and a high nucleic acid content.

Understanding the distinct spectroscopic characteristics of each layer of the colon, we are now in a position to evaluate the effects of azoxymethane upon the colonic mucosa, and to ascertain the extent of interference from absorptions arising from the muscularis externae and the submucosa. Class average spectra of control mucosa and mucosa and tumors from azoxymethane treated animals obtained with an infrared microscope are shown in Figure 6.7. Assignment of the spectra to mucosa or tumor was verified by histological assessment. It can be seen that there is no contamination from either submucosa or muscularis externae in these spectra, based upon the absence of an intense tyrosine absorption at 1515 cm^{-1} and the lack of characteristic collagen absorptions. The spectral profiles of the three tissues are similar. However, subtle differences are apparent. Most noticeably, the PO_2^- symmetric

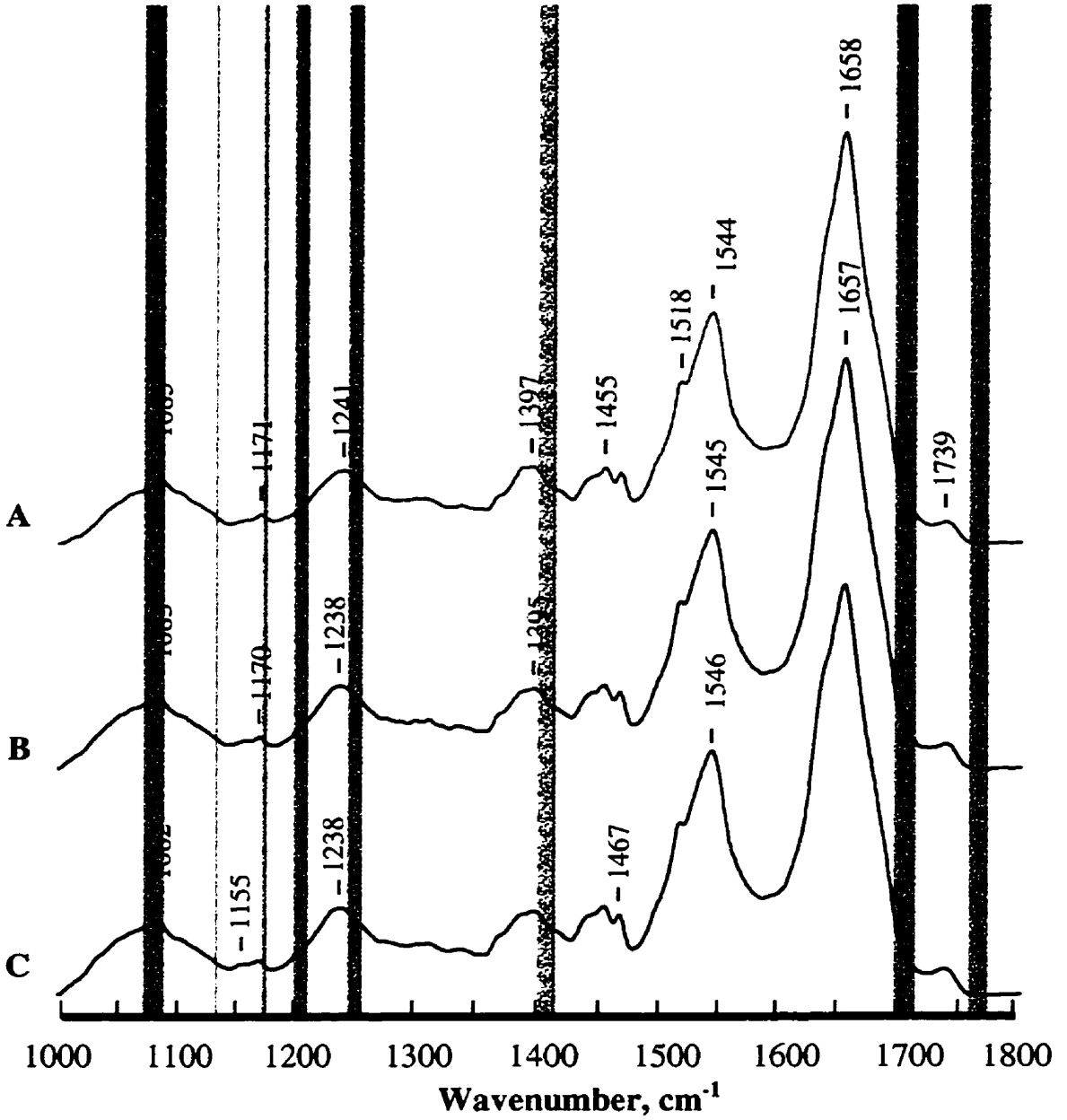

Figure 6.7. Class average FT-IR spectra of cryostat sections of rat colon tissue: (A) tumor (B) AOM-mucosa (C) control mucosa. Shaded areas define the optimal discriminatory subregions.

absorption. Similarly, the PO_2^- asymmetric stretching absorption occurs at a higher frequency in the tumors (1242 cm^{-1}) compared to that in control mucosa (1238 cm^{-1}). These results suggest a progressive alteration in the hydrogen bonding pattern of the epithelial cell nucleic acids (Wong *et al.*, 1993b). The contribution of lipids to this region of the spectrum could be considered minimal. It can be seen in the spectra of the organic phase that the intensity of the ester C=O stretch band (1740 cm^{-1}) is roughly twice the intensity of the phosphate asymmetric and symmetric stretch band. In the present spectra the intensity of the ester C=O stretch band at 1740 cm^{-1} is minimal, so that most of the contributions arise from nucleic acids.

As mentioned before, the amide I band has been used to determine protein conformation. However, because the tissue samples contain a variety of proteins, their spectra are an average of those of all the proteins present in the tissue. We could speculate that most of the proteins in these tissues have α-helical and/ or unordered conformation.

In contrast to previous studies (Wong *et al.*, 1993), spectra of colon tumors presented here do not show appreciable differences in the amide I absorption compared to control mucosa, suggesting that the proteins expressed in the tumors are essentially the same as those found in healthy mucosa. This discrepancy may indicate a species difference, since the tumors studied here are of rodent origin, whereas those studied in previous reports were of human origin. Alternatively, this difference may be due to the induction of the rodent tumors with a carcinogen, rather than the natural process in the human specimens. It is

by no means certain that the molecular mechanisms involved in tumor formation in the colon under these two circumstances are the same (while some colonic tumors are almost certainly the result of the action of dietary carcinogens, others such as familial polyposis are predominantly genetic in origin).

In addition to visual analysis of the spectroscopic data, a multivariate pattern recognition technique was applied to our data in an attempt to classify spectra according to tissue type non-subjectively. Traditionally, differences between spectra are assessed by means of changes in such variables as peak position, peak height, bandwidth and relative changes in these parameters. Obviously, such an approach is highly subjective and depends upon the skill of the spectroscopist. In addition, for a complex data set the number of variables which must be compared to obtained maximum distinction between spectral types can be very large, often greater than 10. Multivariate pattern recognition techniques can be trained to determine intrinsic patterns in a large number of variables (hence the name) which characterize particular groups of spectra. Spectra of unknown origin can then be analyzed to assess the pattern present and a classification of tissue type made based upon this analysis.

One such technique, linear discriminant analysis (LDA), was applied to our data. Spectra were first subjected to a genetic algorithm which identified the spectral subregions which contain the most diagnostic information. These subregions were then used as the input for the LDA pattern recognition algorithm. Data were split into a training set, which was used to train the LDA algorithm to find the discriminatory patterns in the data, and a test set with which to assess the

accuracy of the trained algorithm. The results of LDA analysis using these subregions are presented in Tables 6.1 and 6.2.

In both the training and test sets, the poorest classification was for control mucosa, which was often misclassified as azoxymethane-treated mucosa. However, control mucosa was never misclassified as tumor. AOM mucosa classification was significantly better, and AOM mucosa generally misclassified as control mucosa. Tumor spectra were classified with the greatest degree of accuracy (100% in the test set). These results suggest that control mucosa and mucosa from AOM-treated animals are more similar to each other than to tumors, as expected. However, the results confirm that mucosa from AOM-treated animals gives rise to spectra which are different to those obtained from control mucosa, suggesting that this morphologically normal AOM-treated mucosa is biochemically different from control mucosa.

Table 6.1. Training set for mid FT-IR spectra of cryostat sections of rat colon tissue.

Histological Class	Assigned Class				
	Control	AOM-mucosa	Tumor	% Correct	n
Control	**14**	6	0	70.0	20
AOM-mucosa	3	**16**	1	80.0	20
Tumor	0	1	**19**	95.0	20

Overall accuracy 81.7 %. Numbers on the diagonal indicate the cases where the statistical classification agrees with the histological one. Off-diagonal numbers denote misclassifications.

Table 6.2. Test set for mid FT-IR spectra of cryostat section of rat colon tissue.

Histological Class	Assigned Class				
	Control	AOM-Mucosa	Tumor	% Correct	n
Control	**20**	8	0	71.4	28
AOM-Mucosa	4	**31**	0	88.6	35
Tumor	0	0	**17**	100	17

Overall accuracy: 85 %.

The eight optimally discriminatory spectral regions as calculated by the genetic algorithm are highlighted in Figure 6.7. The discriminatory subregions included 1074-1086 (symmetric stretching PO_2^- of nucleic acids); 1132 cm^{-1} (C-O/C-C stretching); 1170-1171 cm^{-1} (C-OH stretching of protein and RNA); 1200-1208 cm^{-1} and 1246-1254cm^{-1} (asymmetric stretching PO_2^- of nucleic acids); 1401-1411 cm^{-1} (symmetric stretching vibration of carboxylate groups of acidic amino acids); 1699-1711 cm^{-1} (absorbances from the C=O stretching of nucleic acids); 1765-1776 cm^{-1}. Consistent with our earlier observations, these results suggest that the predominant changes in the colon of azoxymethane-treated rats occur in the nucleic acids.

While this infrared microscopic analysis of thin sections allows characterization of tissue of different histological types, it is not without problems. ACF are distributed relatively sparsely along the colon. This means that the majority of sections obtained from the colon will not contain ACF, making ACF difficult to study by this technique. Analysis of excised tissue is preferable. To obtain spectra, ACF were removed from the colon by microdissection. For comparison, spectra of mucosa were acquired from musosal samples obtained by gentle scraping of the internal surface of the colon, while tumor spectra were obtained from small (1 mm^3) samples microdissected from the tumor body. Spectra were obtained from tissue mounted between a pair of CaF_2 windows.

ii. FT IR spectroscopy of rat colon tissue biopsies

The average spectra of the excised tissues (tumor, ACF, untreated and AOM-treated mucosa) between 1000 and 1800 cm^{-1} are shown in Figure 6.8. The most noticeable difference between spectra recorded in this manner and spectra obtained with the microscopic method is the increased intensity at 1650 cm^{-1} with respect to the other absorptions. This is due to a strong contribution from the OH bending vibration of water in this spectral region. Since tissues examined by the microscopic method have been allowed to dry prior to measurement, this absorption is not present in microspectroscopic measurements. The strongest contributions from water are seen in spectra of excised mucosa, as expected, given that the tissue were acquired by lightly scraping the moist mucosal surface.

This dominant water absorption makes a visual comparison between spectra of the four tissues difficult and unreliable. We therefore applied multivariate analysis to the excised tissue spectra. Again, a genetic algorithm was applied to the data to determine the spectral subregions which contained the most diagnostic information, and these subregions were used as input into an LDA algorithm. In this analysis, the ACF spectra were the most difficult to classify correctly, ACF being misclassified as control and treated mucosa and also as tumor (Tables 6.3 and 6.4). This is perhaps to be expected, given that ACF arise from the mucosa and are believed to be a precursor of tumors. Such a result indicates that ACF share biochemical features with both tumor and mucosal samples. Tumors were

misclassified tumor spectra, four were classified as ACF, again indicating shared biochemical characteristics.

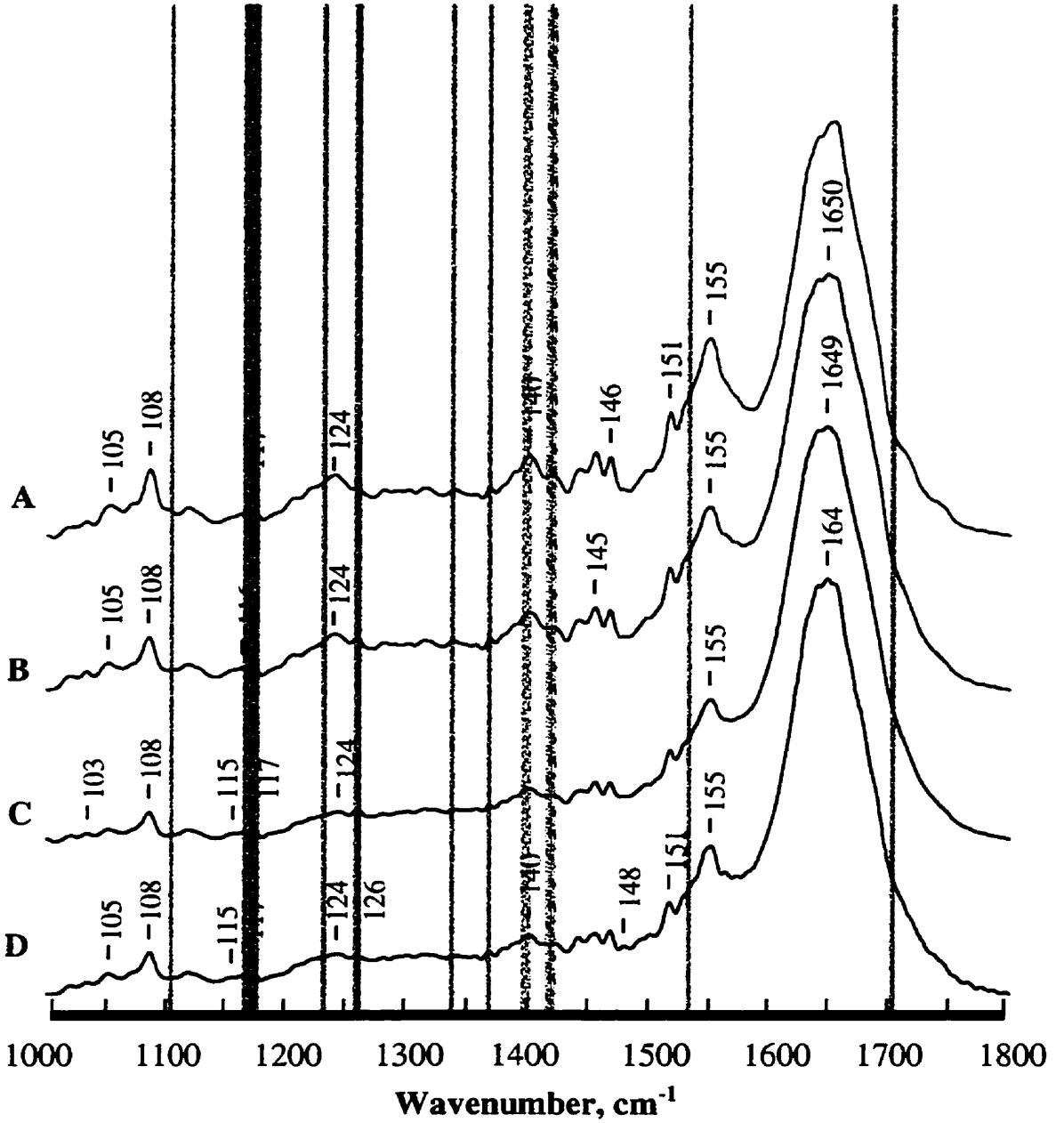

Figure 6.8. Class average FT-IR spectra of rat colon tissue biopsies: (A) tumor (B) ACF (C) AOM-mucosa (D) control mucosa. Shaded areas define the optimal discriminatory subregions.

misclassified tumor spectra, four were classified as ACF, again indicating shared biochemical characteristics.

The optimal set of ten spectral subregions used to classify biopsy samples are shown in Figure 6.8. The discriminatory regions included: 1104-1107 cm^{-1} (C-O/C-C stretching), 1167-1178 cm^{-1} (C-OH stretching of proteins and RNA), 1235-1239 cm^{-1} (asymmetric stretching PO_2^- of nucleic acids), 1259-1264 cm^{-1} (asymmetric stretching PO_2^- of nucleic acids), 1343-1345 cm^{-1} (alkane C-H bending), 1371-1373 cm^{-1} ($-CH_3$ symmetric bending), 1397-1406 cm^{-1} (symmetric stretching vibrations of carboxylate groups of acidic amino acids), 1420-1427 cm^{-1} (C-H in-plane bending), 1540-1542 cm^{-1} (amide II), 1704-1709 cm^{-1} (C=O stretching of nucleic acids). Although the precise frequencies of the absorptions, which carry the most diagnostic information, differ from those found for microscopic studies, they are in the same spectral regions and arise from the same chromophores.

Table 6.3. Training set for mid FT-IR spectra of excised rat colon tissue.

Histological Class	Assigned Class					
	Control	AOM-Mucosa	ACF	Tumor	% Correct	n
Control	**17**	3	0	0	85.0	20
AOM-Mucosa	1	**19**	0	0	95.0	20
ACF	2	3	**14**	1	70.0	20
Tumor	1	0	1	**18**	90.0	20

Overall accuracy: 85.0%. Numbers on the diagonal indicate the cases where the statistical classification agrees with the histological one. Off-diagonal numbers denote misclassifications.

Table 6.4 Test set for mid FT-IR spectra of excised rat colon tissue.

Histological Class	Assigned Class					
	Control	AOM-Mucosa	ACF	Tumor	% Correct	n
Control	**19**	7	0	0	73.1	26
AOM-Mucosa	2	**20**	1	0	87.0	23
ACF	2	3	**18**	2	72.0	25
Tumor	0	0	3	**19**	86.4	22

Overall accuracy: 79.2%.

6.6.3 Conclusions

The results of this FT-IR study support the hypothesis that ACF are putative preneoplastic lesions. The multivariate analysis clearly classified these lesions between normal colonic tissue and colonic tumors. Furthermore, these results support the idea that cancer is a multiple step process. Control mucosa only misclassified as AOM-mucosa. AOM-mucosa misclassified as control mucosa and ACF. ACF misclassified as control and AOM-mucosa as well as tumors. Tumors only misclassified as ACF. According to the adenoma-carcinoma sequence, carcinomas arise from adenomas. If this hypothesis were true, we should be able to find the precursors of the adenomas themselves. ACF could represent an early event of this sequence.

With both the objective multivariate analysis and our qualitative analysis of the data, the major differences among the four classes of tissue used in our study can be found in the protein and phosphate bands. Those bands were assigned mainly to nucleic acids and acidic amino acids.

6.7 Future perspectives

The *in vivo* diagnostic potential of mid-infrared spectroscopy is limited by the strength of absorptions from biological compounds in the mid-infrared. As a consequence, pathlengths greater than 10-15 μm result in artifacts due to complete absorption of the infrared radiation. In addition, the strong absorption of water

presents problems with pathlengths greater than 10 μm. Obviously, a diagnostic technique with a pathlength limitation of 10-15 μm is of little value for *in vivo* studies. This problem can in principle be alleviated by near infrared (NIR) radiation. The reduced absorption in the NIR allows much greater pathlengths to be utilized. The reduced absorption in the NIR could also be a drawback, as less spectroscopic information is obtained. With the development of improved fiber optics and detector designs, the potential exists in the future for the development of an IR colon analyzer using near-infrared spectroscopy as a non-invasive diagnostic tool.

6.8 References

Bezabeh, T., Smith, I.C.P., Krupnik, E., Somorjai, R.L., Kitchen, D.G., Bernstein, C.N., Pettigrew, N.M., Bird, R.P., Lewin, K.J. and Briere, K.M. Diagnostic potential for cancer via ^{1}H magnetic resonance spectroscopy of colon tissue, Anticancer Res., **16**, 1553-1558, 1996.

Carney, J.M., Landrum, W., Mayes, L., Zou, Y., Lodder, R.A. Near-infrared spectrophotometric monitoring of stroke-related changes in the protein and lipid composition of whole gerbil brains, Anal. Chem., **63**, 1305-1313, 1993.

Choo, L.P., Jackson, M., Halliday, W.C., and Mantsch, H.H. In situ characterization of beta-amyloid in Alzheimer's diseased tissue by synchrotron Fourier transform infrared microspectroscopy, Biochim. Biophys. Acta, **1182**, 333-337, 1993.

Colthup, N.B., Daly, L.H., and Wiberley, S.E. *Introduction to infrared and Raman spectroscopy*, Academic Press, Inc. New York, 1990.

Fabian, H., Jackson, M., Murphy, L., Watson, P.H., Fichtner, I., and Mantsch, H.H. A comparative infrared spectroscopic study of human breast tumor cell xenografts, Biospectroscopy, **1**, 37-45, 1995.

Folch, J., Lees, M., and Sloane Stanley, G.H. A simple method for the isolation and purification of total lipides from animal tissues, J. Biol. Chem., **226**, 497-509, 1957.

Griffiths, P.R. and de Haseth, J.A. *Fourier Transform Infrared Spectrometry.* John Wiley, Toronto, 1986.

Jackson, M. and Mantsch, H.H. Biomembrane structure from FT-IR spectroscopy, Spectrochimica Acta Rev., **15**, 53-69, 1993.

Jackson, M. and Mantsch, H.H. The use and missuse of FTIR spectroscopy in the determination of protein structure, Critical Reviews in Biochemistry and Molecular Biology, **30**, 95-120, 1995.

Jackson, M., Choo, L.-P., Watson, P.H., Halliday, W.C. and Mantsch, H.H., Beware of connective tissue proteins: assignment and implications of collagen absorptions in infrared spectra of human tissues, Biochim. Biophys. Acta, **1270**, 1-6, 1995.

Lewis, R.N.A.H. and McElhaney, R.N. Fourier transform infrared spectroscopy in the study of hydrated lipids and lipid bilayer membranes. In *Infrared Spectroscopy of Biomolecules.* H.H. Mantsch and D. Chapman eds., Wiley-Liss, Inc., Toronto, 131-158, 1996.

Liu, K-Z., Jackson, M., Sowa, M.G., Ju, H., Dixon, I.M., and Mantsch, H.H. Modification of the extracellular matrix following myocardial infarction monitored by FT-IR spectroscopy, Biochim. Biophys. Acta, **1315**, 73-77, 1996.

Mantsch, H.H., Casal, H.L., and Jones, R.N. resolution enhancement of infrared spectra of biological systems. In *Spectroscopy of Biological Systems.* R.J.H. Clark and R.E. Hester, eds. John Wiley and Sons, Toronto, 1-46, 1986.

Mathies, R.A. Biomolecular vibrational spectroscopy. In *Methods in Enzymology.* K. Sauer, ed. Academic Press, Toronto, **246**, 377-389, 1995

Nikulin, A., Brière, K.M., Friesen, L., Smith, I.C.P., and Somorjai, R.L. Genetic algorithm-guided optimal attribute selection: a novel preprocessor for classifying MR spectra, Proc. Soc. Magn. Reson., **3**, 1940, 1995.

Parker, F.S., *Applications of infrared, Raman, and resonance Raman spectroscopy in biochemistry*, Plenum Press, New York, 1983.

Schultz, C.P., Liu, K-Z., Johnston, J.B., and Mantsch, H.H. Study of chronic lymphocytic leukemia cells by FT-IR spectroscopy and cluster analysis, Leuk. Res., **20**, 649-655, 1996.

Silverstein, R.M. and Webster, F.X. *Spectrometric identification of organic compounds*, John Wiley & Sons, Inc., New York, 1998.

Rigas, B., Morgello, S., Goldman, I.S., and Wong, P.T.T. Human colorectal cancers display abnormal Fourier-transform infrared spectra, Proc. Natl. Acad. Sci. USA., 87, 8140-8144, 1990.

Rigas, B. and Wong, P.T.T. Human colon adenocarcinoma cell lines display infrared spectroscopic features of malignant colon tissues, Cancer Res., 52, 84-**88**, 1992.

Schrader, B. Vibrational spectroscopy of different classes and states of compounds. In *Infrared and Raman Spectroscopy. Methods and* Applications. B. Schrader, ed. VCH Verlagsgesellschaft mbH, New York, 189-410,1995

Skoog, D.A. *Principles of Instrumental Analysis*. Saunders College Publishing, Toronto, 1985.

Somorjai, R.L., Nikulin, A., Pizzi, N., Jackson, D., Scarth, G., Dolenko, B., Gordon, H., Russel, P., Lean, C.L., Delbridge, L., Mountford, C.E., and Smith, I.C.P. Computerized consensus diagnosis: a classification strategy for the robust analysis of MR spectra. I. Application to ^{1}H spectra of thyroid neoplasms, Magn. Reson. Med., **33**, 257-263, 1995.

Wong, P.T.T. and Rigas, B. Infrared spectra of microtome sections of human colon tissues, Appl. Spec., **44**, 1715-1718, 1990.

Wong, P.T.T., Cadrin, M., and French, S.W. Distinctive infrared spectral features in liver tumor tissue of mice: evidence of structural modifications at the molecular level, Exp. Mol. Pathol., **55**, 269-284, 1991a.

Wong, P.T.T., Wong, R.K., Caputo, T.A., Godwin, T.A., and Rigas, B. Infrared spectroscopy of exofiliated human cervical cells: evidence of extensive structural changes during carcinogenesis, Proc. Natl. Acad. Sci. USA, **88**, 10988-10992, 1991b.

Wong,, P.T.T., Goldstein, S.M., Grekin, R.C., Dodwin, T.A., Pivik, C., and Rigas, B. Distinct infrared patterns of human basal cell carcinoma of the skin, Cancer, Res., **53**, 762-765, 1993a.

Wong, P.T.T., Lacelle, Z., and Yazdi, H.M. Normal and malignant human colonic tissues investigated by pressure-tuning FT-IR spectroscopy, Appl. Spectrosc., **47**, 1830-1836, 1993b.

7 Summary of thesis research

In this thesis I have used a combined approach of ^{1}H-MR and FT-IR spectroscopies for the elucidation of the molecular events underlying carcinogenesis and characterization of premalignant tissue of the rat colon. By comparing the different ^{1}H MRS and FT-IRS peaks and bands with those of isolated biomolecules, tissue extractions, and assignments found in the literature, it was possible to characterize the different tissues of the rat colon spectroscopically. I have also shown that those spectroscopic techniques, combined with multivariate statistical analysis, were able to separate the different classes of tissues with high accuracy, even though some of those classes are histologically similar. The multivariate analysis was also able to show links among the different classes of colon tissue that support the multistep model of colon cancer.

In ^{1}H MRS, the main differences were found in the resonances due in part to the amino acids glutamate and glutamine. These amino acids have been shown to be involved in the metabolism of different types of cancers. The results of this thesis support those conclusions.

In FT-IR the main differences between normal and malignant colon tissues lie in the spectral regions due to nucleic acids and acidic amino acids (aspartate and glutamate).

Both in ^{1}H MRS and FT-IR the spectroscopic features of ACF were shown to lie between those of the normal tissues and the tumors. As expected, the two types

of mucosa were the most closely-related groups while the histologically different tumor class was the most homogeneous group.

The ultimate goal in the field of biodiagnostics is the early detection of the disease process. The results provided in this thesis show that it is possible to identify very early premalignant lesions of the colon with high accuracy. The multivariate analysis of the FT-IR and ^{1}H MR spectra resulted in a more objective method of classification than the histopathological classification. Histopathology is the gold-standard for the classification of tissues. However, it is heavily dependent on the experience of the histopathologist and on the accuracy with which the tissue sections are obtained and examined for future diagnosis. Differences in the interpretation of the diagnosis are also an important factor. The spectroscopic-statistical approach presented in this thesis has given above average accuracy in the classification of the different classes of tissues. Given the importance of early diagnosis, the multidisciplinary approach presented in this thesis could serve as an important complement to the routine histopathological assessment for a better and more efficient diagnosis of colorectal cancer.

In conclusion, I have shown that the multidisciplinary approach of using ^{1}H MRS and FT-IR spectroscopy combined with multivariate analysis can be successfully used to investigate changes in colon tissue biochemistry prior to the appearance of tumors.

Appendix I

Table 1. ^{1}H MRS assignment of resonances present in acid extracts of lymphocytes.

Table 2. ^{1}H MRS assignment of resonances of perchloric acid extracts of human colon mucosa and adenocarcinomas.

Abbreviations and key: b = broad, s = singlet, d = doublet, dd = doublet of doublets, ddd = doublet of doublets of doublets, m = multiplet, t = triplet, q = quadruplet, c = complex, U = unidentified metabolites.

Table 1 taken from: Sze, D.Y. and Jardetzky, O. Biochim. Biophys. Acta, **1054**, 181-197, 1990.

Table 2 taken from: Moreno, A., and Arús, C. NMR Biomed., **9**, 33-45, 1996.

Appendix II

Tissue Extractions

Colon tissue samples under 1 mg. were homogenized in 0.75 ml of double distilled H_2O. The homogenate (0.75 ml) was mixed with 3 ml of chloroform/methanol solution (2:1, v/v). The mixture was centrifuged for 5 minutes at 6000 rpm. After centrifugation a biphasic solution was obtained. The upper layer consists of all non-lipid substances (upper phase or aqueous phase); the lower layer contains all the lipids of the tissue (lower phase or organic phase). The two layers were separated with a syringe and transferred to a clean, labeled, glass tube. The solutions were taken to dryness under pure nitrogen. The dried extracts were then reconstituted with either chloroform or water.

^{1}H MRS of tissue extractions

For the ^{1}H MRS experiment, the dried extractions (tumor=4; control mucosa=3; AOM-treated mucosa=4) were reconstituted in either 400 µl of PBS/D_2O or deutereted chloroform. The reconstituted extractions were then immediately transferred to an NMR tube and ^{1}H MR spectra were obtained as with the tissue biopsies.

FT-IR spectroscopy of tissue extractions

For the FT-IR experiment, the dried extractions (tumor=10; control mucosa=10; AOM-treated mucosa=10) were reconstituted in either 50 µl of water or chloroform. Immediately after, the reconstituted solutions were pipetted out, laid on top of a CaF_2 window and let dry. FT-IR spectroscopy was then performed as for the biopsies.

Appendix III

[1] MR spectra of isolated biochemicals.

Creatine

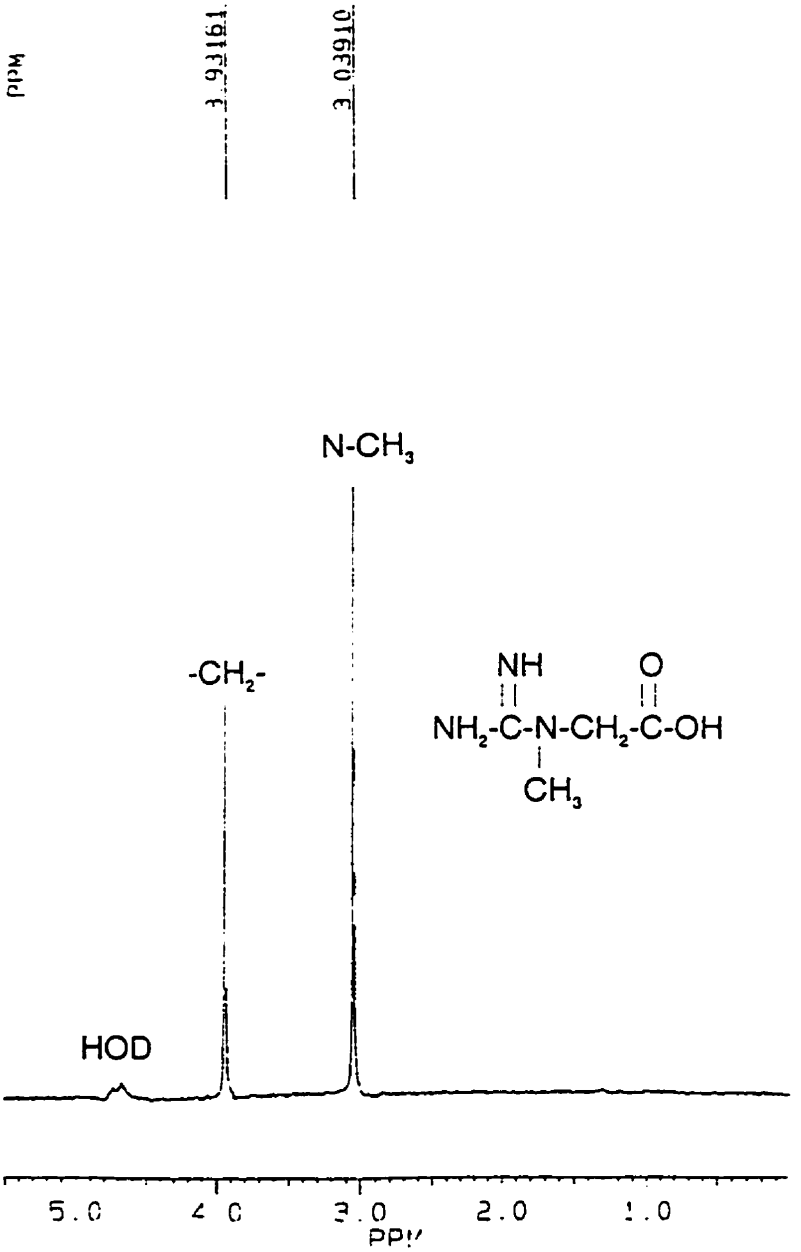

Glutamate

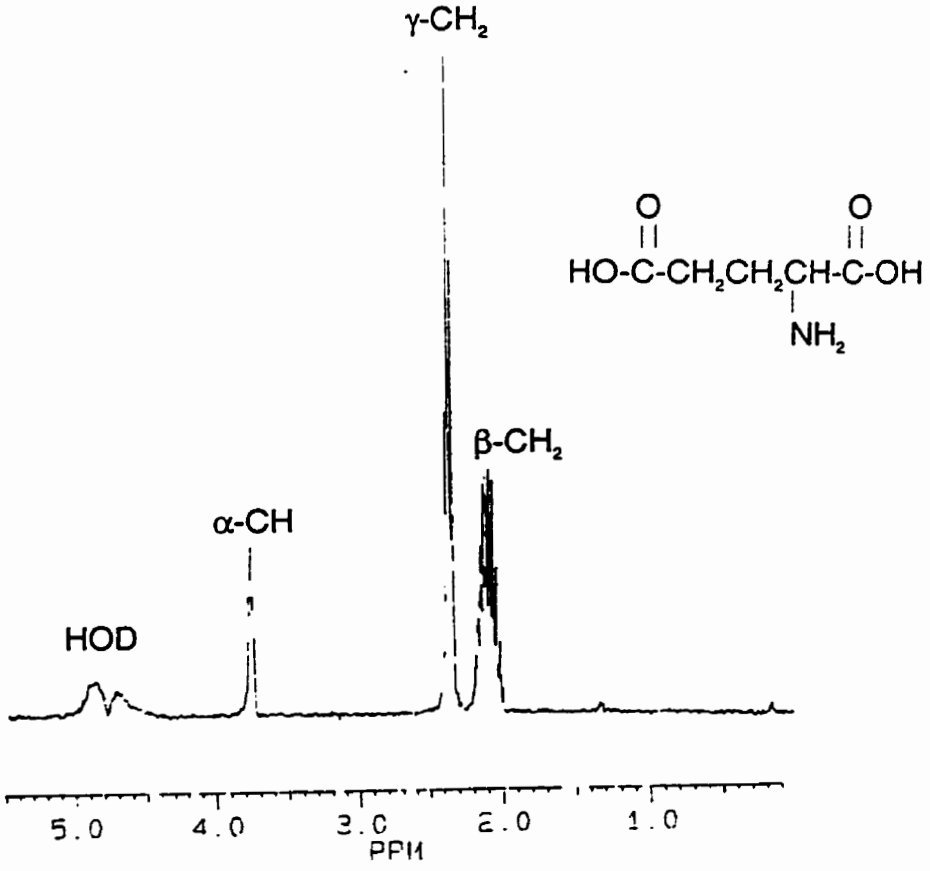

Glutamine

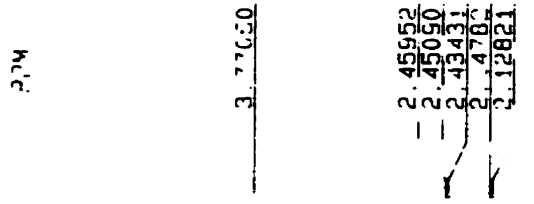

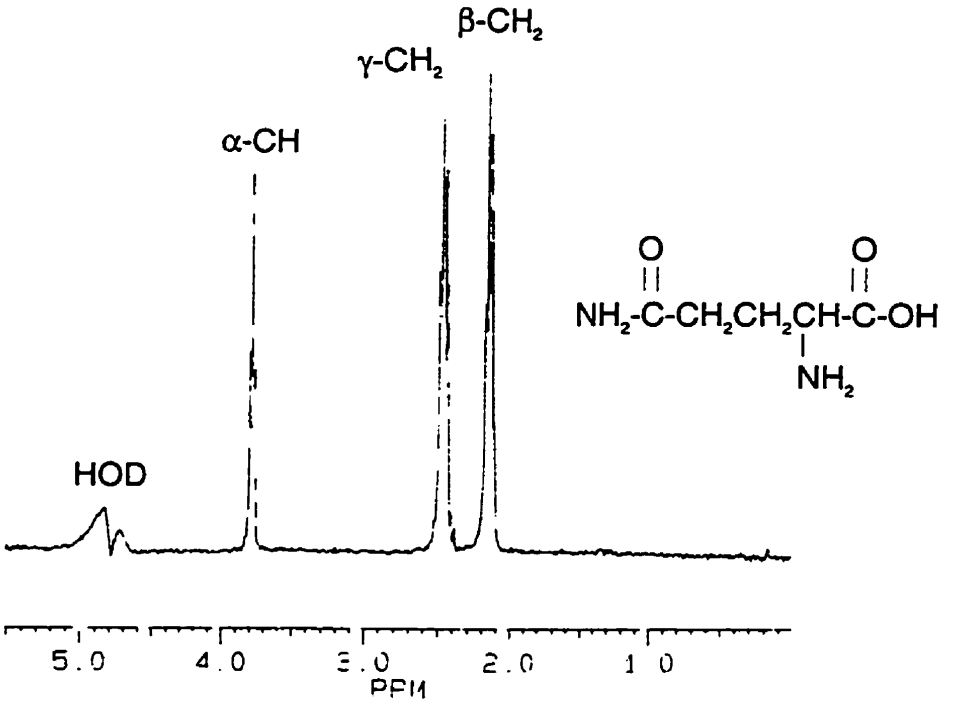

Phosphorylcholine

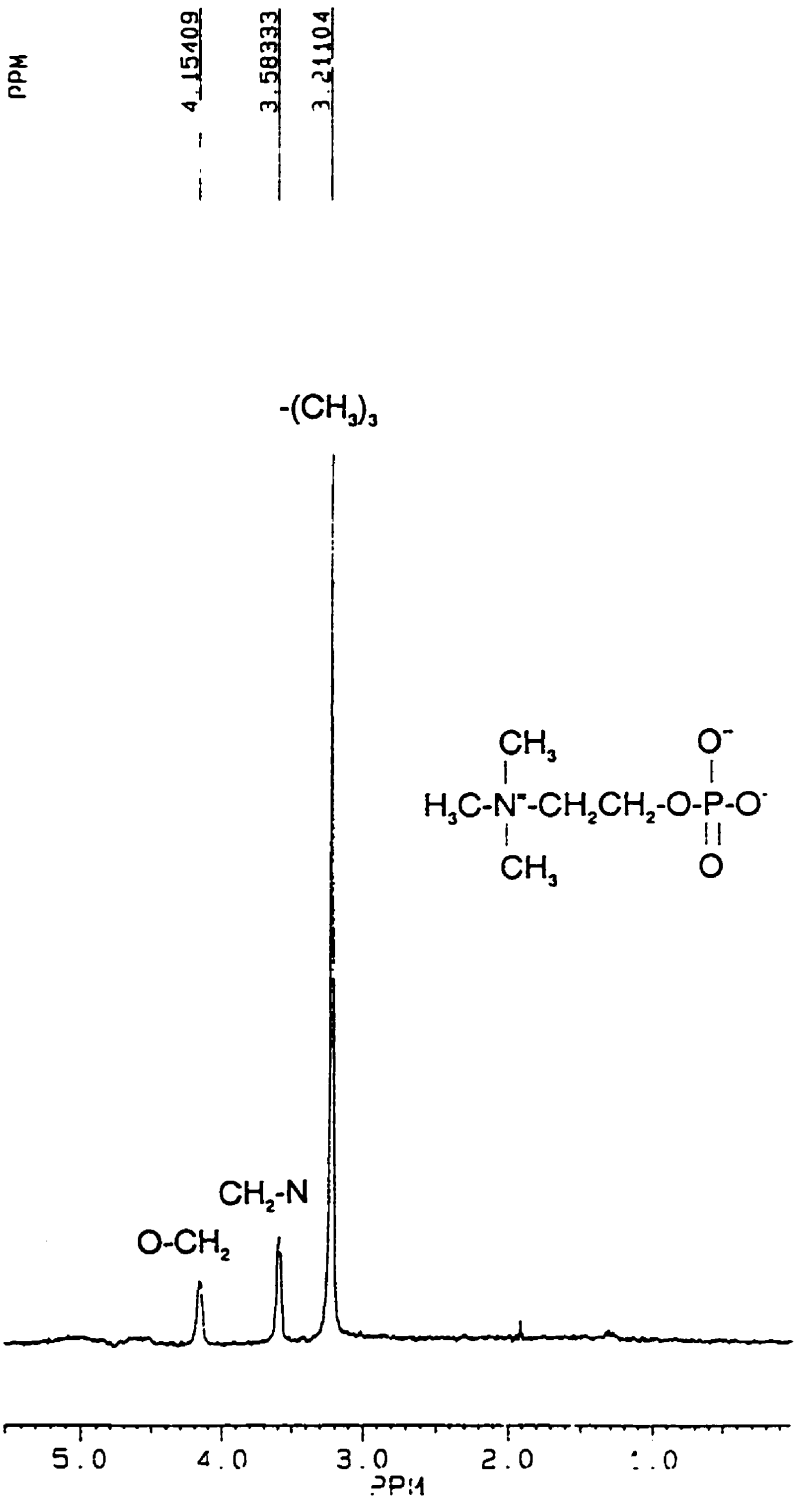

Taurine

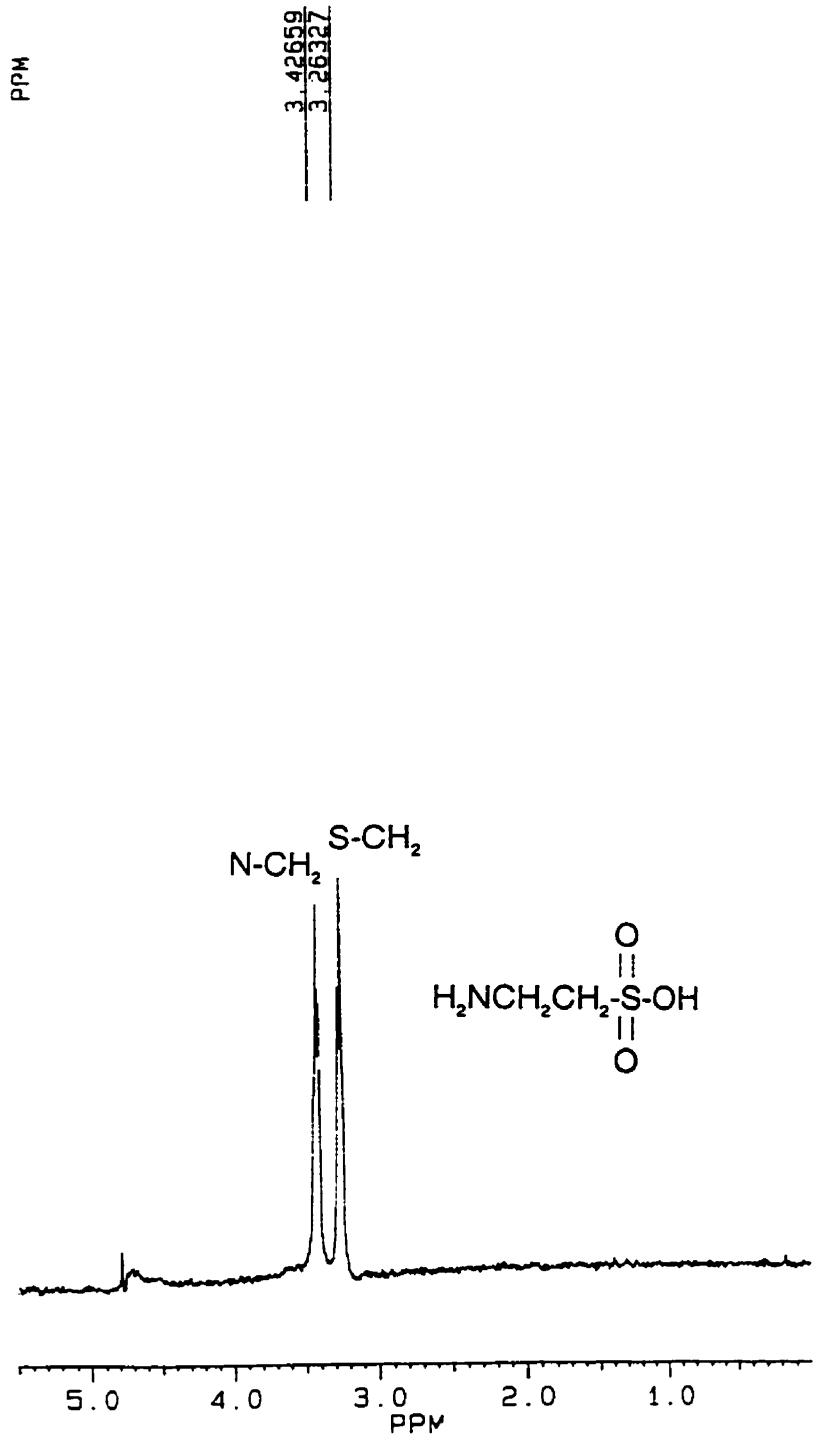
PPM
3.42659
3.26327
N-CH2
S-CH2
O
H2NCH2CH2-S-OH
O
5.0
4.0
3.0
2.0
1.0
PPM

Appendix IV

Genetic algorithm-guided optimal spectral region selection.

For the accurate classification of the ^{1}H MR and FT-IR spectra, a genetic algorithm (GA) developed in-house was applied to the training set to find the best diagnostic spectral subregions. The accuracy of classification based on those best subregions was tested using Linear Discriminant Analysis with the leave-one-out method.

The GA algorithm requires as input the entire spectral range that consisted of 810 attributes for the IR spectra and 570 for the ^{1}H MR spectra. The following parameters must be set to run the analysis: the number of generations, the size of the population, and the ultimate number of subregions required. To start, GA generates a population of P random "chromosomes" which are binary strings used to map the different spectral subregions. A set of consecutive "ones" represents one subregion.

Each generation consists of changing the chromosomes of the population by using genetic –based *point mutations* and *crossover*.

Each chromosome is tested with a fitness function based on LDA with the leave-one-out method and the best P_1 chromosomes are kept intact. The program stops when either the size of the mutations equals zero or the preset number of generations has been reached.

Appendix V

Representative mid-infrared frequencies of various chemical groups.

Range (cm^{-1})	Intensity[a]	Group	Type of vibration[b]	Comments
1030-1090	vs	P-O-C	str	Phosphoric ester
1000-1200	s	C-OH	str	Alcohols
1170-1200	s	C-O	str	Propionic and high esters
1150-1250	vs	P=O	str	Phosphoric ester, H-bonded P=O
1200-1300	s	P=O	str	Phosphoric ester, free P=O
1200-1305	m	N-H	def	Secondary amide, Amide III band
1210-1320	s	C-O	str	Carboxylic acid
~1340	w	C-H	bend	Alkane C-H
1375-1385	m	C-H	bend (sym)	$-CH_3$
1400-1460	s	C-O	sym str	$-COO^-$, carboxylate
1406-1420	w	C-H	i-p bend	$C=CH_2$
~1460	m	C-H	bend (asym)	$-CH_3$
~1468	s	C-H	sc	Alkane, $-CH_2-$
~1500	var	C=C	sk, i-p	aromatic C=C
1515-1570	s	N-H	def.	Amide II band

1520-1580	m	C=N (plus C=C)	int eff	pyrimidines
1540-1610	vs	C-O	asym str	$-COO^-$, carboxylate
1560-1620	m-s	NH_2^+	def	
1590-1620	s	NH	def	primary amide (dil. soln.)
1580-1650	m-s	N-H	def	NH_2;primary amine
1620-1650	s	N-H	def	Primary amide (solid):Amide II band
1620-1670	s	C=O	str	Primary amide (solid), H-bonded: Amide I band
1670-1690	s	C=O	str	-CONHR, primary amide, free (dil. soln.): Amide I
1670-1700	s	C=O	str	-CONHR, secondary amide, free (dil. soln.): Amide I
1700-1720	s	C=O	str	-COOH, aliphatic carboxylic acid
1705-1725	s	C=O	str	Ketone

1720-1740	s	C=O	str	-C(=O)H, aldehyde
1735-1745	s	C=O	str	Saturated esters
1710-1780	s	C=O	str	-O-(C=O)-O-, carbonate
~2850	s	C-H	str (sym)	$-CH_2-$, methylene
~2875	s	C-H	str (sym)	Methyl
~2925	s	C-H	str (asym)	$-CH_2-$, methylene
~2960	s	C-H	str (asym)	Methyl

Abbreviations and key:

[a] br= broad, m= medium, s=strong, sh=sharp, v=very, var=variable, w=weak.

[b] asym= asymmetrical, def=deformation, i-p=in-plane, int eff=interaction effect, sc=scissoring, sk=skeletal, str=stretching, sym=symmetrical.

Adapted from: Parker, F.S., *Applications of infrared, Raman, and resonance Raman spectroscopy in biochemistry*, Plenum Press, New York, 1983.

IMAGE EVALUATION
TEST TARGET (QA-3)

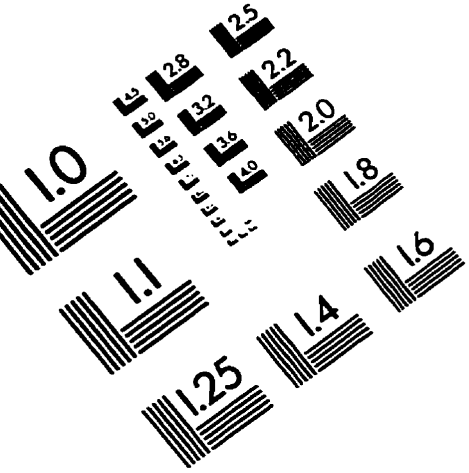

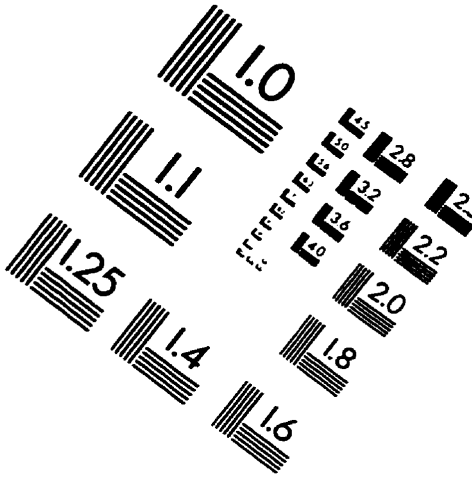

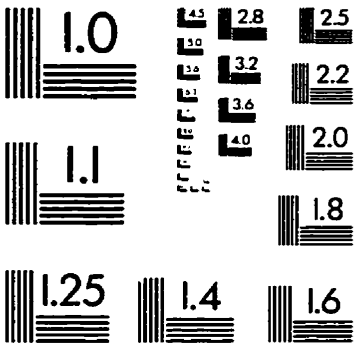

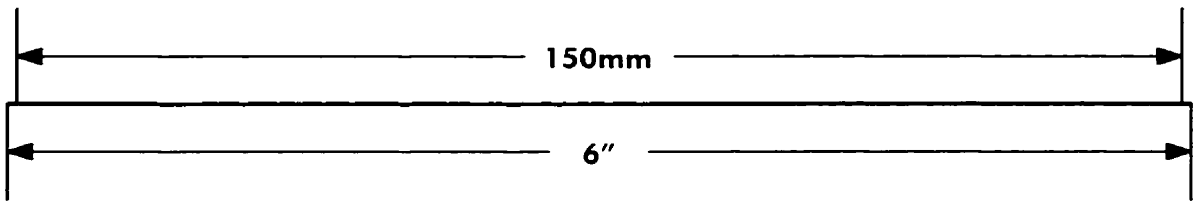

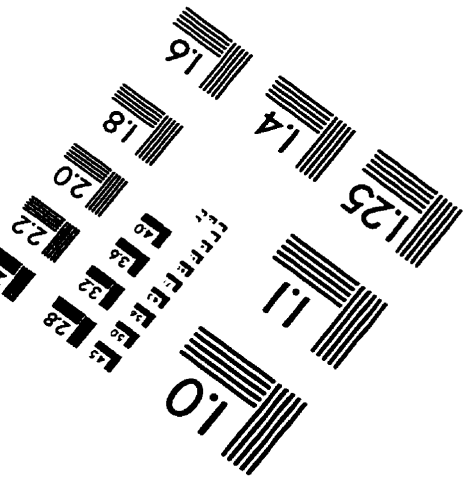

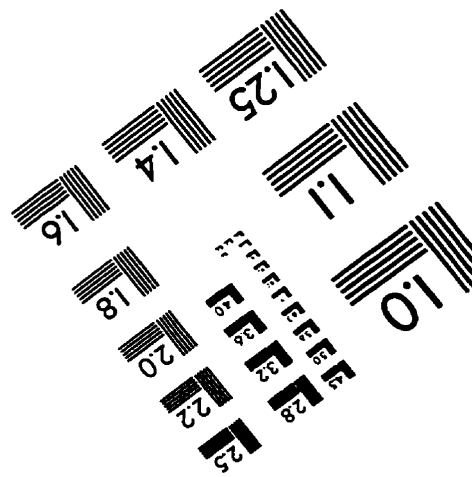

APPLIED IMAGE, Inc
1653 East Main Street
Rochester, NY 14609 USA
Phone: 716/482-0300
Fax: 716/288-5989